Check for updates

Historical development and novel concepts on electrolytes for aqueous rechargeable batteries†

Shigang Chen,[a] Mengfei Zhang, [iD][a] Peimiao Zou,[a] Boyao Sun[a] and Shanwen Tao [iD] *[ab]

In battery systems, aqueous electrolytes are superior in ionic conductivity, interfacial wettability, safety and environmentally benign compared to organic liquids, polymers, inorganic solid-state and ionic liquid electrolytes. However, their narrow electrochemical stability window, electrode dissolution/side reactions and temperature-variation instability result in a low energy density, undesirable cyclic lifespan and limited working temperature window in aqueous rechargeable batteries. Herein, the historical development of aqueous electrolytes in various types of batteries, ranging from monovalent-ion batteries, multivalent-ion batteries, metal–air batteries, metal–chalcogen batteries, and hybrid batteries to redox flow batteries is summarized through the representative pioneering works. Meanwhile, the strategies of electrolyte additive, pH-management, salt-concentrated electrolyte, gelling, solvent hybridizing, interface tuning and beyond concentrated electrolyte to mitigate the challenges associated with aqueous electrolytes are reviewed and discussed in detail. All these new electrolyte concepts mutually stabilize aqueous rechargeable batteries and improve their corresponding energy density in a broad temperature range, ushering in a promising aqueous energy storage era.

Broader context

Batteries are key technology to mitigate carbon emissions, which are closely related to energy and environmental science. The electrolyte is the most important material in batteries, which thermodynamically and kinetically affect their overall performance. Therefore, it is necessary to understand the principles, historical development and new concepts of electrolytes for the development of enhanced batteries, particularly for next-generation batteries such as aqueous rechargeable batteries. Aqueous rechargeable batteries exhibit high safety, excellent rate capability, desirable environmentally benign nature and cost-effective manufacturing, making them suitable for stationary energy storage. Their corresponding electrolytes can be improved in terms of electrochemical stability window, interfacial stability and temperature-variation stability to potentially extend their applications to electric vehicles to achieve a carbon neutral world. In this review, not only the historical development and new concepts of electrolytes for aqueous rechargeable batteries have been comprehensively and systematically summarized, but a visionary perspective is also provided. The perspective part concentrates on both an academic roadmap for fundamental understanding (characterization and modeling) of electrolytes and the electrode/electrolyte interface and industrial routes for commercializing aqueous rechargeable batteries. This review offers readers a convenient and fast way to understand the key electrolytes for aqueous rechargeable batteries, and also promotes research on improving the relevant electrolytes.

1. Introduction

Climate change has attracted global attention, and hence under the UN Paris Agreement, countries are committed to restricting global warming to less than 2 °C and are actively pursuing a 1.5 °C limitation.[1–3] This has triggered a boom in research and

[a] School of Engineering, University of Warwick, Coventry CV4 7AL, UK.
E-mail: S.Tao.1@warwick.ac.uk
[b] Department of Chemical Engineering, Monash University, Clayton, Victoria 3800, Australia
† Electronic supplementary information (ESI) available. See DOI: **https://doi.org/10.1039/d2ee00004k**

practice towards carbon dioxide mitigation, ranging from carbon avoidance (photovoltaic power stations and hydrogen energy) and carbon embedding (methanol) to carbon removal (bioenergy crops and carbon capture technology).[4,5] The popular strategy of using electric energy in automobiles, which are known as electric vehicles (EVs), can reduce the overall energy usage by enhancing energy efficiency, thus reducing carbon emissions, which can also be categorized into carbon avoidance.[4,6,7] Transport is the second largest source of CO_2 emissions, with 24% of the total emissions, where the fuel efficiency of the mode of travel can significantly influence CO_2 emissions largely.[8] Compared with current internal combustion engine vehicles, EVs are expected to reduce well-to-wheel emissions by

This journal is © The Royal Society of Chemistry 2022

Energy Environ. Sci., 2022, **15**, 1805–1839 | 1805

70–85% by 2030 with virtually zero tailpipe emissions and excellent energy utilization efficiency, which requires the total use of EVs in the transport sector.[8] The commercialization of EVs, involving full battery electric vehicles (BEVs), hybrid electric vehicles (HEVs) and hybrid plug-in electric vehicles (HPEVs), demands mature battery technology with the properties of high energy density, high power density and long lifespan, which currently, commercialized batteries especially lithium-ion batteries (LiBs) fail to satisfy.[7,9,10]

In fact, the bottleneck in promoting the use of EVs promotion is the battery requirements, given that the current batteries exhibit undesirable energy densities, low power densities and safety issues, which are caused by the relatively low capacity of their positive electrode, sluggish electrode kinetics and/or electrode/electrolyte interface kinetics, and flammable organic solvent of electrolytes, respectively.[11–15] Furthermore, although the cyclic lifespan of commercial LiBs (electrode) is acceptable, the degradation of their electrolyte can shorten the lifespan of a whole cell and even induce potential safety hazards.[13,14] Concerning these issues, several new concepts ranging from lithium//air batteries, lithium//sulfur batteries and flow batteries (innovations on the cathodes)[16–18] to solid-state batteries, quasi-solid-state batteries and aqueous batteries (innovations in the electrolyte) have been proposed and widely researched.[19–21] Meanwhile, the capacity of the cathode is influenced by the interfacial kinetics and mass transportation between the electrolyte and cathode, where the working potential of the cathode will decrease due to interfacial polarization, thereby reducing the energy density of the whole cell.[22,23] Therefore, electrolytes are of paramount importance for the development of batteries with high energy density and good safety.

An ideal electrolyte material should possess properties such as good electronic insulation, high ionic conductivity, wide

electrochemical stability widow (ESW), thermal stability and safety, facilitate interfacial kinetics, low chemical "cross-talk" between electrodes, be produced via simple large-scale manufacturing process, inexpensive, environmentally friendly and non-toxic;[24,25] however, currently no electrolyte can meet all these criteria. The conventional electrolytes can be classified into organic liquid electrolytes, polymer electrolytes, inorganic solid-state electrolytes, ionic liquid electrolytes and aqueous electrolytes, which are semi-quantitatively compared in Fig. 1. Among them, aqueous electrolytes are impressive in terms of their ionic conductivity, environmentally benign nature and interfacial wettability.[26–33]

Exploring safe and cost-effective electrochemical energy storage systems is of great significance and importance.[34,35] Based on aqueous electrolytes, aqueous rechargeable batteries (ARBs) have move to the forefront, which are destined to avoid the potential flammability and explosion of organic liquid electrolyte-based batteries and sophisticated (atmosphere controlled) manufacturing processes.[36,37] Furthermore, due to the high permittivity and low viscosity of water, the ionic conductivity of aqueous electrolytes is considerably higher than that of organic liquid electrolytes, resulting in an excellent rate capability and power density in ARBs.[29,36] Thus, based on the above-mentioned advantages of aqueous electrolytes, ultrafast charge–discharge energy storage systems can be established on a grid-scale with ARBs.[29,38] However, there is a noticeable gap between conventional LiBs and ARBs in terms of energy density, which restricts the large-scale application and eliminates the low cost and good safety benefits of ARBs in the EV industry.[39,40]

The relatively low energy density of ARBs is basically derived from the low working voltages caused by their narrow ESWs, which is related to the oxygen evolution in high-potential and

Fig. 1 Semi-quantitative comparison of organic liquid electrolyte, polymer electrolyte, inorganic solid-state electrolyte, ionic liquid electrolyte and aqueous electrolyte.

1806 | Energy Environ. Sci., 2022, 15, 1805–1839

This journal is © The Royal Society of Chemistry 2022

hydrogen evolution in low-potential aqueous electrolytes. To some extent, the narrow ESWs of aqueous electrolytes is the Achilles' heel in improving the energy density of ARBs.[36,41] In 2013, Wu *et al.* innovatively utilized a sandwich polymer membrane and LISICON to coat an Li metal anode. Due to the "cross-over" effect of the Li ion in the coated LISICON, this ARB delivered an output voltage of about 4.0 V, a big breakthrough in the theoretically ESW of water; however, it exhibited poor cyclic stability.[42] Furthermore, the issue regarding the ESW can induce a short cyclic lifespan, thus increasing the cost to run energy storage stations based on ARBs.[43] It is noteworthy that electrode dissolution in aqueous electrolytes can hinder the long-term charge–discharge cycling due to the strong polarity of water molecules. Theoretically, mass dissolution is a thermodynamically favorable process, as determined by the Gibbs free energy, regardless of the acid/alkaline environment of the electrolyte in real situations.[44,45] Besides narrow ESWs and electrode dissolution, batteries can become unstable due to the side reactions of the electrodes with water and/or oxygen, especially in the case of aqueous rechargeable lithium-ion batteries (ARLiBs).[41] Moreover, the phase transition of water with a variation in temperature can limit the application of ARBs at elevated or subzero temperatures, thereby confining the operation temperature windows of aqueous electrolytes.[46] Hereon, the methods that can be employed to increase the energy density, expand the cyclic lifespan and extend the working temperature window of ARBs by tailoring aqueous electrolytes are summarized and discussed. Before that, the design concepts (principles) and historical development of aqueous electrolytes are briefly introduced and summarized in the following section.

2. Design concepts and historical development of aqueous electrolytes

2.1. Principles of battery electrolyte

The typical liquid electrolyte used in rechargeable batteries, fuel cells, and electrochemical capacitors is composed of a solvent, anion, and solvent-solvated cation. In the case of organic liquid electrolytes, the solid electrolyte interface (SEI) can function as a critical component to equip electrolytes with both electrochemical and thermal stability as well as excellent rate capability,[47,48] which is absent in conventional aqueous electrolytes. Thus, a reasonable design is necessary for aqueous electrolytes, enabling good stability of the electrolyte/electrode interfaces. The design of an electrolyte is based not only on whether the reactants in both sides may be solid, liquid, or gaseous (processing consideration), but also the limiting electrochemical potentials μ_A and μ_C for the anode and cathode (their Fermi energies), respectively.[49] The ESW of the electrolyte originates from the separation energy (E_g) of the lowest unoccupied molecular orbital (LUMO) and highest occupied molecular orbital (HOMO) of the electrolyte.[50] Thus, to achieve thermodynamic stability in a battery, μ_A and μ_C should be located in the ESW of the electrolyte, as exhibited in the schematic illustration of the electron energies of

the electrode and electrolyte in Fig. 2a. The open circuit potential (V_{OC}) of a battery cell can be defined as follows:[51]

$$eV_{OC} = \mu_A - \mu_C < E_g a \quad (1)$$

where e is the magnitude of the electronic charge, while for organic liquid electrolytes, the passivating SEI film offers kinetic stability to a large V_{OC} with no extra-large.[51] This is because an anode with a μ_A above the LUMO can reduce the electrolyte unless a passivation layer generates a barrier to electron transfer from the anode to the electrolyte LUMO. Similarly, a cathode with a μ_C below the HOMO will oxidize the electrolyte unless a passivation layer blocks electron transfer from the electrolyte HOMO to the cathode.[51]

Experimentally, the ESW can be determined through standard potentiodynamic approaches such as linear sweep voltammetry (LSV) and cyclic voltammetry (CV), despite the various electrochemical environments of electrolytes during actual applications.[52,53] The restricted reduction and oxidation potentials are assigned to a predefined value (reaching the decomposition current). The cutoff criteria may be arbitrary given that it lacks theoretical significance. In fact, the observed total current of the working electrode, i_T, can be expressed as the sum of two parts, as shown in the following equation:[53]

$$i_T = i_{nF} + i_F \quad (2)$$

where i_{nF} represents the nonfaradaic component (capacitive, interface double layer) and i_F represents the faradaic component (impurity reactions, redox process, and decomposition of the electrolyte at the interface).[53] Ideally, i_{nF} should be close to zero if i_T indicates the ESW of the electrolyte exactly. Thus, practically, i_{nF} should be eliminated when predefining the current level for i_T. Normally, i_{nF} and i_F can be distinguished by the slope of the LSV/CV curve. A lower slope in the LSV/CV curve is assigned to i_{nF}, appearing earlier, whereas a higher slope is assigned to i_F, appearing later.[54,55] Also, non-porous electrodes such as Pt and glassy carbon can create the circumstance of $i_{nF} \approx 0$.[53]

Conducting ions are the essential requirement of electrolytes, which affect how fast the energy stored in the electrodes can be delivered. In liquid electrolytes, the transport of ions is realized by the solvation and dissociation of ionic compounds and the migration of these solvated ions through the solvent.[56] In terms of solvation and migration, ionic conductivity can be qualified as follows:[57]

$$\sigma = \sum_i n_i \mu_i Z_i e \quad (3)$$

while for most liquid electrolytes, the conductivity results from the overall migration of both anions and cations. Also, for most batteries, only the portion of current carried by the cation is important, and thus the concept of transference number (t_{cation}) is introduced as follows:[57]

$$t_{cation} = \frac{\mu_{cation}}{\sum_i \mu_i} \quad (4)$$

This journal is © The Royal Society of Chemistry 2022

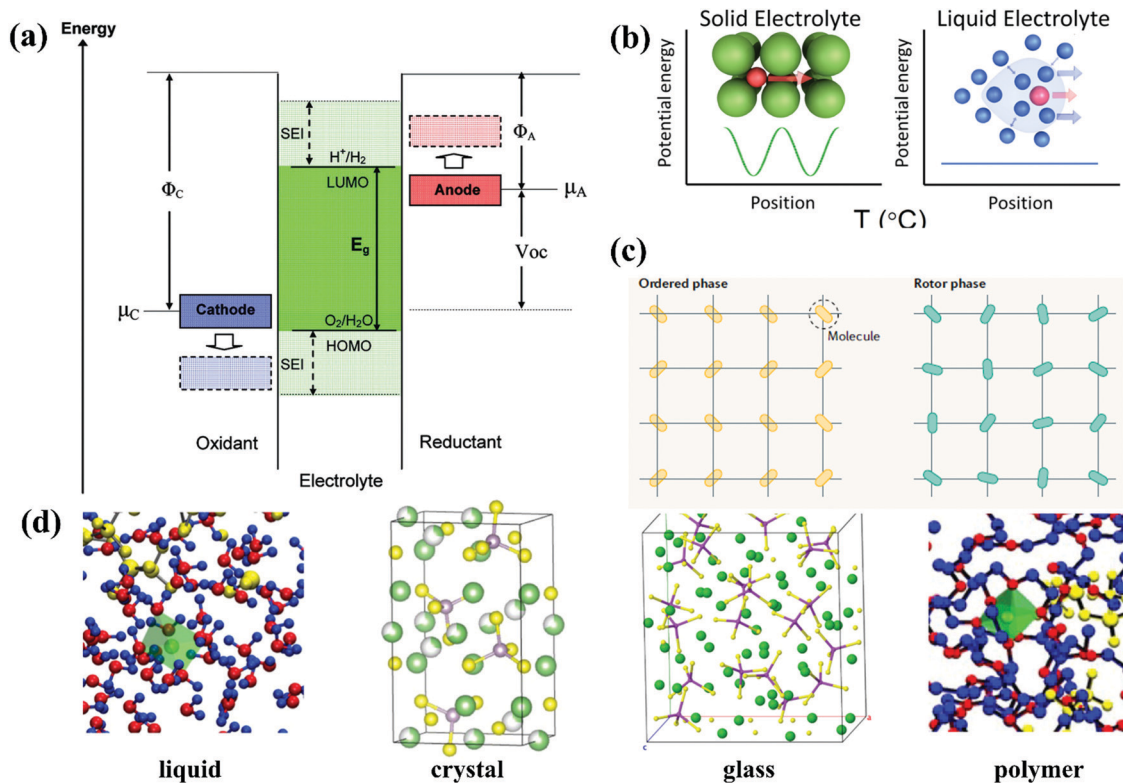*Energy Environ. Sci.*, 2022, **15**, 1805–1839 | **1807**

Fig. 2 (a) Schematic open-circuit energy diagram of an aqueous electrolyte.[51] (b) Potential energy of migration in liquid electrolytes of a charged species in red with a solvation shell of electrolyte molecules (highlighted in blue) and an interstitial mobile ion in a crystalline solid, respectively.[59] (c) Comparison of the orientations of molecules in ordered phases and rotor phases (plastic crystals).[62] (d) Solvation structure of liquid, crystal, glass and polymer examples.[63]

In diluted electrolyte, the transference number of cations is normally 0.2 to 0.4, meaning that anions are much more mobile than cations due to the solvation sheath around cations.[56] A transference number of less than 1 can remarkably induce concentration polarization during battery operation through the resultant overwhelming anion movement and enrichment near the electrode surface, which requires a relatively "naked" cation with a high cation current.[56]

Meanwhile, solvents with lower viscosity (η) can enhance the mobility of ions and ameliorate the concentration polarization according to the Stokes–Einstein relation, as follows:[57]

$$\mu_i = \frac{1}{6\pi\eta r_i} \quad (5)$$

where r_i is the solvation radius. A lower η leads to a higher μ_i, while a lower solvation degree of cation (solvation radius) leads to a higher μ_i. Besides, the dielectric constant, ε, of the solvents is also critical, which determines the charge carrier number (n_i). With a higher ε, ions have a higher probability of remaining free.[58] Therefore, in terms of ionic conductivity, an ideal solvent should demonstrate a high ε and low η, which is difficult to realize in organic solvent systems, while water can be an optimized option, thereby offering desirable ionic conductivity to high power density ARBs.

The ion conduction mechanisms between liquid and solid electrolytes are different. The potential energy profile of mobile ions in liquid electrolytes can be considered flat (Fig. 2b, right) due to the reasonably fast exchange between the solvating molecules and the solvent molecules, and the uniform surroundings. In contrast, the diffusion of mobile species in a solid-state crystalline network needs to pass through periodic bottleneck points, which define an energetic barrier that separates two local minima (typically crystallographic sites for ions) along the minimum energy pathway (Fig. 2b, left).[59] Therefore, the ion conduction mechanism in liquid electrolytes is concentration diffusion, whereas that in solid especially crystal solid electrolytes is ion hopping between the ground-state stable sites and/or intermediate metastable sites of the crystalline framework. In the crystalline case, vacancies of cations or interstitials are perceived as the mobile charged species, the migration mechanisms of which can be summarized as ion migration to a neighboring vacant site, direct interstitial mechanism between sites not fully occupied and concerted or correlated interstitially (knock-on) mechanism.[22] The ionic conductivity of a solid crystal electrolyte can be thermally activated, the process of which is described by a modified Arrhenius relationship, while the ion absolute mobility, μ, can be linked to the ion diffusion coefficient, D, through the Nernst–Einstein relationship.

In the case of polymer and glass, which are two solid electrolytes exhibiting no long-range structural order, their mechanisms vary accordingly. In polymer electrolytes, the

relationship curve between σ and $\frac{1}{T}$ is bent and is best fitted to VTF behavior (after Vogel, Tammann, and Fulcher). T_o (equilibrium glass-transition temperature) is introduced for amendment, which is related to the (kinetic) measured glass-transition temperature.[60] Glass is a promising electrolyte for use in solid-state batteries. Although the Arrhenius relationship and Nernst–Einstein relationship can still be applied to glass electrolytes, cation migration occurs *via* a mechanism that combines the concerted motion of cations with the large, quasi-permanent reorientation of anions. This effect, known as the 'paddlewheel' mechanism, is typically observed in high-temperature crystalline polymorphs. In contrast to the behavior of crystalline materials, the glass paddlewheel dynamics contribute to ion mobility at room temperature.[61] The dynamics of ion motions in these materials are often described as being strongly coupled to the structural modes, whereas intermediate degrees of coupling are observed in organic ionic plastic crystals. Owing to the relatively weak interactions between molecules, reorientational processes occur with little hindrance. The orientations of molecules in ordered phases and rotor phases are illustrated in Fig. 2c.[62] Recently, in one study, a unified framework was built for all liquid and solid (crystal, polymer and glass) electrolytes based on the concepts of solvation shell for liquids and solvation cage for solids. An LiTFSI aqueous solution, β-Li_3PS_4 at 537 K, amorphous Li_3PS_4 glass at 298 K and LiTFSI in polyethylene oxide (PEO) at 363 K were utilized as examples in that work for liquid, crystal, glass and polymer, respectively (Fig. 2d), to study the Li-ion solvation structure.[63] The ultimate goal was enabling the rational design of the solvation environment to propel the migration of the working ions in a unified framework.

Based on this design concept, numerous aqueous electrolytes have been developed and applied in various types of ARBs. In the following sections, the historic development of aqueous electrolytes is summarized in different types of ARBs, ranging from monovalent-ion batteries, multivalent-ion batteries, metal//air batteries, metal//chalcogen batteries, and hybrid batteries to redox flow batteries.

2.2. Monovalent-ion battery

Among the monovalent-ion batteries, LiBs are the most popular and practical, while sodium-ion batteries (SiBs), potassium-ion batteries (PiBs), even proton batteries (PBs) and ammonium-ion batteries (AiBs) are starting to play an important role at this stage owing to the growing concern regarding lithium resources, manipulating the development of the corresponding aqueous electrolytes.[64] In 1994, the first ARLiB was introduced by Jeff Dahn and co-workers with VO_2//$LiMn_2O_4$ chemistry in 5 M $LiNO_3$ aqueous solution, delivering an energy density of 75 W h kg^{-1}, which was regarded as a breakthrough in energy storage systems.[65] In 2009, Na_2SO_4 aqueous solutions were employed as electrolytes for realizing Na^+ reversible intercalation/deintercalation in an $NaMnO_2$ cathode,[66] which were further developed in 2010, coupling an $NaTi_2(PO_4)_3$ anode and $Na_4Mn_9O_{18}$ cathode.[67,68] Compared with lithium, sodium

offers multiple advantages ranging from its wide abundance in the Earth's crust and dramatically lower cost to even distribution worldwide, and hence has attracted a great deal of attention.[69,70] Meanwhile, K_2SO_4 aqueous solution facilitated K^+ reversible intercalation/deintercalation in the $K_{0.27}MnO_2 \cdot 0.6H_2O$ cathode in 2010.[71] Subsequently, a Prussian blue analogue (PBA), nickel hexacyanoferrate was proposed to function as a cathode for PiB with 1 M KNO_3 aqueous electrolyte. Its open-framework structure allowed the retention of 66% of the initial capacity even at a C rate of 41.7. The high power density, safety, and low-cost production method of this device make an attractive candidate for use in large-scale energy storage to support the electrical grid.[72] Proton insertion/extraction involving electrochemical energy chemistries have been reported as hybrid devices,[73] until the discovery of a pure proton rocking-chair capacitor with anthraquinone (AQ)//tetrachlorohydroquinone (TCHQ) redox couple and 0.5 M H_2SO_4 aqueous electrolyte.[74] Recently, 62 wt% (9.5 m, molality, molar salt in kg solvent) H_3PO_4 was reported as an electrolyte for a high-rate aqueous proton battery, with Mn_2O_3 as the anode and CuFe-Turnbull's blue analogue (H-TBA) as the cathode. It is noteworthy that the unit of m is different from the conventional solution concentration unit of M (molarity, molar salt in liter solution) because of the evident variation in the density of solution, and thus the volume change caused by a high salt concentration.[75–77] As a eutectic mixture electrolyte with a low melting point, the 9.5 m H_3PO_4 electrolyte enhanced the low-temperature performance of PBs even at -78 °C.[78] In 2017, the first rocking-chair ammonium-ion battery was demonstrated with an ammonium Prussian white analogue cathode, organic solid as the anode and 1.0 M $(NH_4)_2SO_4$ aqueous solution as the electrolyte. Although the average working voltage and energy density of that battery were $\sim$1.0 V and $\sim$ 43 W h kg^{-1}, respectively, this performance was still encouraging, inspiring research towards the utilization of ammonia waste.[79] Subsequently, Wu and co-workers further introduced sodium iron hexacyanoferrate and copper hexacyanoferrate cathodes in 1 M $(NH_4)_2SO_4$ (pH $\approx$ 5.4) aqueous solution to enhance the rate performance and stability of ammonium-ion batteries.[80,81]

2.3. Multivalent-ion Battery

The energy density of multivalent-ion batteries (MViBs) is theoretically higher than that of the presently commercialized LiBs due to the higher capacity induced by the multivalent ion insertion in the cathode.[82] Magnesium (Mg), aluminum (Al), calcium (Ca) and zinc (Zn) ion batteries dominate among the MViBs, while iron (Fe) and copper (Cu) ion batteries have also emerged recently.[83–85] Similar with ARLiBs, aqueous electrolytes make MViBs safe and environmentally friendly, even perform bettering than ARLiBs because of their higher energy density, and hence water in MViBs can open doors to new opportunities.[86] Among them, aqueous rechargeable zinc ion batteries (ARZiBs) can be further selected as the crown jewel due to their features of high abundance, large-scale production, nontoxicity, low redox potential (-0.76 V *vs.* standard hydrogen electrode (SHE)) and high overpotential for hydrogen evolution
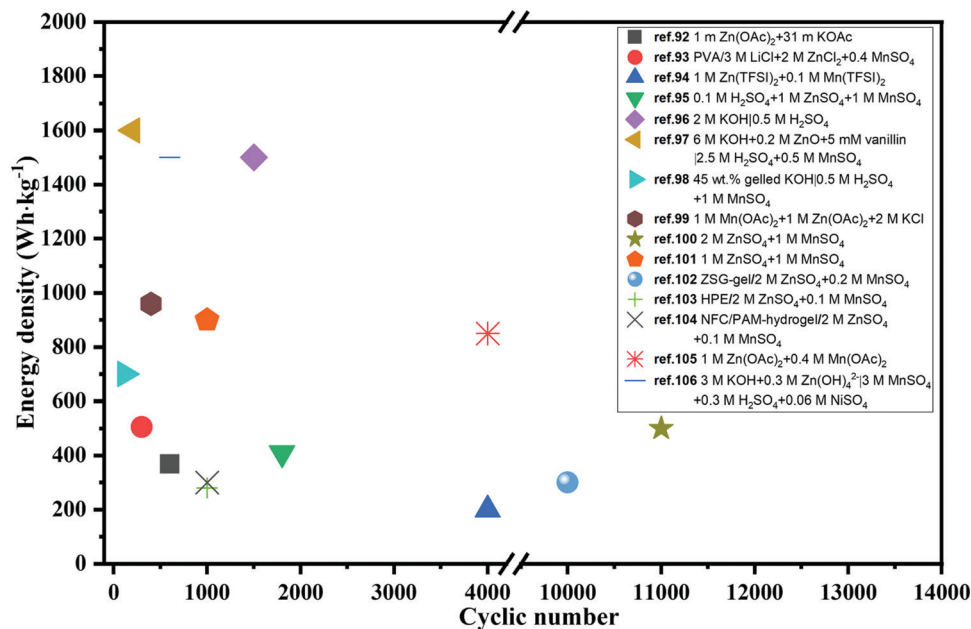
This journal is © The Royal Society of Chemistry 2022

Energy Environ. Sci., 2022, **15**, 1805–1839 | **1809**

Fig. 3 Performance comparison of recently reported Zn//MnO$_2$ batteries based on various aqueous electrolytes in terms of energy density and cyclic number.

reactions (contributing to the thermodynamic stability against aqueous electrolytes).[87,88] Alkaline Zn//MnO$_2$ batteries with KOH aqueous solution served as the primary battery since the 1960s, and efforts to make them rechargeable started in the 1990s, even expanding manganese-based cathodes to vanadium-based materials and PBA.[89–91] In the last three years, remarkable progress has been achieved in the case of ARZiBs, especially for aqueous Zn–MnO$_2$ batteries through the technical routines towards aqueous electrolytes such as hydrogel, salt-concentrated, pH-adjusting and decoupling electrolytes. Some representative works are exhibited with the employed electrolytes and compared in terms of energy density and lifespan (cyclic number) in Fig. 3,[92–106] where the energy density of various aqueous Zn//MnO$_2$ batteries is unified based on the mass of MnO$_2$, and some of them are basically estimated. There is an obvious tendency to employ aqueous Zn//MnO$_2$ batteries as high-energy storage devices, which are almost ready for further commercialization on a large scale, while their flexible and stretchable properties enabled by hydrogel electrolytes extend their applications from electric grids to daily-use, wearable electronic devices.[96,107]

Besides Zn, Al is also an abundant and cheap element, which possesses a superior volumetric capacity to that of Mg and Ca.[108] As early as around 1980, an NaCl aqueous solution was used as the electrolyte for Al-alloy//air batteries.[109] In 2012, Liu *et al.* demonstrated Al-ion insertion/extraction in anatase TiO$_2$ electrode with an AlCl$_3$ aqueous solution as the electrolyte;[110] however, it is highly acidic in nature and enhances the dissolution of the active material and corrosion of auxiliary battery parts.[108] To overcome this drawback, Al(NO$_3$)$_3$ and Al$_2$(SO$_4$)$_3$ aqueous solutions have been developed as electrolytes for aqueous rechargeable aluminum-ion batteries (ARAiBs).

However, the corresponding electrochemical activity was weakened in these electrolytes, especially for Al-ion insertion/extraction in anatase TiO$_2$ electrodes. Therefore, mesoporous nanosized electrodes have been demonstrated to improve the electrode and interfacial kinetics, and thus enhance the discharge capacity.[108] Mg is regarded another alternative to Li, but it suffers a lot from sluggish kinetics in organic liquid electrolytes. Therefore, water was introduced in a non-aqueous system to enhance the kinetics in electrolytes and cathodes, and thus the rate capability of the whole cell.[111] Since 2013, numerous works focused on aqueous Mg chemistries have been reported in half-cells (mostly using Mg(NO$_3$)$_2$ aqueous solutions as electrolytes);[112,113] however, it was only in 2017 that Chen *et al.* reported the fabrication of a full Mg-ion battery (MiB) based on 1 M MgSO$_4$ aqueous solution with a polyimide//nickel hexacyanoferrate redox couple.[114] In the same year, Wang *et al.* used a 4 m (molar salt in kg solvent) magnesium bis(trifluoromethane sulfonyl)imide (Mg(TFSI)$_2$) super-concentrated electrolyte to expand the ESW to 2.0 V, enabling poly pyromellitic dianhydride//lithium vanadium phosphate battery chemistry with a working voltage of 1.9 V.[111] Likewise, water was introduced in a Ca ion battery to improve the electrolyte and electrode/electrolyte kinetics, while a super-concentrated aqueous electrolyte (8.37 m Ca(NO$_3$)$_2$) was used with a CuHCF working electrode in a half-cell system, delivering a capacity of almost 70 mA h g^{-1}.[115] In 2017, the combination of 2.5 M Ca(NO$_3$)$_2$ aqueous electrolyte with an organic polyimide anode and CuHCF cathode as a full cell was reported, displaying 1000 cycles of charge–discharge under 400 mA g^{-1} current density with a cut-off voltage of 0.5–1.9 V.[116] Among the metal elements used as cations (charge carriers) in MViBs, Fe element is even more abundant than Zn, Mg and Ca, which has a content of ~46 500 ppm in the

1810 | *Energy Environ. Sci.*, 2022, **15**, 1805–1839

This journal is © The Royal Society of Chemistry 2022

Earth's crust.[84] Reversible Fe plating/stripping was realized in an $FeSO_4$ aqueous electrolyte with Fe-based PBAs, which exhibited an excellent cycling performance of 1000 cycles. The authors also showed that the Fe metal anode could pair with an $LiFePO_4$ cathode as a hybrid cell, displaying a discharge capacity of ~155 mA h g^{-1}.[84] In summary, ARZiBs and ARAiBs are more suitable to be industrialized than the other types of ARBs at this stage in terms of reliable performance and cost. Particularly, ARZiBs are almost ready for application in portable electronic devices and large-scale energy storage stations, especially Zn// MnO_2 batteries, as shown in Fig. 3, but their energy density needs to be further improved for EV applications.

2.4. Metal//air battery

Since the 1960s and early 1970s, considerable work has been carried out on metal//air batteries (MABs) for a variety of applications.[117] MABs are unique compared with other batteries owing to the fact that their electroactive material (oxygen) does not require storage. In this respect, this type of battery is similar to fuel cells and is essentially a fuel cell/battery hybrid, which principally simplifies the battery design and increases the energy density.[117] Therefore, MABs have attracted much attention as a possible alternative due to their extremely high energy density compared to that of other batteries, as shown in Fig. 4a.[118] The electrolytes utilized for MABs can be basically classified into aqueous electrolytes (not sensitive to moisture) and non-aqueous electrolytes (water-sensitive system with aprotic solvents). Li and Na are intrinsically suitable for non-aqueous electrolytes, while metals such as Al, Fe and Zn are appropriate for aqueous systems.[118] For the first time, a water-stable Li metal anode with water-stable lithium-conducting glass ceramics (Li super ion conductor, LISICON) and a

lithium-conducting polymer electrolyte was proposed as the anode for an Li//air battery (LAB) with LiCl aqueous electrolyte at the air electrode in 2008,[119] possessing a similar cell configuration to that shown in Fig. 4b. Although the nonaqueous electrolyte-based LABs possessed a higher energy density/power density than that of the aqueous electrolyte-based LABs, the uncertain side reactions in the oxygen electrode and aprotic solvent-insoluble Li_2O_2, which usually occur in the former, can be avoided in the latter.[120] In 2014, the application of a gel polymer/LISICON multilayer-coated Li metal anode was expanded to an Li//Br_2 battery with 1 M $LiBr_2$ as the electrolyte.[121] Based on a similar design concept, in 2013, a mixed aqueous (NaOH)/aprotic electrolyte was realized through a separator of $Na_3Zr_2Si_2PO_{12}$ (NASICON) ceramics and applied in an Na//air battery (SAB), discharging a capacity of ~600 mA h g^{-1} (energy density of ~1500 W h kg^{-1}) and outputting an areal powder density of 11 mW cm^{-2}.[122] Unlike LABs and SABs, Zn//air batteries (ZABs) naturally suit aqueous electrolytes, which mostly operate in alkaline media, such as KOH and NaOH, due to the higher activity of both the zinc electrode and air electrode since the first invention in 1878.[123] The structures of cells based on alkaline aqueous electrolytes are much simpler than that of aqueous LABs and SABs, as shown in Fig. 4c, because no protection layers are required for Zn metal anodes. For ZABs with open structures, water loss from the aqueous electrolyte is a crucial cause of performance degradation, whereas the alkalinity of these electrolytes leads to the problem of insoluble carbonate precipitation and promotes zinc-dendrite growth and hydrogen evolution, all limiting the performance of ZABs.[124] Thus, to overcome these problems through electrolytes, a molten $Li_{0.87}Na_{0.63}K_{0.50}CO_3$ eutectic electrolyte with added NaOH was prepared and employed in a ZAB, which was cycled for 110 cycles
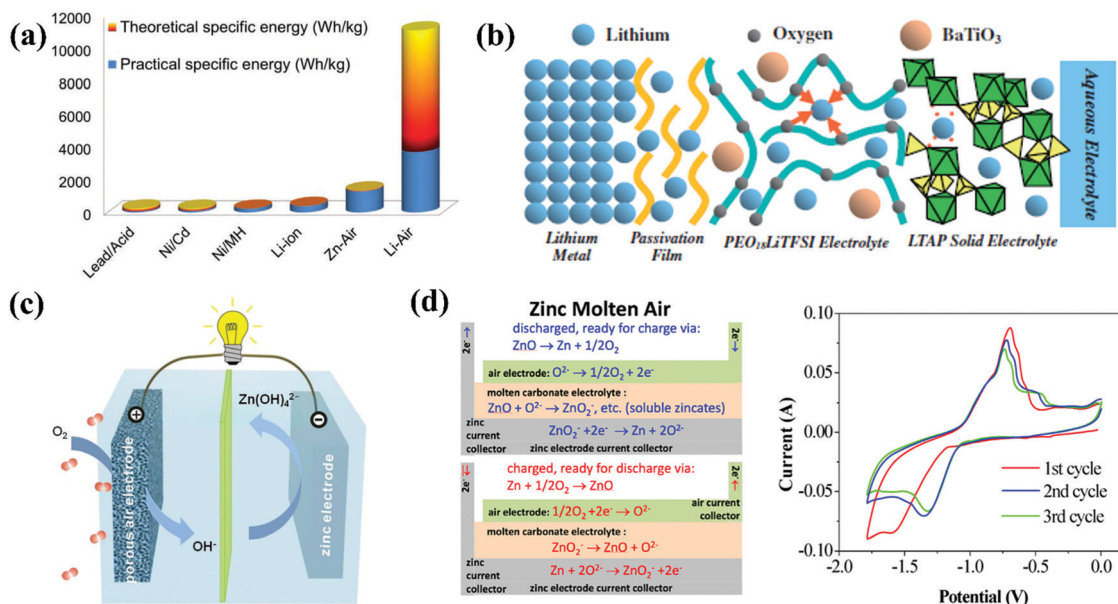

Fig. 4 (a) Theoretical and practical energy densities of various types of rechargeable batteries.[118] (b) Schematic diagram of the proposed water stable lithium metal electrode with polymer buffer layer and glass ceramic separator.[120] (c) Schematic principle of operation for Zn//air batteries.[123] (d) Schematic representation of the molten Zn//air battery and CV curve of Zn redox reaction in that electrolyte with a sweep rate of 100 mV s^{-1}.[125]

This journal is © The Royal Society of Chemistry 2022

Energy Environ. Sci., 2022, **15**, 1805–1839 | **1811**

at 550 °C, having an average charging potential of ~1.43 V and discharge potential of ~1.04 V.[125] The relevant cell configuration is shown in Fig. 4d, together with the CV curve upon Zn plating/stripping (~1.38 V *vs.* Ni/Ni(OH)$_2$ for zinc deposition and ~0.7 V *vs.* Ni/Ni(OH)$_2$ for the oxidation of Zn to Zn^{2+}).[125] Al and Fe are deemed as the first and second most abundant metallic elements in the Earth's crust. The theoretical energy density of Al//air batteries (AABs, 8140 W h kg^{-1}) is much higher than that of ZABs (1350 W h kg^{-1}), while that of Fe//air batteries (IABs) is 1200 W h kg^{-1}.[126,127] Considering this, AABs should be more promising; however, they suffer significantly from self-corrosion of the anode and sluggish kinetics, which demand a rational electrolyte with good stability and electrode/electrolyte interface process. Initially, NaCl aqueous solution was utilized as the electrolyte for AABs, but the energy density was restricted in the neutral condition, and then an alkaline system was introduced for not only AABs (KOH) but also IABs (KOH + LiOH).[117,128]

2.5. Metal//chalcogen battery

Besides MABs, metal//chalcogen batteries (MCBs) are promising alternatives because they can provide remarkable capacities, while using cheaper and more reliable electrodes of sulfur (S), selenium (Se) and tellurium (Te) than air electrodes.[129,130] MCBs possess an exceptional energy density (for instance, 2600 W h kg^{-1} for Li//S batteries, LSBs) and may be readily sealed, alleviating electrolyte leakage/loss issues, hence making them a safe option. However, this type of secondary batteries (especially for LSBs) faces the challenges of inferior electrical conductivity of their cathodes, polysulfide dissolution and their shuttling between electrodes, and considerable volume variation during charge/discharge cycles.[129] In conventional LSBs,

ether solvents were mostly used in the liquid electrolytes, which can dissolve polysulfides. Traditional carbonate-based LiB electrolytes (carbonates) and ionic liquids, which are either polysulfide incompatible or sparingly polysulfide-soluble, have been adopted in some special cases. Unfortunately, the use of these flammable liquid electrolytes raises the risk of electrolyte fire.[131] Therefore, some studies attempted to introduce aqueous electrolytes in metal–chalcogen chemistry.[132] Aqueous Al//S batteries (ASBs) were reported as early as 1993, which used KOH aqueous solution with both K$_2$S$_4$ and In(OH)$_2$ additives as the electrolyte, while the relevant working voltage was only 1.3 V; however, their cyclic performance was not demonstrated.[133] In 2019, one Fe//S battery (ISB) was reported with 0.5 M FeSO$_4$ aqueous solution as the electrolyte, although its working voltage was very low (0.6–0.8 V), its cyclic performance was improved to 200 charge/discharge cycles by changing the Fe metal anode midway, avoiding polysulfide shuttling.[134] In the case of LSBs and Na//S batteries (SSBs), analogous to LABs/SABs, protection layers (membrane electrolytes) were necessary in the metal anode side when introducing aqueous electrolytes. Li *et al.* integrated a photocatalyst in a hybrid LSB involving 0.01 M Li$_2$S$_4$ and 0.2 M LiOH aqueous electrolyte (catholyte) to store solar energy directly. At the Li anode side, an organic liquid electrolyte of 1 M LiClO$_4$ in ethylene carbonate (EC)/dimethyl carbonate (DMC) was used, coupled with an Li$_{1.35}$Ti$_{1.75}$-Al$_{0.25}$P$_{2.7}$Si$_{0.3}$O$_{12}$ (LATP) glass ceramic separator.[135] The structure of this solar energy directly stored LSB and the reaction mechanism is shown in Fig. 5a. For the Na metal anode-based LSB, 0.25 M Na$_2$S$_4$ + 0.1 M NaOH aqueous electrolyte (catholyte) was matched with 1 M NaClO$_4$ in EC: propylene carbonate (PC) + 5% fluoroethylene carbonate (FEC) organic electrolyte (anolyte) with the assistance of an NASICON membrane, as shown in Fig. 5b.[136]
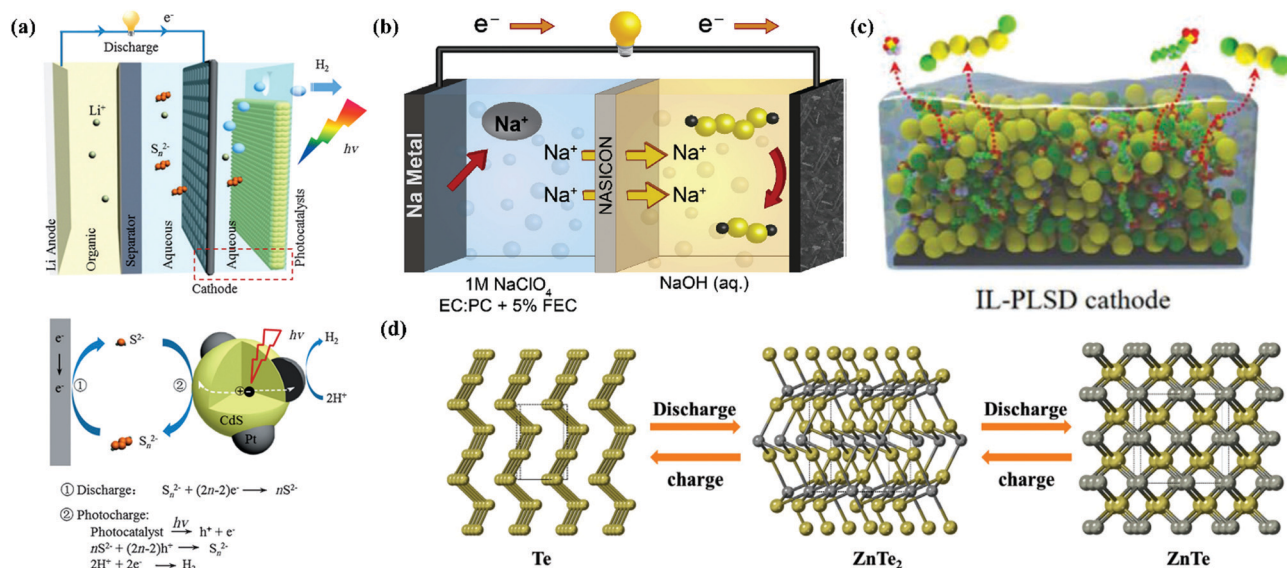

Fig. 5 (a) Battery consisting of an Li anode with organic electrolyte, Li-ion conductive LATP glass ceramic separator, and aqueous Li$_2$S$_n$ alkalic catholyte containing Pt/CdS photocatalyst and corresponding photocharging and discharging processes.[135] (b) Schematic of a sodium−aqueous polysulfide hybrid battery with a sodium−metal anode, organic anolyte, NASICON separator, and alkaline aqueous polysulfide catholyte.[136] (c) Schematic of PLSD cathodes coated with Zn^{2+}-conducting IL.[137] (d) Schematic representation of phase transformation during discharging (yellow: Te atoms and grey: Zn atoms).[139]

1812 | *Energy Environ. Sci.*, 2022, **15**, 1805–1839

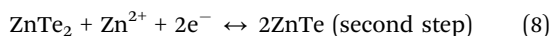This journal is © The Royal Society of Chemistry 2022

This configuration for both LSBs and SSBs not only stabilized the Li/Na metal anodes in aqueous electrolytes, but also prevented dendrite formation and polysulfide shuttling and increased the utilization of the active materials.

Zn stands out among the aqueous systems, and recently aqueous Zn//chalcogen batteries have also become eye-catching, as reported by Zhi's group. An aqueous Zn//S battery was initially realized using a "liquid film"-comprising ionic liquid encapsulated in a copolymer (working as the cathode, as shown in Fig. 5c) and 1 M $Zn(TFSI)_2$ aqueous electrolyte. This Zn//polysulfide system delivered an extraordinary capacity of 1148 mA h g^{-1} and an overwhelming energy density of 724.7 W h kg^{-1} (calculated based on the cathode mass, under a current density of 0.3 A g^{-1}).[137] The same aqueous solution (1 M $Zn(TFSI)_2$) was also used as the electrolyte of a Zn//Se battery, but its performance was undesirable. Thus, a 2 M $Zn(TFSI)_2$/polyethylene glycol (PEG)/water electrolyte was prepared, extending the ESW of the aqueous electrolyte and enhancing the performance of the Zn//Se battery.[138] The overall reaction mechanism of this battery was also studied, as follows:[138]

$$Zn + Se \leftrightarrow ZnSe \quad (6)$$

which was same conversion reaction mechanism in both the organic electrolyte and aqueous electrolyte. Meanwhile, an aqueous Zn//Te battery was also reported by Zhi's group, utilizing a 1 M $ZnSO_4$ polyamide (PAM) hydrogel as the electrolyte, which displayed an ultra-flat discharge plateau and high volumetric capacity (2619 mA h cm^{-3} under 0.05 A g^{-1} current density).[139] This battery exhibited obvious flat discharge plateaus at about 0.59 and 0.48 V, originating from the reduction of Te. Furthermore, this was proved to be a two-step solid-to-solid conversion with the successive formation of $ZnTe_2$ and ZnTe, obeying the following two equations:[139]

$$2Te + Zn^{2+} + 2e^- \leftrightarrow ZnTe_2 \text{ (first step)} \quad (7)$$

$$ZnTe_2 + Zn^{2+} + 2e^- \leftrightarrow 2ZnTe \text{ (second step)} \quad (8)$$

as demonstrated in Fig. 5d. This work presented a new direction to design conversion-type aqueous MCBs with high capacity, stable output potential, excellent rate capability and long cyclic performance.
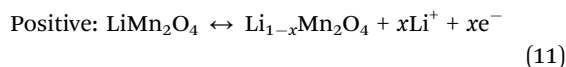
2.6. Hybrid battery

Aqueous hybrid batteries (AHBs) are new members of the ARB family, attracting great interest from researchers, which can be classified into hybrid ion batteries (HiBs), dual ion batteries (DiBs) and capacitor batteries (CBs). Besides CBs integrating battery behaviour in one side and capacitor behaviour in the other side, the mechanism of HiBs and DiBs is similar to that of single-ion ARBs, while their electrolytes are composed of various electrochemically active ions, diffusing from the electrolyte to electrodes simultaneously (for DiBs) or individually (for HiBs).[140] Compared with the ARBs of single ions, AHBs exhibit several significant benefits, which can be summarized as follows: (1) enhanced rate performance by combining the

ions of sluggish diffusion with that exhibiting better kinetics; (2) superior coulombic efficiency (CE) by avoiding ion trapping; (3) high flexibility and adaptability (more options for electrode materials); (4) low cost due to the less occupancy of Li/other costly elements in the whole cell; and (5) wide applications (energy storage and lithium purification).[141] HiBs are the most popular among AHBs, which can be further divided into monovalent/monovalent ion batteries and monovalent/multivalent ion batteries.[140] In 2013, Xia's group initially reported two monovalent/monovalent systems ($Na_{0.22}MnO_2$//$LiMn_2O_4$ and TiP_2O_7/$Na_{0.44}MnO_2$) based on Li_2SO_4 + Na_2SO_4 mixed electrolytes, exhibiting a specific energy of 17 W h kg^{-1} and 25 W h kg^{-1} based on the total weight of the active electrode materials, respectively.[142] In 2018, a low-cost aqueous Mg–Na battery was proposed as a monovalent/multivalent system, employing Mn_3O_4 as the cathode of MiB, $NaTi_2(PO_4)_3$ as the anode of SiB and 2 M $MgSO_4$ + 1 M Na_2SO_4 aqueous solution as the electrolyte, which avoided the cathode problems of SiBs and anode problems of MiBs.[143] A Pb//$LiMn_2O_4$ battery was reported in 0.5 M Li_2SO_4 aqueous solution as a monovalent/multivalent system, which realized the reversible dissolution/deposition of Pb $\leftrightarrow$ $PbSO_4$ in a neutral environment.[144] Furthermore, an Mg//$LiFePO_4$ battery was developed in a hybrid electrolyte comprised of a non-aqueous electrolyte (1 M PhMgBr and 0.1 M LiBr in tetrahydrofuran) against an Mg anode and aqueous electrolyte (0.5 M H_2SO_4) against an $LiFePO_4$ cathode, while LISICON was utilized as the separator to stabilize both the non-aqueous and aqueous electrolytes.[145] In the case of monovalent/multivalent systems, Zn metal anode-based HiBs have been reported intensively,[140] especially that in mild aqueous electrolytes, which can overcome poor cyclic performances and the formation of Zn dendrites in alkaline conditions, as shown by the following equation:

$$Zn + 4OH^- \leftrightarrow Zn(OH)_4^{2-} + 2e^- \leftrightarrow ZnO + 2OH^- + H_2O + 2e^-$$
$$(9)$$

In 2012, Chen et al. proposed Zn metal anode-based HiBs for the first time, which employed $LiMn_2O_4$ as the cathode and 3 M LiCl + 4 M $ZnCl_2$ solution (pH = 4) as electrolyte.[146] Afterwards, aqueous Zn–$LiMn_2O_4$ batteries were investigated frequently, while the relevant reaction mechanism was determined as follows:

$$\text{Negative: } Zn^{2+} + 2e^- \leftrightarrow Zn \quad (10)$$

$$\text{Positive: } LiMn_2O_4 \leftrightarrow Li_{1-x}Mn_2O_4 + xLi^+ + xe^-$$
$$(11)$$

In 2018, Wang's group made a breakthrough in aqueous Zn//$LiMn_2O_4$ batteries via the use of 1 m $Zn(TFSI)_2$ + 20 m LiTFSI highly concentrated electrolyte, which was cycled for 4000 cycles under a rate of 4C. In their work, a symmetrical Zn cell based on the highly concentrated electrolyte was cycled for 500 cycles ($\sim$170 h) under a current density of 0.2 mA cm^{-2} without any dendrite and ZnO observed.[147] The Zn-based monovalent/multivalent system was extended by Wu's group from Zn//$LiMn_2O_4$ to the Zn//$Na_{0.95}MnO_2$ redox couple with 0.5 M $Zn(OAc)_2$ + 0.5 M

This journal is © The Royal Society of Chemistry 2022

Energy Environ. Sci., 2022, **15**, 1805–1839 | **1813**

NaOAc electrolyte, which was charged/discharged for 1000 cycles under a rate of 4C in the voltage range of 1–2 V.[148] Meanwhile, Wu's group made a noticeable contribution to rechargeable Zn-based HiBs in an alkaline environment, reporting the fabrication of $Zn//Co_3O_4$ and $Zn//NiO$ batteries in 1 M KOH + 10 mM $Zn(OAc)_2$ electrolyte with $[Zn(OH)_4^-]^{2-}$ and OH^- as the charge carriers.[149,150] These works achieved a balance between high energy and high stability in alkaline battery systems.

The ions in HiBs participating in the electrode reaction are only cations, while both cations and anions are involved in DiBs, which need to be considered as active species. The typical cathodes of DiBs are graphitic carbons, metal organic frameworks (MOFs), organic cathodes or electroactive polymers and MXenes, among which graphitic carbon cathodes are the most suitable candidates for practical applications due to their unique layered structure, environmentally friendly nature, and low cost.[151,152] An aqueous DiB using 1 M $(NH_4)_2SO_4$ aqueous solution as the electrolyte was reported by Zhang et al. in 2019, in which the n-type polyimide anode reacted with NH_4^+, while the p-type radical polymer reacted with SO_4^{2-} to obtain a large cell voltage of 1.9 V.[134] Alternatively, Ji's group made contributions to aqueous DiBs by using concentrated $ZnCl_2$ aqueous solutions (30 m) with the $ZnCl_4^{2-}$-insertion molecular solid of ferrocene as the anode and Zn^{2+}-insertion PBA as the cathode. This electrolyte not only minimized the dissolution of the ferrocene anode, but also widened the voltage of the full cell by 0.35 V compared with dilute $ZnCl_2$ electrolyte.[153] Both cations and anions contribute to the capacity in CBs, which is similar to that in DiBs, while the cations are involved in the redox-active oxide cathode and anions are absorbed/desorbed by an inert activated carbon (AC) anode in CBs. Therefore CBs is one type of relatively new device that is intermediate in energy between batteries and supercapacitors, whilst principally offering supercapacitor-like power and cyclability values.[154] The high ionic conductivity of aqueous electrolytes can induce a high electrical double layer (EDL) capacitance in the active carbon anode/electrolyte interfaces, and hence can be a good option for CBs.[29] An Li_2SO_4 aqueous solution was assembled with an $LiMn_2O_4$ cathode and AC anode as an Li^+ ion capacitor by Wang and Xia in 2005,[155] and before that, an $Ni(OH)_2$ cathode was demonstrated as a good cathode for aqueous systems with an AC anode in alkaline aqueous electrolyte (KOH).[156] Brousse et al. prepared an Na^+ ion capacitor based on an Na_2SO_4 aqueous solution with AC anode, while MnO_2 was utilized as a cathode for Na ion intercalation/deintercalation in the bulk according to the following equation:[157]

$$MnO_2 + Na^+ + e^- = MnOONa \quad (12)$$

while the surface redox could be enhanced once the cathode was nanosized as follows:

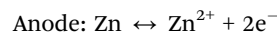$$(MnO_2)_{surface} + Na^+ + e^- = (MnOONa)_{surface} \quad (13)$$

Recently, a Zn-ion capacitor was innovatively proposed by Kang et al., in which AC, Zn metal and $ZnSO_4$ aqueous solution

served as the cathode, anode and electrolyte, respectively. A metric of 121 mA h g⁻¹ capacity (84 W h kg⁻¹ energy density), 14.9 kW kg⁻¹ power output and excellent cycling stability (over 10 000 cycles with 91% capacity retention) was exhibited.[158] Numerous works towards Zn ion capacitors have been reported since then, indicating another feasible route to perfect electrochemical energy storage systems.

2.7. Redox flow battery

Redox flow batteries (RFBs) are novel electrochemical energy storage devices, storing electrical energy in two redox-active matters with distinct redox potentials. The redox species are usually dissolved or suspended in the electrolyte tanks (negolyte and posolyte, as shown in in Fig. 6a). Electrochemical charge-transfer reactions occur on the electrode stack, consisting of a pair of porous electrodes separated by an ion-conducting membrane. The capacity of the RFB depends on the available charges stored in the electrolyte tank, whilst the current output of the RFB is determined by the rate of the electrochemical reaction on the electrode stack. This unique configuration enables design flexibility in decoupling energy and power, which is critical for large-scale energy storage and energy distribution.[159] Aqueous redox flow batteries (ARFBs) are one of the most important candidates for large-scale energy storage, which can be applied over a wide power range with long lifetimes over a flexible discharge duration. Moreover, the natural scalability induced by their unique design of decoupled power and energy is considered the most prominent advantage. Since the first ARFB was invented by NASA in the 1970s with Fe(III)/Fe(II) and Cr(III)/Cr(II) as the active species and $FeCl_2$- and $CrCl_3$-containing HCl solution as the electrolyte, a vast number of ARFBs have been invented, which are classified as vanadium (V)-, Zn-, Fe-, polysulfide (PS)-based (inorganic) and organic-based ARFBs.[160] In 1985, a V(III)/V(II) redox couple was introduced as the first V-based ARFB with VCl_3-dissolved HCl/H_2SO_4 solution as the electrolyte, but there was considerable room for ameliorating the reversibility of the redox reactions.[161] Furthermore, V-based ARFBs face the challenges of low thermal stability, crossover of V-species, and limited kinetics, which are basically correlated with the electrolyte issues, where porous nanofiltration-enhanced Nafion membranes (perfluorinated cation exchange membranes), as shown in Fig. 6b, can be the effective solutions.[162,163] Besides V-based ARFBs, Zn-based ARFBs are widely reported due to the high adaptability of Zn metal anodes towards aqueous systems, and $Zn//Br_2$ systems were the first to be reported among Zn-based species, in which KCl/NH_4Cl-containing $ZnBr_2$ concentrated solutions served as the electrolytes.[164] However, Br_2 is considered a hazardous substrate and the corresponding redox potential exceeds the ESW of water. Hence, Li et al. introduced $Zn//I_2$ species with a battery structure scheme, as shown in Fig. 6c, consisting of a Nafion membrane and ZnI_2 solution as the electrolyte. The redox mechanism was revealed as follows:[165]
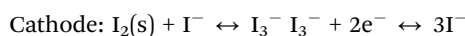
Anode: $Zn \leftrightarrow Zn^{2+} + 2e^-$

$$E^0 = -0.7626 \text{ V } vs. \text{ SHE} \quad (14)$$

1814 | *Energy Environ. Sci.*, 2022, **15**, 1805–1839

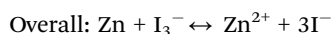This journal is © The Royal Society of Chemistry 2022

Fig. 6 (a) Schematic representation of a general RFB cell. The solid and dashed curly arrows represent the charging and discharging process, respectively. N/N′, negolyte in oxidized/reduced state; P/P′, posolyte in oxidized/reduced state.[159] (b) Two views of an inverted-micelle cylinder and schematic diagram of the approximately hexagonal packing of several inverted-micelle cylinders.[163] (c) Schematic representation of the proposed Zn//I$_2$ system.[165] (d) CV curves of 0.085 M ZnI$_2$ on a glassy carbon electrode at the scan rate of 50 mV s^{-1}.[165] (e) Schematic illustration of the proposed aqueous polysulfide/iodide redox flow batteries.[190] (f) CV curves of 5 mM K$_2$S$_2$−0.5 M KCl solution (blue) and 5 mM KI−0.5 M KCl solution (red) at 5 mV s^{-1} on a gold electrode.[190]

Cathode: $I_2(s) + I^- \leftrightarrow I_3^-$ $I_3^- + 2e^- \leftrightarrow 3I^-$

$$E^0 = 0.5360 \text{ V } vs. \text{ SHE} \tag{15}$$

Overall: $Zn + I_3^- \leftrightarrow Zn^{2+} + 3I^-$

$$E = 1.2986 \text{ V} \tag{16}$$

with the relevant CV curve shown in Fig. 6d. In this case, ZnI$_2$ electrolytes with various concentrations were investigated, and

the concentration of 3.5 M was selected for further cyclic performance tests due to the optimum CE, energy efficiency (EE) and voltage efficiency (VE) dependent on that condition, whereas ethanol was further added for expanding the stable electrolyte temperature window from −20 °C to 50 °C.[165] Similar to Zn-based ARFBs, Fe-based ARFBs have been widely studied and applied. As mentioned above, the initially studied ARFB was an Fe-based battery with Fe^{3+}/Fe^{2+} and Cr^{3+}/Cr^{2+} as the active species and HCl solution as the electrolyte, which was

This journal is © The Royal Society of Chemistry 2022

Energy Environ. Sci., 2022, **15**, 1805–1839 | **1815**

limited by the sluggish reaction kinetics of Cr^{3+}/Cr^{2+}, parasitic hydrogen evolution reaction (HER), and the crossover of active materials. Thus, management of the electrolyte pH was chosen as an effective strategy to mitigate these challenges,[160] which will be discussed in detail in the next section. The first PS-based ARFB was invented by Regenesys Ltd in 1991 with NaBr on the positive side and Na_2S_4 on the negative side as the electrolyte,[166] extending the utilization of PS from MCBs to ARFBs. Analogous to Zn-based ARFBs, the Br^-/Br_3^- chemistry was replaced by I^-/I_3^- in the PS system, demonstrating higher solubility, faster kinetics and a lower vapour pressure.[167] This cell was comprised of KI and K_2S_2 + KOH aqueous solution and Nafion 115/117 membranes with the cell structure shown in Fig. 6e and CV curves of the redox species shown in Fig. 6f. Compared with inorganic-based ARFBs, organic-based ARFBs demonstrate large Earth abundance and high tunability through functionalization. In 2009, Xu et al. innovatively reported the concept of organic-based ARFBs by adopting 1,2-dihydrobenzoquinone-3,5-disulfonic acid (BQDS) or 1,4-dihydrobenzoquinone-2-sulfonic acid (BQS) as the cathode and conventional $PbSO_4$ in iron-containing aqueous H_2SO_4 solution as the anolyte, which delivered an average CE of 99% and EE of 70% over 100 cycles. The obtained high performance indicated that soluble quinones are promising positive materials for ARFBs.[168] Recently, reversible ketone hydrogenation and dehydrogenation were realized in an organic-based ARFB using a design based on the molecular structure of 9-fluorenone (FL) as an example. An ARFB consisting of a ferro/ferricyanide catholyte and 1.36 M 4-carboxylic-7-sulfonate fluorenol (4C7SFL)/1 equiv. NaOH anolyte (equivalent to 2.72 M electron transfer) was subjected to current density testing and extended cycling, which delivered 1000 charge–discharge cycles at 25 °C (75% capacity retention) and 780 cycles (70% capacity retention) at 50 °C.[169]

Overall, the historical development of aqueous electrolytes for ARBs in various species was briefly introduced with the timelines of representatively innovative works summarized in Fig. 7. The flourishing of aqueous electrolytes facilitated the all-around development of ARBs, while their challenges of low energy density, poor cyclic stability and narrow working temperature window were exposed during practice. From the perspective of electrolytes, the narrow ESWs, electrode dissolution/side reactions, and phase transition/instability of water at different working temperatures can account for the issues associated with ARBs. Therefore, it is critical to develop more mature aqueous electrolytes via new concepts.

3. New concepts for better aqueous electrolyte

Electrolytes in battery systems have been tailored to the specific chemistry and structure of the electrodes and reactions present in the cell.[48] Although the requirements vary with the electrodes, there are still some common demands towards electrolytes such as wide ESW, high ionic conductivity, desirable thermal stability and wide working temperature range, while negligible electrode dissolution/side reactions in the case of aqueous electrolytes.[170] In 2013, Wu et al. published a pioneering work on ARBs with an exceptionally high working voltage above 3 V, which inspired intensive and extensive research towards better aqueous electrolytes, and consequently better ARBs.[42] The recently developed concepts for better aqueous electrolytes can be categorized into electrolyte additive, salt-concentrated electrolyte, gelled electrolyte, solvent-hybrid electrolyte, electrode/current collector-electrolyte interface tuning, and beyond salt-concentrated electrolyte, which have formed a dense network with different working mechanisms and different specific routes (as shown in Fig. 8). The concepts presented in this review are the common strategies for liquid-phase electrolytes, except pH management (including two-pH decoupling electrolyte), which is a unique strategy for aqueous electrolytes.

3.1. Electrolyte additive

For conventional LiBs, the use of electrolyte additives is one of the most economic ways to improve their performance. Usually, the amount of additive in the electrolyte is no more than 5% either by weight or by volume, but it significantly improves the reversibility and cyclic life of LiBs.[171] The strategy of electrolyte additives is also appropriate for ARBs, which was intensively reported in ARZiBs in the last five years. The additives added to aqueous electrolytes can be classified as ion, metal, organic and inorganic, offering the function of enhancing ion transportation, manipulating ESWs, and tuning electrode surfaces/interfaces.[172]

3.1.1. Suppressing OER on electrode surface.
In a typical study on widening the ESWs of aqueous electrolytes, sodium dodecyl sulfate (SDS) was adding to 1 M Na_2SO_4 + 1 M $ZnSO_4$ aqueous electrolyte, which equipped the HiB of $Zn//Na_2Mn-Fe(CN)_6$ with a 2.0 V operation voltage and capacity retention of 75% over 2000 cycles. In this study, the surfactant additive could effectively suppress the oxygen evolution reaction (OER), and thus extended the ESW to 2.5 V, which was attributed to the SDS adsorption layer and theoretically confirmed by density functional theory (DFT) calculation, as shown in Fig. 9a–f.[173] Beside SDS, Mn ion additive was proven to suppress the OER and broaden the ESW through the competition mechanism of the dissolution/deposition reaction of MnO_2/Mn^{2+} and the OER in the solvent.[95]

3.1.2. Inhibiting corrosion and dendrite formation in Zn metal anode.
The above-introduced two additives expanded the ESWs by suppressing the OER, while additives such as $PbSO_4$, diethyl ether (Et_2O) and sodium dodecyl benzene sulfonate (SDBS) were used for inhibiting corrosion and suppressing the formation of dendrites in the Zn metal anode, thus enhancing the cyclability. $PbSO_4$ was added to 1 M Li_2SO_4 + 2 M $ZnSO_4$ electrolyte gelled by 5% fumed silica until saturation, which provided a 20% lower corrosion current density on the Zn anode. The Zn metal anode in the tested $Zn//LiMn_2O_4$ HiB with $PbSO_4$-containing electrolyte was determined to possess a dendrite-free morphology through scanning electron microscopy (SEM).[174] In the $Zn//MnO_2$ system, 2 vol% Et_2O was added to 3 M $Zn(CF_3SO_3)_2$ + 0.1 M $Mn(CF_3SO_3)_2$ electrolyte,

1816 | Energy Environ. Sci., 2022, 15, 1805–1839

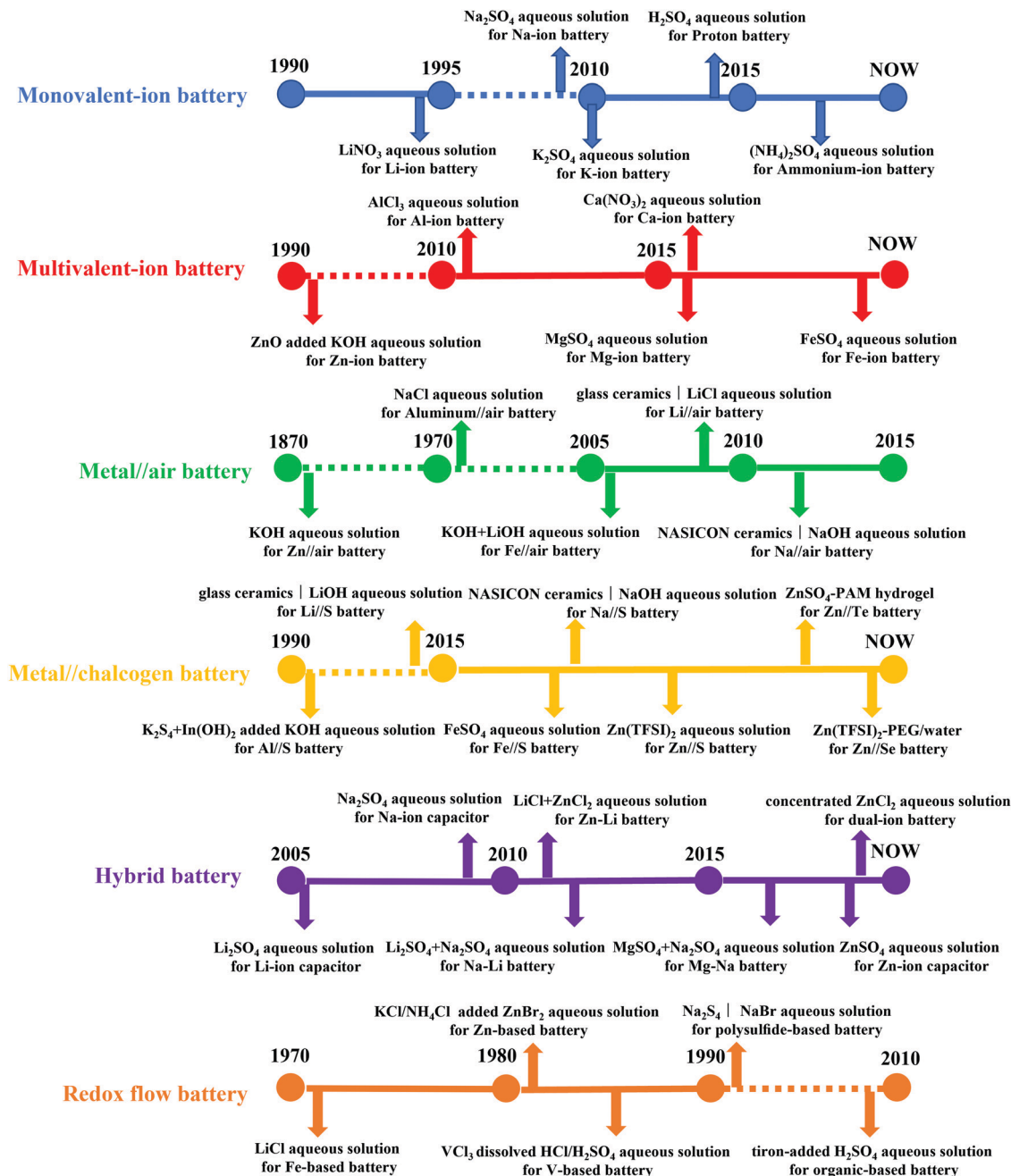This journal is © The Royal Society of Chemistry 2022

Fig. 7 Historical development of aqueous electrolytes with representative innovative works for various ARBs.

which was believed to be absorbed near the tip of the metal anode substrate surface, inducing an electrostatic shield and suppressing dendrite formation by maintaining a smooth deposition layer, as shown in Fig. 9g.[175] SDBS was reported to improve the electrochemical behaviors of a Zn//LiFePO$_4$ HiB. With the assistance of this additive, Zn ions were deposited smoothly on the surface of the Zn metal instead of participating in the vertical growth of flake-shaped Zn dendrites. Simultaneously, the Li-ion diffusion coefficient was increased from 1.78×10^{-11} to 8.22×10^{-11} cm^2 s^{-1} by ameliorating the wettability of the LiFePO$_4$ cathode, contributing to the high power density of the whole cell.[176]

3.1.3. Interfacial engineering. In LiBs, additives are used intensively for engineering interfaces, especially engineering SEIs, which are also employed to tailor the interfaces of ARBs. Recently, Wang's and Xu's group reported the use of trimethyl-ethyl ammonium trifluoromethanesulfonate (Me$_3$EtNOTF) as an additive in the fluorinated interface between a Zn metal anode and aqueous zinc trifluoromethanesulfonate (Zn(OTF)$_2$) electrolyte, which enabled the stable cycling of both a Zn//VOPO$_4$ full cell (136 W h kg^{-1} and retained 88.7% of its capacity for >6000 cycles) and Zn//O$_2$ cell (325 W h kg^{-1} for >300 cycles). The ZnF$_2$-rich composition in that interface was caused by the additive, while ZnCO$_3$, ZnSO$_3$ and poly-species

This journal is © The Royal Society of Chemistry 2022

Energy Environ. Sci., 2022, **15**, 1805–1839 | **1817**
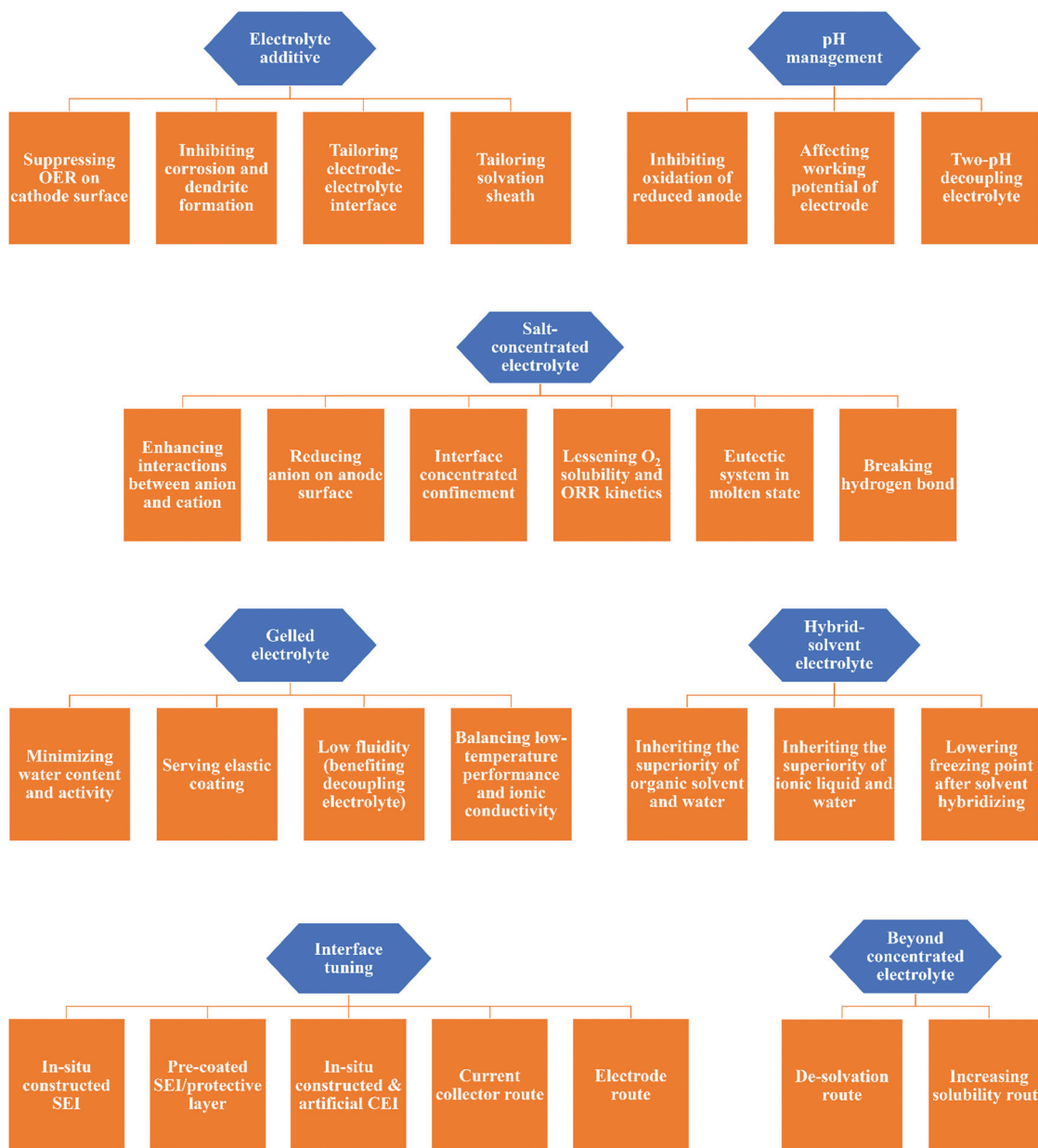
Fig. 8   Summary of specific working mechanisms and implementation paths of various strategies for mitigating aqueous electrolyte challenges.

were also discovered there (Fig. 9h). DFT calculation suggested that the downstream reactions resulting from alkylammonium decomposition were responsible for the formation of $ZnCO_3$.[177] In another work, ZnF_2 was added to 2 M $ZnSO_4$ electrolyte directly for the formation of a stable F-rich interfacial layer. The F-rich interfacial layer could not only regulate the growth orientation of zinc crystals, but also serve as an inert protection layer against side reactions such as the HER. Under the protection of that interfacial layer, Zn stripping/plating was stably repeated for 600 h, and an anode-free Zn//LiMn$_2$O$_4$ HiB was realized.[178] Besides the interfaces between the Zn metal anode and aqueous electrolytes, the additive can also function on the cathode. In 2016, Wang's group constructed a cathode electrolyte interphase (CEI) between an LiCoO$_2$ cathode and

LiTFSI aqueous electrolyte through the electrochemical oxidation of tris(trimethylsilyl) borate. The LiCoO$_2$ cathode was stabilized at a high cut-off voltage corresponding to 0.7 e^- electron charge transfer, which delivered a working voltage of 2.5 V and 120 W h kg^{-1} energy density.[179]

3.1.4. Solvation sheath tailoring. To widen the working temperature windows of ARBs, some efforts focused on tailoring their solvation sheath, which adjusted the correlated ARBs to the frozen environments. Dimethyl sulfoxide (DMSO), a highly polar aprotic solvent, can form strong H-bonds with water molecules and significantly change the original H-bond structure of water molecules.[180] According to previous studies, the HER of water molecules is a competitive process with the H-bond formation process in solution,[181] and hence DMSO is
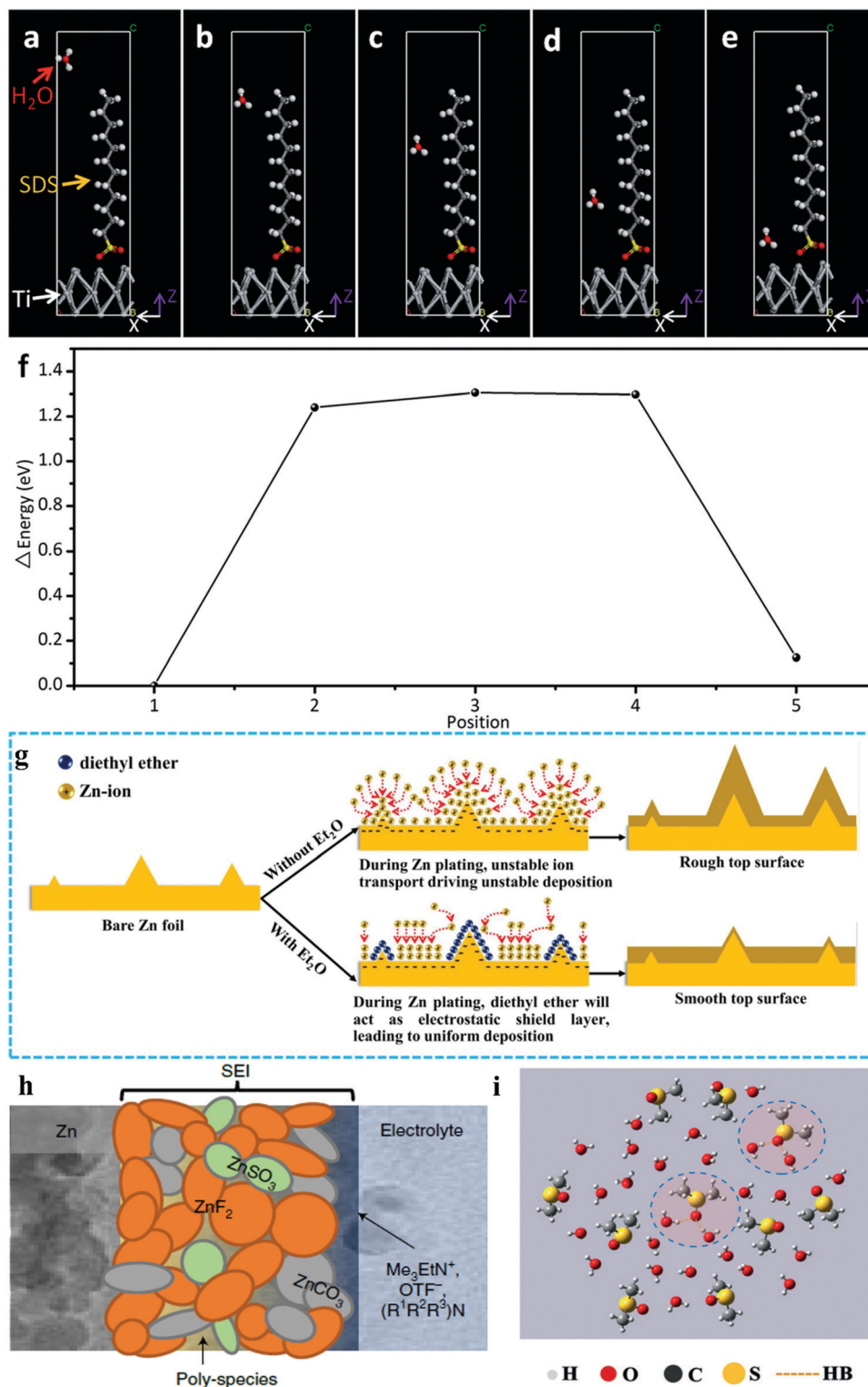
Fig. 9 (a−e) Models of density functional theory calculations, showing a water molecule passing through the SDS adsorption interlayer at different positions.[173] (f) Energy change tendency at different positions.[173] (g) Schematic of the morphology evolution of Zn anodes in mild aqueous electrolyte with and without Et$_2$O additive during Zn stripping/plating.[175] (h) Cartoon of proposed Zn^{2+}-conducting SEI, characterized by small nodular particles embedded in a polymeric framework.[177] (i) Local structure of the χ_{DMSO} = 0.3 system from MD simulations.[46]

an effective additive to suppress the HER. Thus, DMSO was added to an aqueous solution of 2 M NaClO$_4$ with a molar fraction of 0.3 (2M-0.3 electrolyte). The 2M-0.3 electrolyte exhibited a sufficient ionic conductivity of 0.11 mS cm^{-1} at

This journal is © The Royal Society of Chemistry 2022

Energy Environ. Sci., 2022, **15**, 1805–1839 | **1819**

−50 °C. The Raman and Fourier transform infrared (FTIR) spectra proved that hydrogen bonds were stably formed between DMSO and water molecules, facilitating the operation of the electrolyte at ultra-low temperatures, while molecular dynamics (MD) modelling, as shown in Fig. 9i, demonstrated consistent results.[46] In ARFB systems, additives are also employed to widen their working temperature windows. For example, 10 vol% ethanol served as an additive in a near-neutral 5 M ZnI_2 electrolyte of Zn//I_2 ARFB, enabling a stable battery performance in the temperature range of −20 to 50 °C. Nuclear magnetic resonance (NMR) study and DFT-based simulation together with flow test data illustrated that the addition of ethanol induced ligand formation between the oxygen on the hydroxyl group and the zinc ions, which not only extended the stable electrolyte temperature window but ameliorated the interface of the zinc metal anode.[165] In the PB system, anions such as BF_4^- and SO_4^- were discovered to enhance the adaptability of relevant aqueous electrolytes towards frozen conditions. In one work on a PB, FTIR, Raman and NMR analyses synergistically demonstrated that the introduction of BF_4^- anions efficiently broke the hydrogen-bond networks of the original water molecules, resulting in an ultralow freezing point. Therefore, the alloxazine//MnO_2 redox couple could run regularly even at −90 °C and displayed a high specific discharge capacity of 85 mA h g^{-1}.[182] Similarly, the hydrogen bonds between water molecules in the electrolyte could be remarkably damaged by modulating the interaction between SO_4^{2-} and water molecules, lowering the freezing point of the electrolyte. Consequently, the *p*-chloranil-reduced graphene oxide redox couple of the proton insertion mechanism delivered an extraordinary electrochemical performance even at −70 °C.[183] Basically, the electrolyte additive strategy can be a feasible route to improve the stability and widen working temperature windows of ARBs. The performance of representative works is summarized in Table S1 (ESI†). However, some additives probably fail to become a universal way to achieve better main aqueous electrolytes. Furthermore, electrolyte additives only function as minor modification to some cases rather than a fundamental transformation, while solvents and salts have a greater effect on aqueous electrolytes.

## 3.2. pH management and two-pH decoupling electrolyte

In aqueous electrolytes, the pH value can have a considerable impact on the ESW by thermodynamically affecting the HER and OER. Furthermore, the pH and H_2O in aqueous electrolytes with or without O_2 can influence the stability and working potential of the electrodes in ARLiBs, as follows:[41]

$$Li(intercalated) + \frac{1}{4}O_2 + \frac{1}{2}H_2O \leftrightarrow Li^+ + OH^- \quad (17)$$
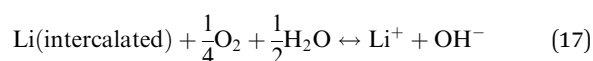
Based on the chemical potential of intercalated Li in the electrode ($\mu_{LI}^{int}(x)$) and Li in Li metal (μ_{LI}^0), the working potential of the electrode ($V(x)$) can be derived as follows:[184]

$$V(x) = 4.268 - 0.059 \text{ pH (V)} \quad (18)$$

where x for both $\mu_{LI}^{int}(x)$ and $V(x)$ is the amount of intercalated Li in the lithium-ion intercalated compounds. According to eqn (18), $V(x)$ in equilibrium condition is determined to be 3.85 V at pH 7 and 3.50 V *vs.* Li/Li$^+$ at pH 13, indicating that the reduction state of all usual anode materials in ARLiBs would theoretically be chemically oxidized by O_2 and H_2O rather than undergoing the electrochemical redox process. However, after eliminating O_2 in aqueous electrolytes, the reaction becomes:[185]

$$Li(intercalated) + H_2O \leftrightarrow Li^+ + OH^- + \frac{1}{2}H_2 \quad (19)$$
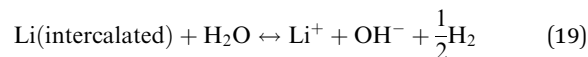
and the correlated $V(x)$ can be further determined as:[41]

$$V(x) = 3.039 - 0.059 \text{ pH(V)} \quad (20)$$

revealing that H_2O can also chemically oxidize some reduction-state anodes in ARLiBs.

3.2.1. pH management for higher stability. Theoretically, the pH value of aqueous electrolytes can serve as a benchmark to determine whether the electrodes are stable against the corresponding aqueous electrolytes. Practically, pH adjusting can be another route to manipulate the stability of ARBs.[41] Base on this idea, Cui's group used 1 M KH_2PO_4 (pH = 1) solution as an electrolyte for a PiB with a copper hexacyanoferrate cathode and AC/polypyrrole hybrid anode, which had zero-capacity loss after 1000 deep-discharge cycles.[38] Xie *et al.* adjusted the pH value of 5 M $LiNO_3$ aqueous electrolyte by controlling the concentration of LiOH, and found that when the pH was ∼8.5, the ARLiB with the CuV_2O_5//$LiMn_2O_4$ redox couple demonstrated the optimum cyclic performance.[186] pH management of aqueous electrolytes is also a popular strategy to stabilize ARFBs. For example, Xie *et al.* utilized a 1.5 M HAc/NaAc buffer electrolyte to maintain the pH value of negative electrolyte in a Zn//Fe-based ARFB in the range of 2.0–6.0. The chemical reaction of Zn species with proton species was very insignificant, while the electro-reduction of protons on the negative electrode was significantly suppressed in this pH range.[187] In a PS-based ARFB system, PS could be stabilized in alkaline electrolyte by avoiding the formation of H_2S in neutral and acidic conditions. The equilibrium potential of polysulfide was pH-dependent for pH < 11.5, while it remained at −0.51 V *vs.* SHE when pH > 11.5. The reaction of PS in water was as follows:[188]

$$S_2^{2-} + 2H_2O + 2e^- \leftrightarrow 2HS^- + 2OH^-$$

$$E^0 = -0.51 \text{ V } vs. \text{ SHE} \quad (21)$$
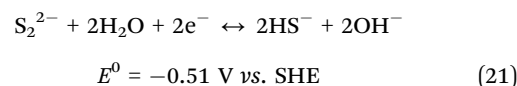
In a Zn//I_2 ARFB, fast overcharge self-protection ability was demonstrated with a smart pH-responsive electrolyte. Once overcharged, the electrolyte pH increased, which was induced by hydrogen evolution, and consequently the irreversible formation of insulating ZnO at the anode side and soluble $Zn(IO_3)_2$ at the cathode side, which could rapidly switch off the Zn//I_2 ARFB with capacity degrading to 6% of the initial capacity, thereby avoiding continuous battery damage. Noticeably, the stimulus-responsive ARFB could be switched on with

1820 | *Energy Environ. Sci.*, 2022, **15**, 1805–1839

This journal is © The Royal Society of Chemistry 2022

nearly 100% capacity recovery by re-adjusting the electrolyte pH, delivering excellent stability.[189]

3.2.2. pH management for higher energy density. Besides stability, pH management even can improve the energy density of ARBs, especially for the Zn//MnO$_2$ system, in which the cathode mechanism can be classified as proton-participating conversion in mild/strong alkaline environment,[190,191] reversible Zn ion insertion/extraction in neutral/mild acidic aqueous electrolyte,[91,192] proton and Zn ion co-insertion in mild acid condition,[193] and cathode dissolution/deposition mechanism under strong acid condition.[95,194] Various cathode mechanisms generate different working potentials in the cathode, among which the that of the dissolution/deposition mechanism is the highest. Therefore, the pH value of 1 M ZnSO$_4$ + 1 M MnSO$_4$ aqueous electrolyte was adjusted using H$_2$SO$_4$ to create a strong acid environment, while 0.1 M was chosen as the optimized concentration of H$_2$SO$_4$ for balancing between a high working voltage and wide ESW (desirable cyclic stability). The discharge profiles of the pH-adjusted electrolyte-based Zn–MnO$_2$ battery exhibited three discharge regions including D1 (2.0–1.7 V), D2 (1.7–1.4 V), and D3 (1.4–0.8 V), which represented MnO$_2$ dissolution, proton insertion, and Zn ion insertion, respectively (Fig. 10a). The average out-put voltage of that cell was 1.95 V, together with ∼570 mA h g^{-1} capacity (active matter of both cathode and anode), exhibiting ∼409 W h kg^{-1} energy density.[95] Based on the dissolution/deposition mechanism of MnO$_2$, a membrane-free Zn//MnO$_2$ ARFB was proposed for large-scale energy storage with the corresponding schematic illustration and digital image, and schematic cross-section of the cell shown in Fig. 10b and c, respectively.[101]

3.2.3. Two-pH decoupling electrolyte. Actually, the pH of aqueous electrolytes not only affect the working mechanism of the MnO$_2$ cathode but also the Zn metal anode. The redox potential of Zn stripping/plating is −0.76 V vs. SHE, while that for Zn/Zn(OH)$_4^{2-}$ conversion in an alkaline environment can be extended to −1.199 V vs. SHE.[98] Thus, decoupling the working conditions of the MnO$_2$ cathode and Zn anode to enable both acidic MnO$_2$ and alkaline Zn redox reactions in a single cell can break the 2.0 V barrier of the aqueous Zn//MnO$_2$ battery. One design (Fig. 10d) used both an alkaline (6 M KOH + 0.2 M ZnO + 5 mM vanillin) and an acidic (3 M H$_2$SO$_4$ + 0.1 M MnSO$_4$) electrolyte in two chambers separated by a neutral (0.1 M K$_2$SO$_4$) electrolyte to avoid their neutralization. The neutral electrolyte chamber was encapsulated by two membranes (cation-exchange or bipolar membrane) with ion selectivity on each side. Basing on this design, the decoupled Zn//MnO$_2$ battery exhibited an exceptionally high open-circuit voltage of 2.83 V and a specific energy density of 1621.7 W h kg^{-1} (based on the active mass of MnO$_2$).[97] The three-chamber structure was sophisticated to some extent, and hence one study attempted to construct this type of decoupled Zn//MnO$_2$ battery into a ARFB with one anolyte of 2.4 M KOH + 0.1 M Zn(CH$_3$COO)$_2$ and one catholyte of 0.5 M H$_2$SO$_4$ + 1.0 M MnSO$_4$, separated by a bipolar membrane (Fig. 9e).[96] Recently, a polyacrylate (PAA)-based alkaline hydrogel and PAM-cellulose-based acid hydrogel were prepared and employed as a two-pH

decoupling electrolyte. The commonly used cellophane worked as a separator, effectively solving the problem of electrolyte neutralization caused by diaphragm ruptures. The flexible Zn//MnO$_2$ battery displayed a high working voltage of 2.7 V, high area capacity of 2.63 mA h cm^{-2}, and acceptable cyclic stability of 86.7% capacity retention after 400 cycles.[195]

The alkaline/acid decoupling electrolytes were designed for an aqueous Zn//MnO$_2$ battery, whereas alkaline/mild ones were proposed by Wu's group for Zn–Li HiBs. In that system, 5 M LiNO$_3$ and 5 M LiOH + 1 M Zn(OAc)$_2$ aqueous solutions were selected as the cathodic and anodic electrolytes, respectively, coupling the waste Nafion NR117 membrane treated with 3 wt% H$_2$O$_2$ and 1 M H$_2$SO$_4$ as the separator (Fig. 9f). Before that, the same membrane was employed in an aqueous Zn//MnO$_2$ battery and an aqueous Li-ion capacitor with alkaline/mild electrolytes, showing its feasibility and validity as a separator.[196,197] While in the Zn–Li HiB, a Zn anode in alkaline solution and LiMn$_2$O$_4$ cathode in mild solution together equipped the whole cell with a working voltage of above 2.3 V. This battery system delivered a steady energy density of 208 W h kg^{-1} (based on the total weight of active materials) at 1.69C with a high average output voltage of up to 2.31 V, and could be cycled for over 1000 cycles with an average CE of >98%.[198] In summary, the pH of aqueous electrolytes can influence the redox potential and even the reaction mechanism of electrodes, thereby influencing the stability and working voltages of the whole cell, which is an important move towards overcoming the disadvantages of ARBs. The performance of representative works is summarized in Table S2 (ESI†). However, managing the pH of aqueous electrolytes may fail to shift the electrode redox potential considerably according to eqn (18) and (20). In contrast, for two-pH decoupling electrolytes, their complicated cell structures probably restrict their application and popularization in ARBs, together with the unwanted HER and OER at the electrode/electrolyte interfaces under a high working voltage. Therefore, the strategies of pH management and two-pH decoupling electrolyte need more studies and further optimization to maturely enhance the stability and working voltage/energy density of ARBs.

3.3. Salt-concentrated electrolyte

Liquid electrolytes are a combination of solvents and salts, while salt concentration is a critical parameter, impacting the ESWs, ionic conductivity, and electrode/electrolyte interfaces through solvation structures, viscosity, ionic mobility and overall electrolyte structure (morphology).[56,199] Based on this, salt concentration manipulation is an easy and effective way to tailor the corresponding liquid electrolytes. Increasing the salt concentration in liquid electrolytes will result in enhanced interactions between cations and anions/solvents and a decrease in the content of free-state solvent molecules, which will demonstrate unusual physicochemical and electrochemical properties that are remarkably distinct from conventional dilute electrolytes.[199]

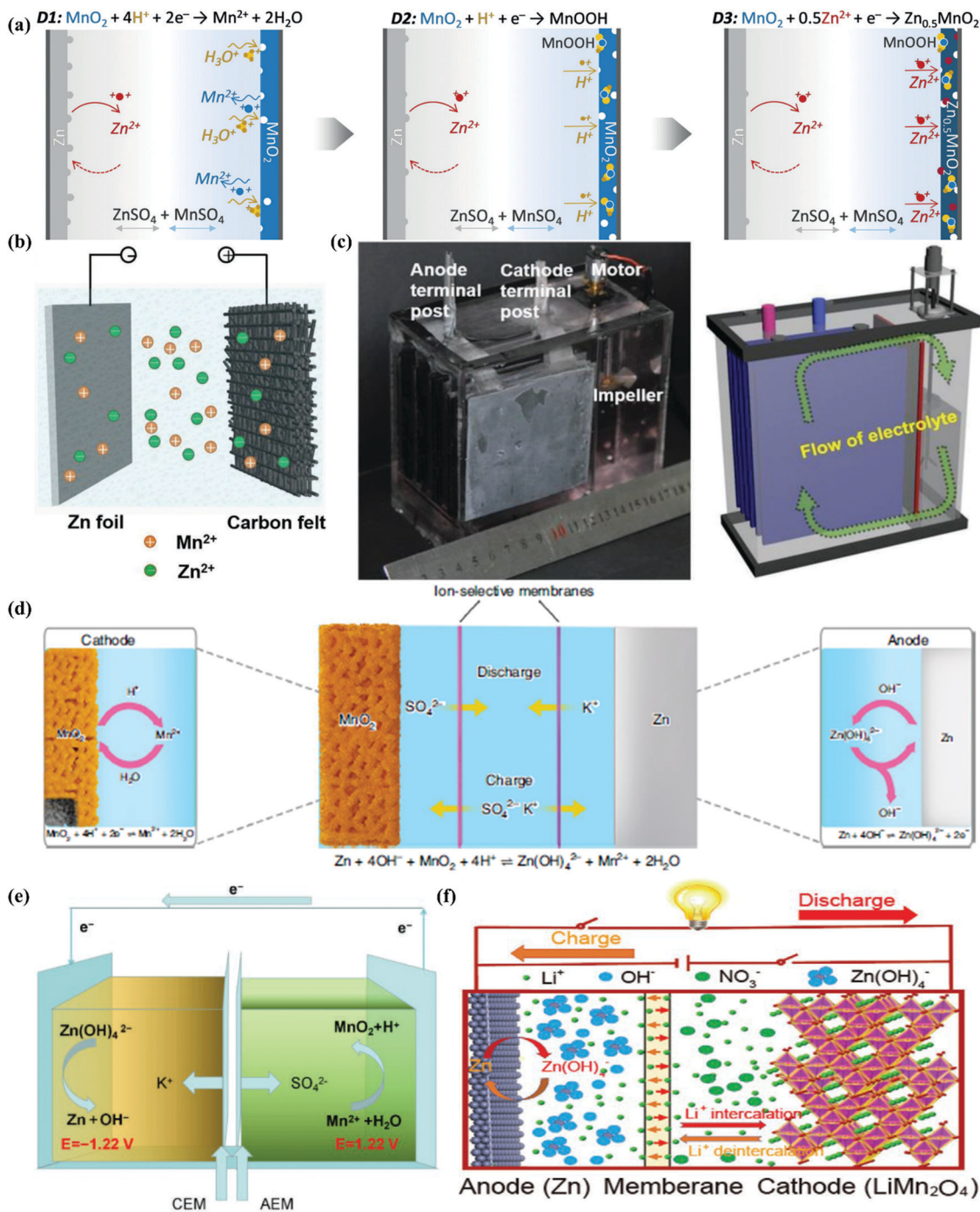**3.3.1. "Water-in-salt" electrolyte.** In 2015, one significant breakthrough was made by Wang's and Xu's group, proposing

Fig. 10 (a) Schematic representation and charge storage mechanism of the aqueous Zn//MnO$_2$ battery in H$_2$SO$_4$-adjusted 1 M ZnSO$_4$ + 1 M MnSO$_4$ electrolyte.[95] (b) Configuration of a membrane-free Zn//MnO$_2$ ARFB.[101] (c) Digital image and cross-section schematic of the cell, where the electrolyte flow propelled by the impeller is indicated by a green arrow.[101] (d) Schematic diagram of the cell structure and chemical reactions at the cathode and anode during the discharge and charge based on decoupled reactions in acidic and alkaline electrolytes separated by a neutral electrolyte in the central chamber.[97] (e) Schematic illustration and mechanism of Zn//MnO$_2$ ARFB battery using an acid/alkaline decoupling electrolyte.[96] (f) Schematic representation of the structure and working mechanism of the assembled Zn–Li HiB with alkaline/mild decoupling electrolyte.[198]

the concept of "water-in-salt" electrolyte (WiSEs), which ushered salt-concentrated electrolytes and ARBs into a new era.[75] The flourished salt-concentrated electrolytes in ARBs can be categorized into WiSEs, hydrate-melt electrolytes (HMEs) and regular super-concentration electrolytes (RSCEs), which generate wide

ESWs, and then high energy density. The definition of WiSEs is that salt outnumbers the solvent in a binary system in terms of both weight and volume, leading to an anion-containing Li-ion solvation sheath (Fig. 11a) and the formation of a dense interphase on the anode surface (mainly arising from anion
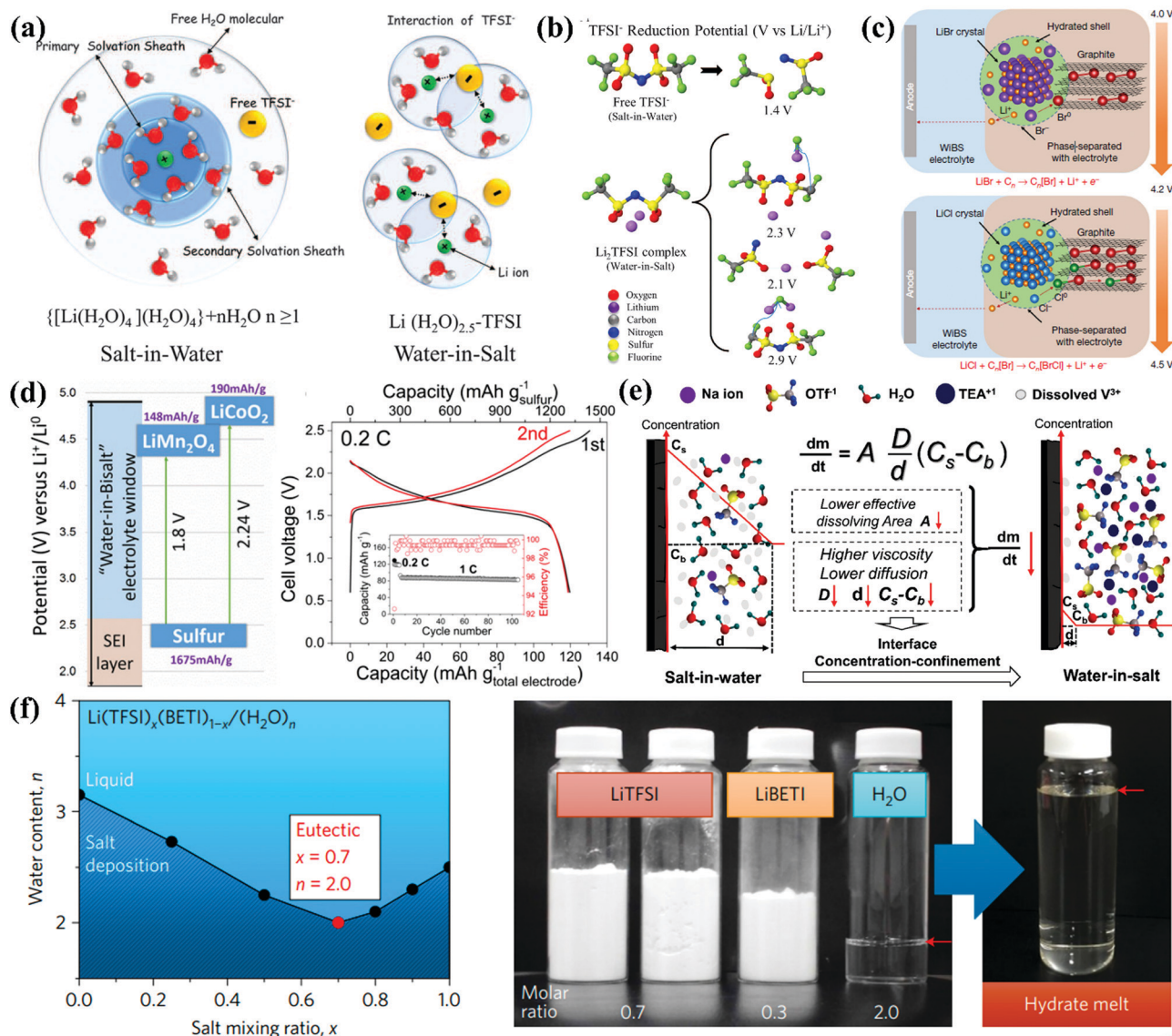
1822 | *Energy Environ. Sci.*, 2022, **15**, 1805–1839

This journal is © The Royal Society of Chemistry 2022

Fig. 11 (a) Illustration of the evolution of the Li-ion primary solvation sheath in diluted and WiSE.[75] (b) Predicted reduction potentials of free and complex TFSI⁻ from G4MP2 quantum chemistry calculations.[75] (c) Schematic drawing of the conversion-intercalation mechanism occurring in $(LiBr)_{0.5}(LiCl)_{0.5}$-graphite during its oxidation in the WiSE. Two-stage reactions involved in the oxidation of Br⁻ (~4.0 V) and Cl⁻ (~4.2 V) and their subsequent intercalation into the graphitic structure.[76] (d) Illustration of $S//LiMn_2O_4$ and $S//HV$-$LiCoO_2$ full cell in WiSE with expanded ESW. Voltage profiles of $S//HV$-$LiCoO_2$ full cell in WiSE at a rate of 0.2C. (inset) Capacity stability and CE during cycling.[201] (e) Schematic illustration of vanadium dissolution according the Noyes−Whitney equation.[45] (f) Liquidus line of $Li(TFSI)_x(BETI)_{1-x}$ salt−water mixtures and stoichiometric amounts of LiTFSI, LiBETI and water used to prepare an $Li(TFSI)_{0.7}(BETI)_{0.3} \cdot 2H_2O$ hydrate melt. The red arrows indicate the liquid levels.[208]

reduction, Fig. 11b). Combined with the substantially reduced electrochemical activity of water in a WiSE of 21 m LiTFSI, an ESW of ~3.0 V was provided, which equipped a full ARLiB $(Mo_6S_8//LiMn_2O_4)$ with a working voltage of 2.3 V and 1000 charge/discharge cycles.[75] Since that, WiSEs have demonstrated all-round versatility in raising the energy density, enhancing the stability and widening the working temperature windows of ARBs. In terms of energy density enhancement, Wang's and Xu's groups applied WiSEs to an ARLiB with halogen conversion–intercalation chemistry in graphite (Fig. 11c), delivering a capacity of 243 mA h g⁻¹ (based on the total weight of the electrode) at an average potential of 4.2 V vs. Li/Li⁺. Pairing a graphite anode

with an artificial SEI, a 4 V class ARLiB was created with an energy density of 460 W h kg⁻¹.[76] Furthermore, Wang's and Xu's group employed the WiSE in ZAB chemistry with a porous carbon air cathode, demonstrating an energy density of 1000 W h kg⁻¹ (based on the mass of the cathode) in 200 cycles.[147] Meanwhile, in the LAB system, WiSEs provide the necessary functionalities to support aprotic $Li//O_2$ operations via reversible Li_2O_2 formation and decomposition. The lack of organic solvent molecules was a highlight there, eliminating the known reaction pathways towards by-product formation in organic electrolyte systems.[200] In another theoretically high energy density system of LSB, a WiSE played a role as well, coupling a sulfur anode with

This journal is © The Royal Society of Chemistry 2022

Energy Environ. Sci., 2022, **15**, 1805–1839 | **1823**

solid–liquid two-phase, and $LiMn_2O_4/LiCoO_2$ cathode, delivering a working voltage of 1.8/2.24 V (Fig. 11d). The capacity of the sulfur anode was tested as 1327 mA h g^{-1}, while the energy density of the full cell was determined to be 200 W h kg^{-1} (total electrode mass) for >1000 cycles at ~100% CE.[201]

The stability endowed by WiSEs is also significant among ARBs, not only suppressing the HER/OER of water but also dissolution of the electrodes in aqueous electrolytes. In the above-described LSB system, excellent cyclic stability was induced by the solid–liquid two-phase reaction pathway, where the liquid polysulfide phase in the sulfide electrode was thermodynamically phase-separated from the WiSE.[201] The phenomenon of negligible polysulfide dissolution in WiSEs can also be discovered in SiB chemistry. Yue et al. investigated concentration-controlled cathode dissolution through a susceptible $Na_3V_2(PO_4)_3$ cathode, whose time-, cycle-, and state-of-charge-dependent dissolubility were evaluated by multiple electrochemical and chemical methods. In that study, a novel mechanism of interface concentrated-confinement was proven with WiSEs, which enhanced the cyclic stability of the $NaTi_2(PO_4)_3//Na_3V_2(PO_4)_3$ full cell. The high viscosity, low vanadium ion diffusion, low polarity of solvated water and scarce solute-water dissolving surfaces in WiSEs (9 m NaOTf + 22 m tetraethylammonium triflate, TEAOTf), remarkably decreased the thermodynamic-controlled solubility, the dissolving kinetics, and physical space local mass interfacial confinement (Fig. 11e).[45] It was discovered that the WiSEs could reduce the O_2 solubility in water and the kinetics of the oxygen reduction reaction (ORR) by slowing down O_2 diffusion, as shown by the Koutecky–Levich equation.[202] Hence, the WiSE-based cells could work with an open configuration, which exhibited superior ability to dissipate heat and pressure and eliminated the risk of explosion.[202] Besides stability, WiSEs can also expand the working temperature widows of ARBs. A WiSE of 22 m KCF$_3$SO$_3$ (KFSI) was prepared for a PiB, matched with an Fe-substituted Mn-rich PBA $K_{1.85}Fe_{0.33}Mn_{0.67}[Fe(CN)_6]_{0.98}\cdot0.77H_2O$ (KFeMnHCF-3565) cathode and 3,4,9,10-perylenetetracarboxylic diimide (PTCDI) anode. Beside the impressive performance of 80 W h kg^{-1} and superior capacity retention of 85% at 20C after more than 10 000 charge–discharge cycles at room temperature (RT), the full PiB was assembled in a pouch cell, demonstrating a superior performance at a wide temperature range of −20 °C to 60 °C.[203] In the study reported by Reber et al., a key factor limiting the application of WiSEs at low temperatures was recognized due to their salt crystallization tendency even near RT. Thus, 10 m sodium (fluorosulfonyl)(trifluoromethylsulfonyl)imide (NaFTFSI) with asymmetric anions was introduced into 25 m NaFSI with symmetric anions. Subsequently, an SiB based on the asymmetric anion optimized WiSE in combination with an $NaTi_2(PO_4)_3$ anode and $Na_3(VOPO_4)_2F$ cathode demonstrated excellent capacity retention and high energy density down to a temperature of −10 °C.[204] However, in WiSEs, expensive organic salts were intensively used, which increased the cost of the whole cell. Some studies attempted to use cost-effective salts as substitutions, and obtained some notable achievements, especially for that based on acetates and chlorates. Ji's group applied potassium acetate (KOAc) to form a WiSE, which was capable of cycling

relevant PiBs up to 11 000 cycles under a current density of 1 A g^{-1} with an ESW of ~3.2 V.[205] Through blending with LiOAc and $Zn(OAc)_2$, this acetate-based WiSE could be used in ARLiBs and $Zn//MnO_2$ systems with desirable performances and potentials on a large scale.[92,206] Meanwhile, Ji's group reported the preparation of $ZnCl_2$-based WiSE (30 m $ZnCl_2$), enabling a dendrite-free Zn metal anode with high CE and a novel DiB with high reversibility.[153,207]

3.3.2. Hydrate-melt electrolyte. Among the salt-concentrated systems, another significant electrolyte reported was HMEs, which utilize a eutectic system thereof. LiTFSI and $LiN(SO_2C_2F_5)_2$ (LiBETI) salts were firstly selected for HMEs because these anions are weakly Lewis basic and only interact with Li$^+$ weakly, thereby promoting the solvation of Li$^+$ by water molecules rather than the abundant formation of ion pairs. Furthermore, the anions exerted a 'plasticizing' effect, avoiding the crystallization of the salts and hydrates. Fig. 11f demonstrates the miscibility limits of the blended LiTFSI–LiBETI salts in water at RT, while the eutectic composition of $Li(TFSI)_{0.7}(BETI)_{0.3}$ was determined to exhibit the highest miscibility, forming a stable, transparent liquid with an extremely low water content (H$_2$O : Li$^+$ = 2.0 molar ratio), equalling a water molar concentration of 10.1 mol L^{-1} (Fig. 10f). Because of this low water concentration, the water molecules could be isolated from each other by the bulky anions, thus suppressing the activity of water by decreasing the opportunity for the formation of clusters of free water molecules. This HME equipped $Li_4Ti_5O_{12}//LiNi_{0.5}Mn_{1.5}O_4$ redox couples with an upper limitation working voltage of 3.1 V and energy density of >130 W h kg^{-1} within 100 cycles.[208] Besides, the concept of HME was applied to SiBs and PiBs, employing $Na(PTFSI)_{0.65}(TFSI)_{0.14}(OTf)_{0.21}\cdot3H_2O$ and $K(PTFSI)_{0.12}(TFSI)_{0.08}(OTf)_{0.8}\cdot2H_2O$ hydrate melts with ternary anions including TFSI$^-$, OTf$^-$ and especially asymmetric the $N(SO_2CF_3)(SO_2C_2F_5)^-$ (PTFSI$^-$) anion, which significantly expanded the ESWs to 2.7 and 2.5 V, respectively. Na(PTFSI) and K(PTFSI) with asymmetric anions normally possess high solubility, which is attributed to their high vibrational mobility and flexibility offered by their asymmetric structure, realizing Na and K hydrate melts at super-high concentration.[209] The HMEs were also appropriate in LABs, coupling LiSICON glass ceramic-protected Li metal anode and Ketjen Black (KB) cathode, which showed a low charge potential of ~3.16 V, a high discharge capacity of 38 mA h cm^{-2}, and a stable cyclic ability of 50 cycles with a capacity limitation of 1000 mA h g^{-1} under a current density of 500 mA g^{-1}.[210] After substituting into $ZnCl_2\cdot2.33 H_2O$, the HME could work with a Zn metal anode and Pt/C cathode as a ZAB, delivering a reversible capacity of 1000 mA h g^{-1} (based on catalyst) over 100 cycles.[211] In the WiSE system, a similar concept to HME was proposed, namely "water-in-bisalt" electrolyte (WiBSE), which could dissolve another unhydrated salt with similar chemical properties and form binary salt systems in the molten state with higher cation/water ratios. In the typical WiBSE of 21 M LiTFSI + 7 m LiOTf, a more compact SEI than that in WiSE was created, allowing a 2.5 V $TiO_2//LiMn_2O_4$ full LiB with an average discharge voltage of 2.1 V and an energy density of 100 W h kg^{-1} (total electrode mass).[77] Additionally, the acetate could replace the organic FSI$^-$ anion-based salts in WiBSEs,

1824 | Energy Environ. Sci., 2022, 15, 1805–1839

This journal is © The Royal Society of Chemistry 2022

while the cation-size effect on ESWs in the acetate system was further investigated.[212]

3.3.3. Regular super-concentration electrolyte. Normally, the cation/water ratio of WiSEs and HMEs reach above 2.0 for aqueous electrolytes with a high salt concentration but fail to approach the ratio or meet the definitions of WiSEs/HMEs, which can be categorized as RSCEs. Pan *et al.* investigated the thermodynamic and kinetic contributions to the ESW of an $LiNO_3$-based RSCE ($LiNO_3 : H_2O = 1 : 2.5$) through MD simulation and spectral analysis. The local structure of the intimate Li^+–water interaction was discovered at a super-concentration, inducing $(Li^+(H_2O)_2)_n$ polymer-like chains rather than the ubiquitous hydrogen bonding between water molecules, thereby extending the ESW to 2.55 V.[213] Based on RSCEs, a universal strategy was proposed to ameliorate the specific energy, reversibility and safety of MViBs, which used $Ca(NO_3)_2$-based electrolytes as an example, driving the Ca-ion/sulfur–metal oxide full cell stably.[214] A 3 M $Zn(FSI)_2$ aqueous electrolyte was employed by Chen's group to fabricate a $Zn//ZnMn_2O_4$ battery, which exhibited excellent stability by suppressing Mn dissolution (capacity retention of 94% over 500 cycles under a high current density of 500 mA g^{-1}).[192] Subsequently, the same group optimized the concentration of $ZnCl_2$ to 7.5 m, which achieved an ultralow solid–liquid transition temperature *via* the breakage of H-bonds, and thus an ultra-wide temperature window from -90 to $60\ ^\circ C$.[215] Xue *et al.* introduced superconcentrated sugars into 2 M $NaNO_3$ to reduce the free water molecules and destroy the tetrahedral structure, thus expanding the ESW to 2.812 V by breaking the hydrogen bonds. Consequently, LiBs, SiBs, PiBs and supercapacitors with excellent electrochemical performances were derived from the sugar-based electrolytes.[216]

Briefly, salt-concentrated electrolytes can be a universal strategy to improve the energy density and cyclic stability and widen the working temperature windows of ARBs, which have been employed intensively and extensively, as summarized in Table 1 (both units of m and M were used herein, according to the different salt concentrations of various electrolytes).[45,75–77,92,147,153,192,200–222] However, their cost probably impedes their large-scale applications because of the large amount of salt in these systems, although desirable performances have been obtained. The unit price of some representative salts utilized in salt-concentrated electrolytes is compared in Fig. 12, in which the corresponding information was collected from Sigma-Aldrich in USA, Sinoreagent in China and Alfa Aesar in the UK.[190–192] It can be concluded from Fig. 12 that some organic salts are exceptionally expensive but only a little better in electrolyte performance than the cost-effective salts ranging from nitrites, perchlorates, and chlorates to acetates, and hence it is important for us to strike a balance between the properties of electrolytes and their cost in real applications.

3.4. Gelled electrolyte

Gelled aqueous electrolytes can be deemed as hydrogel electrolytes, consisting of a crosslinked network of polymer chains with interstitial spaces filled with solvent water, which endows the aqueous electrolyte with quasi-solid state and flexible property. Hydrogel electrolytes can be fabricated and applied in flexible and stretchable ARBs not only because of their physical properties but also highly available and tunable polymer chemistries. Hydrogel-based ARBs with self-healing property, shape memory and stretchability can enable the fabrication of wearable devices for health care, implantable devices, soft electronics, and strain sensors.[107,223] The frequently used polymer host materials in hydrogel electrolytes include polyvinyl alcohol (PVA), PAA, PAM, gelatin, alginate, agarose, chitosan, poly(ethylene oxide)-*block*-poly(propylene oxide)-*block*-poly(ethylene oxide) (PEO–PPO–PEO) and poly(*N*-isopropylacrylamide-*co*-acrylamide) (PNIPAM/AM), which possess various features, functional groups, crosslinking/gelation methods (Fig. 13a), and cooperate with aqueous solutions of different cations, anions and pH values.[223]

3.4.1. Minimizing water content for higher stability. The original function of hydrogel electrolytes based on their polymers was endowing ARBs with quasi-solid properties,[224] while additional functions were also discovered to mitigate the challenges of ARBs. In a 5 M LiCl–PVA hydrogel electrolyte for supercapacitors, PVA could prevent the chemical dissolution of the V_3O_7 electrode by minimizing the water content, providing a neutral pH medium, and serving as an elastic coating.[225] With further development, PVA was found to further extend the ESW of an $LiClO_4$ aqueous solution, hence resulting in a higher energy density and cyclic stability in Zn–Li HiBs.[226] By integrating PVA with the currently popular WiSE (21 m LiTFSI), a flexible and wearable symmetrical ARLiB was developed with an energy density of 141 W h kg^{-1} during 4000 cycles using a single $LiVPO_4F$ as both the anode and cathode. In that cell, high energy and power density and flexibility were realized mutually in the presence of PVA.[227] Besides PVA, carboxymethyl cellulose (CMC) was added to an acetate-based WiSE (20 m KOAc) in a small amount (2 wt%) for gelling, which maintained a similar ESW as 32 m KOAc WiSE with less salt dissolved. The existence of CMC reduced the dissolution of Mn and Fe in the KMHCF cathode, and then enhanced the cyclic stability of this PiB to 400 cycles.[212] In 2020, a significant work was reported by Lu's group using LiTFSI salt and poly(ethylene glycol) (PEG) polymer based on the common phenomenon of molecular crowding in living cells, which changed the hydrogen-bonding structure in water molecules, and thus reduced the activity of the water solvent. This molecular crowding electrolyte was optimized to 2 m LiTFSI–94% PEG–6% H_2O, delivering an ESW of 3.2 V and especially excellent stability against the HER (Fig. 13b), which endowed the $Li_4Ti_5O_{12}/LiMn_2O_4$ full cell with an energy density ranging from 75 to 110 W h kg^{-1} over 300 charge–discharge cycles (Fig. 13c).[228] Another similar work was reported in 2021 as a "water-in-gel" electrolyte, which consisted of water, NaCl, $ZnCl_2$ and sodium alginate (SA), expanding the ESW to 2.72 V. A "passway" for cation transportation was built within that electrolyte through coordinate bonds between the carboxylate groups of SA and Na/Zn ions. Also, due to the random coil conformation of the alginate chains, which was affected by dissolved ions, the 3D-fibrilar, porous polymer network ensured the uniform

This journal is © The Royal Society of Chemistry 2022

Energy Environ. Sci., 2022, **15**, 1805–1839 | 1825

Table 1 A summary of recent representative works on salt-concentrated electrolytes for ARBs

Electrolyte	Electrode	ESW (V)	Energy density	Cyclic stability	Working temperature	Ref.
$LiNO_3 \cdot 2.5H_2O$	$AC//LiMn_2O_4$ or $Li\,Ni_{1/3}Mn_{1/3}Co_{1/3}O_2$	2.55	n/a	n/a	RT	213
8.37 m $Ca(NO_3)_2$–PVA	$S|C//Ca_{0.4}MnO_2$	2.6	110 W h kg^{-1} (total electrode)	150 cycles (0.2C)	RT	214
2 M $NaNO_3$/66.7 wt% sucrose	AC//PBA	2.8	n/a	2000 cycles (2 A g^{-1})	−50 °C to 80 °C	216
7.5 m $ZnCl_2$	Zn//polyaniline	n/a	n/a	2000 cycles (0.2 A g^{-1})	−90 °C to 60 °C	215
$ZnCl_2 \cdot 0.03KBr \cdot 2H_2O$	Zn//graphite	n/a	∼440 W h kg^{-1} (cathode)	100 cycles (0.25 A g^{-1})	RT	217
30 m $ZnCl_2$	Zn symmetrical cell	2.3	n/a	600 hours (∼1800 cycles, 0.2 mA cm^{-2})	RT	207
30 m $ZnCl_2$	Fc/C//PBA	2.3	n/a	2000 cycles (5C)	RT	153
$ZnCl_2 \cdot 2.33\,H_2O$	Zn//Pt/C	n/a	n/a	100 cycles (0.1 A g^{-1})	30 °C	211
30 m KOAc	$KTi_2(PO_4)_3$/AC	3.2	n/a	11 000 cycles (1 A g^{-1})	RT	205
8 m LiOAc + 32 m KOAc	$TiO_2//LiMn_2O_4$	∼3.0	n/a	50 cycles (0.5C)	RT	206
7 m LiOAc + 45 m CsOAc	$VO_2//LiNi_{0.5}Mn_{1.5}O_4$	∼3.0	114.8 W h kg^{-1} (total electrode)	1200 cycles (4C)	RT	212
1 m $Zn(OAc)2$ + 31 m KOAc	$Zn//MnO_2$	3.1	232.7 W h kg^{-1} (activated electrode and electrolyte)	600 cycles (C/3)	RT	92
4 M KOH + 16 M KOAc	Al alloy//Mn_xO_y@Ag	2.2	436.1 W h kg^{-1} (activated electrode and electrolyte)	2300 min (∼30 cycles, 25 mA cm^{-2})	RT	218
17 m $NaClO_4$	$NaTi_2(PO_4)_3//Na_4$-$Fe_3(PO_4)_2(P_2O_7)$	2.7	36 W h kg^{-1} (total electrode)	>200 cycles (1C)	RT	221
21 m LiTFSI	$Mo_6S_8//LiMn_2O_4$	∼3.0	84 W h kg^{-1} (total electrode)	1000 cycles (4.5C)	RT	75
21 m LiTFSI	$LICGC|Li//Ru/TiSi_2$	∼3.0	n/a	300 cycles (0.05 A g^{-1})	RT	200
9.26 m NaOTf	$NaTi_2(PO_4)_3//Na_{0.66}$-$[Mn_{0.66}Ti_{0.34}]O_2$	2.5	31 W h kg^{-1} (total electrode)	>1200 cycles (1C)	RT	219
22 m KFSI	PTCDI//KFeMnHCF-3565	∼3.0	80 W h kg^{-1} (total electrode)	10 000 cycles (100C)	−20 °C to 60 °C	203
3 M ZnFSI	$Zn//ZnMn_2O_4$	n/a	∼202 W h kg^{-1} (total electrode)	500 cycles (0.5 A g^{-1})	RT	192
21 m LiTFSI + 7 m LiOTf	$C/TiO_2//LiMn_2O_4$	∼3.1	100 W h kg^{-1} (total electrode)	100 cycles (0.5C)	RT	77
21 m LiTFSI + 7 m LiOTf-PEO/PVA	passivated graphite//$(LiBr)_{0.5}(LiCl)_{0.5}$-graphite	∼3.1	460 W h kg^{-1} (total electrode)	∼250 cycles (0.08 A g^{-1})	RT	76
21 m LiTFSI + 7 m LiOTf-PVA	S-KB//$LiMn_2O_4$ or $LiCoO_2$	∼3.1	200 W h kg^{-1} (total electrode)	>1000 cycles (1C)	RT	201
21 m LiTFSI + 7 m LiOTf (open battery configuration)	$Al_2O_3@LiTi_2(PO_4)_3//LiMn_2O_4$	∼3.1	170 W h kg^{-1} (total electrode)	1000 cycles (5C)	RT	202
42 m LiTFSI + 21 m $Me_3EtN \cdot TFSI$	$Li_4Ti_5O_{12}//LiMn_2O_4$	3.25	145 W h kg^{-1} (total electrode)	150 cycles (0.2C)	RT	216
1 m $Zn(TFSI)_2$ + 20 m LiTFSI	$Zn//LiMn_2O_4$	n/a	180 W h kg^{-1} (total electrode)	4000 cycles (4C)	RT	147
1 m $Zn(TFSI)_2$ + 20 m LiTFSI	Zn//Super P	n/a	300 W h kg^{-1} (total electrode)	200 cycles (0.05 A g^{-1})	RT	147
9 m NaOTf + 22 m TEAOTf	$NaTi_2(PO_4)_3//Na_3V_2(PO_4)_3$	n/a	n/a	100 cycles (1C)	RT	45
25 m NaFSI + 10 m NaFTFSI	$NaTi_2(PO_4)_3//Na_3(VOPO_4)_2F$	2.7	64 W h kg^{-1} (total electrode)	500 cycles (C/5, 1C)	−10 °C, 10 °C, 30 °C	204
$Li(TFSI)_{0.7}(BETI)_{0.3} \cdot 2H_2O$	$Li_4Ti_5O_{12}//LiNi_{0.5}Mn_{1.5}O_4$	3.8	>130 W h kg^{-1} (total electrode)	100 cycles (6.8C)	RT	208
$Na(PTFSI)_{0.65}(TFSI)_{0.14}$-$(OTf)_{0.21} \cdot 3H_2O$	$NaTi_2(PO_4)_3//Na_3(VOPO_4)_2F$	2.7	77.9 W h kg^{-1} (total electrode)	500 cycles (5C)	RT	209
$Li(TFSI)_{0.7}(BETI)_{0.3} \cdot 2H_2O$	$LiSICON|Li//KB$	3.8	950 W h kg^{-1} (activated electrode and electrolyte)	50 cycles (0.5 A g^{-1})	RT	210
$Zn(ClO_4)_2 \cdot 6H_2O$–succinonitrile	Zn//poly(2,3-dithiin-1,4-benzoquinone)	2.55	n/a	3500 cycles (0.3C)	−20 °C, −10 °C, RT	222

distribution and efficient transportation of Na/Zn ions in an aqueous environment. A Zn–Na hybrid battery based on this electrolyte was proposed, achieving a high extraction voltage of Na ions (2.1 V *vs.* Zn/Zn^{2+}) and high capacity retention of 96.8% after 450 cycles.[229]

3.4.2. Lowering fluidity for higher energy density. Besides wide ESWs, the quasi-solid state and poor fluidity of hydrogel electrolytes also contribute to the high energy density of ARBs based on their decoupling structure. As noted above,

a PAA-based alkaline hydrogel and PAM-cellulose-based acid hydrogel were prepared as a two-pH decoupling electrolyte, enabling a high working voltage in a $Zn//MnO_2$ battery (2.7 V). and thus high energy density. Compared with liquid decoupling electrolytes, hydrogel-based electrolytes simplify the three-chamber into a two-chamber structure, thus improving the relevant processability.[195] A gelled decoupling electrolyte with gelatin/$ZnSO_4$ analyte, gelatin/$CuSO_4$ catholyte, and anion-exchange separator was proposed, in which decoupling charge

1826 | *Energy Environ. Sci.*, 2022, **15**, 1805–1839

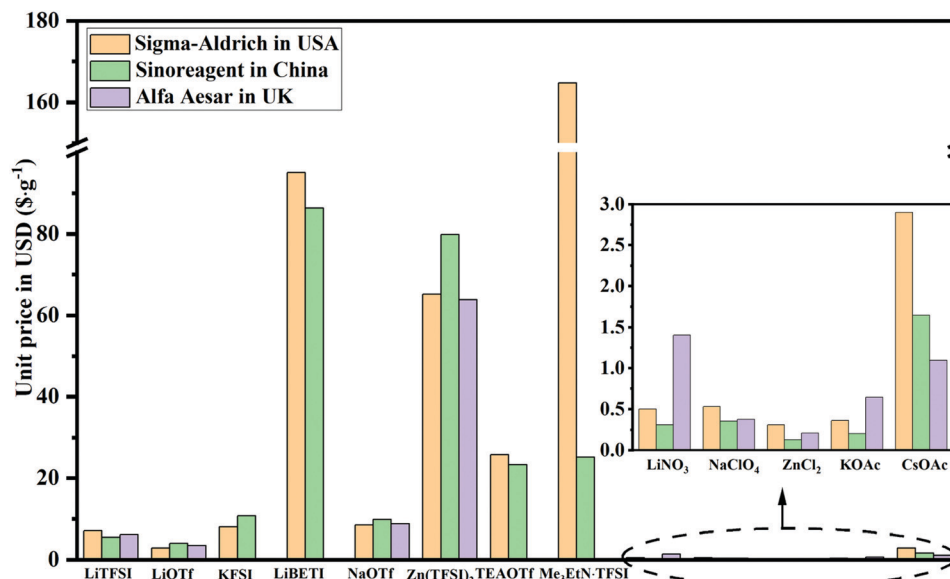This journal is © The Royal Society of Chemistry 2022

Fig. 12 Comparison of the unit price of various representative salts utilized in salt-concentrated electrolytes.
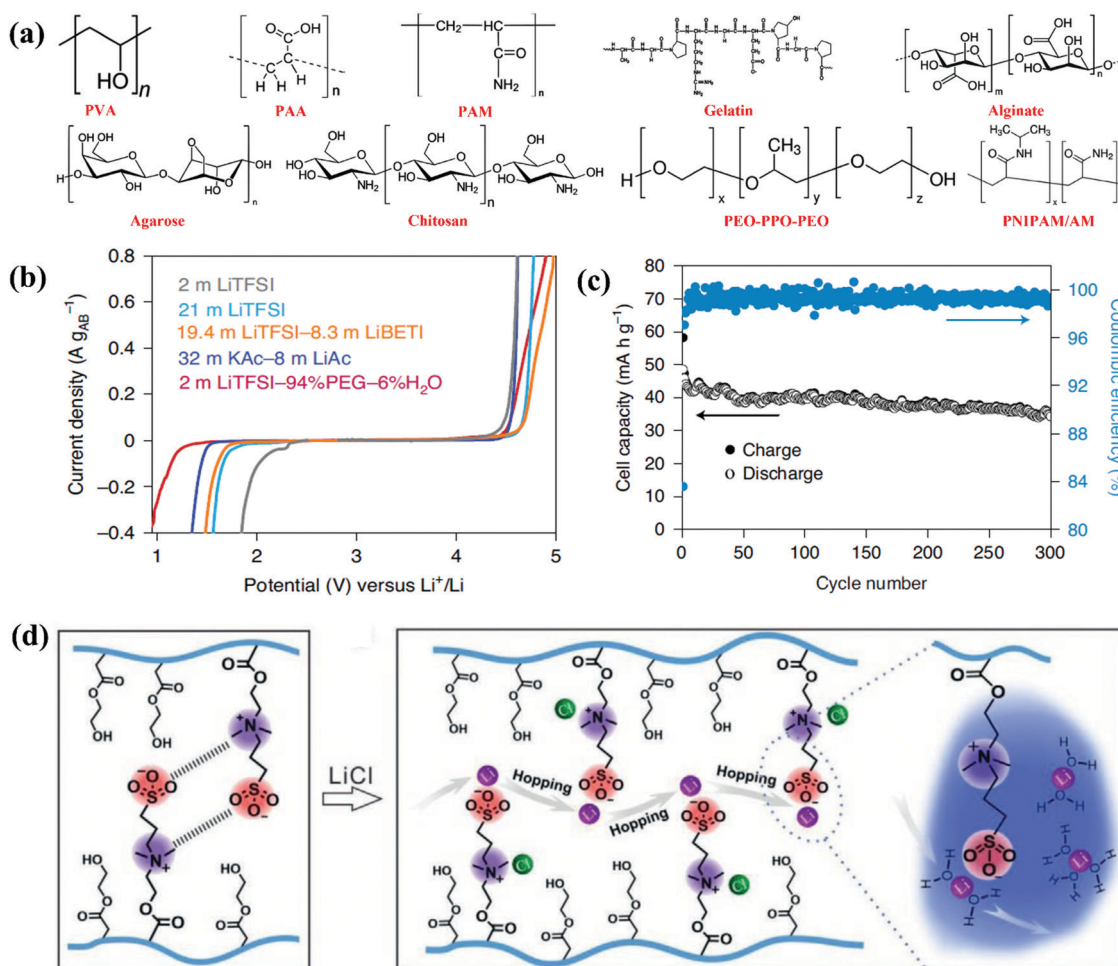

Fig. 13 (a) Molecular structure of frequently used polymer host materials for hydrogel electrolytes.[223] (b) Comparison of ESWs between molecular crowding electrolyte and other salt-concentrated electrolytes.[228] (c) Cyclic stability and CE of Li$_4$Ti$_5$O$_{12}$//LiMn$_2$O$_4$ cell based on molecular crowding electrolyte under 1C rate.[228] (d) Schematic diagram of electrostatic interaction between anionic and cationic groups without salts, and proposed Li$^+$ migration mechanism in zwitterionic polymer hydrogel electrolyte.[231]

This journal is © The Royal Society of Chemistry 2022

Energy Environ. Sci., 2022, **15**, 1805–1839 | **1827**

carriers of anolyte and catholyte simultaneously endowed the Zn anode and S cathode with optimal redox chemistry, as follows:[230]

$$\text{Cathode: } S + 2Cu^{2+} + 4e^- \leftrightarrow Cu_2S \qquad (22)$$

$$\text{Anode: } Zn \leftrightarrow Zn^{2+} + 2e^- \qquad (23)$$
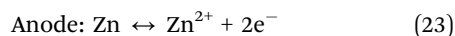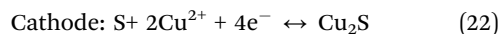
Derived from this, the theoretical volumetric energy density of this flexible HiB was regarded as 3868 W h L^{-1}, while the battery delivered a stable output voltage (released 92% of its full capacity within a small voltage drop of 0.15 V) and an ultrahigh reversible capacity of 2063 mA h g^{-1} (based on mass of S) under a current density of 100 mA g^{-1}.[230]

3.4.3. Anti-freezing for wider temperature window. Hydrogel electrolytes also possess anti-freezing function, which guarantees the stable operation of ARBs at low temperatures. A new type of zwitterionic polymer hydrogel electrolyte was fabricated, achieving high conductivity without sacrificing the flexibility of hydrogels at subzero temperatures. The anionic and cationic counterions on the zwitterionic chains facilitated the dissociation of the LiCl salt, while the salt concentration significantly affected the conductivity and anti-freezing performance of the electrolytes. A direct hopping migration mechanism of hydrated Li$^+$ through the channel of zwitterion groups was further proposed (Fig. 13d). The ultrahigh ionic conductivity of 12.6 mS cm^{-1} was achieved at −40 °C, owing to the synergistic effects including the electrostatic interactions between the zwitterionic groups and Li$^+$ and the formation of an Li$^+$(H$_2$O)$_n$ hydration structure.[231] Furthermore, a borax-crosslinked PVA/glycerol hydrogel electrolyte with a freezing point of below −60 °C was developed, in which glycerol could strongly interact with the PVA chains, thereby effectively prohibiting the formation of ice crystals in the whole gel network. This type of hydrogel electrolyte with 10.1 mS cm^{-1} at −35 °C, drove a Zn//MnO$_2$ battery to charge/discharge for over 2000 cycles with around 90% capacity retention at that temperature.[232] In summary, the performance of representative works is listed in Table S3 (ESI†). To some extent, hydrogel electrolytes are a solvent strategy to solidify/inactivate water and achieve wider ESWs, higher stability, and a wider working temperature range, which are effective and economic for better ARBs. In next section, another method for solvent manipulation, named hybrid solvent, will be reviewed.

3.5. Hybrid-solvent electrolyte

The SEIs formed in WiSEs were found to be predominantly inorganic metal fluorides, originating from the reduction of salt anions of TFSI$^-$ or OTf$^-$. However, the formation of this anion-originating SEI faces a severe "cathodic challenge" as result of the repulsion of anions by the negatively polarized anode surfaces, making the expansion of the cathodic limits extremely difficult.[233,234] Therefore, a new class of electrolytes hybridizing aqueous and non-aqueous solvents was reported, which inherited the intrinsic merits of each system and successfully resolved the conflicts among performance, cost, interfacial chemistry, ambient control, and environmental concerns.

3.5.1. Hybridization with organic (aprotic) solvent. Dimethyl carbonate (DMC) was blended with an LiTFSI WiSE, introducing a secondary ingredient (alkylcarbonate) in the protective interphase on the anode in addition to LiF from anion reduction. This hybrid interphase, consisting of LiF and alkylcarbonate, stabilized the electrolyte down to 1.0 V vs. Li/Li$^+$, allowing 3.2 V Li-ion cell chemistry of Li$_4$Ti$_5$O$_{12}$ anode and LiNi$_{0.5}$Mn$_{1.5}$O$_4$ cathode.[233] Subsequently, the LiTFSI-DMC/water hybrid-solvent electrolyte was applied for DiBs, in which Li$^+$ intercalation/deintercalation occurred on the Li$_4$Ti$_5$O$_{12}$ side, while intercalation/deintercalation occurred on the graphite side.[235] Furthermore, DMC was introduced in an LiTFSI + LiOTf WiBSE with both broad ESW and excellent safety, and assembled with a KS6 graphite cathode and Nb$_2$O$_5$ anode as DIB, which exhibited a good comprehensive performance including capacity, cycling stability, rate performance, and medium discharge voltage.[236] Besides Li$^+$-based chemistries, the hybrid solvent concept also suits SiBs. 7 m NaOTf aqueous solution was mixed with 8 m NaOTf propylene carbonate (PC) solution. Through Raman spectral characterization, intensified cation–anion association was observed in this electrolyte, which benefited the formation of an interphase at the electrode/electrolyte interface, thereby stabilizing the water molecules against the reducing surfaces of the electrodes. The Na$^+$-based solvent-hybrid electrolyte offered an ESW of up to 2.8 V and enabled the NaTi$_2$(PO$_4$)$_3$//Na$_3$V$_2$(PO$_4$)$_3$ redox pair.[237]

3.5.2. Hybridization with ionic liquid. The abovementioned DMC and PC are regular organic solvents for conventional LiBs, while some ionic liquids were also mixed with aqueous solutions in some studies.[238,239] Ionic liquids exhibit unique properties such as flame-retardant ability, nonvolatility, and high thermal stability, but their high viscosity may hinder their further applications. Therefore, a "water in salt/ionic liquid" electrolyte composed of a salt of LiTFSI and a molten salt of 1-ethyl-3-methylimidazolium bis(trifluoromethanesulfonyl) imide (EMIM-TFSI) was mixed with an extremely small amount of water (water/LiTFSI/EMIM-TFSI molar ratio of 1 : 1 : 2). In this electrolyte, the ESW was considerably widened without sacrificing the ionic conductivity, allowing accessibility to the full capacity of a commercial Nb$_2$O$_5$ material at a low potential window (−1.6 V vs. Ag/AgCl).[239] Meanwhile, deep eutectic solvents (DESs), generally obtained by simply mixing Lewis acids and bases in a eutectic molar ratio, have emerged as attractive alternatives to ionic liquids due to their high degree of design freedom. 6 wt% water was added to a urea-based DES, endowing the Zn anode with unusual reversibility and durability. The intensified water–DES interactions significantly suppressed the water reactivity, while the merits of the aqueous system on the ionic conductivity and viscosity were conserved.[238]

3.5.3. Hybridization with low-freezing point solvent. Some organic solvents possessing low freezing points can be employed to enhance the low-temperature performance of ARBs by hybridizing aqueous electrolytes. For instance, the freezing point of acetonitrile (AN) is −48 °C, together with the properties of high dielectric constant (35.9), high oxidation stability (> 5 V vs. Li$^+$/Li), and high miscibility with water, enabling an ARLiB with the Li$_4$Ti$_5$O$_{12}$//LiMn$_2$O$_4$ redox pair to

Table 2 A summary of recent representative works on hybrid-solvent electrolytes for ARBs

Electrolyte	Electrode	ESW	Energy density	Cyclic stability	Working temperature	Reference
14 M LiTFSI in DMC/water	$Li_4Ti_5O_{12}$//$LiNi_{0.5}Mn_{1.5}O_4$	4.1 V	165 W h kg^{-1} (total electrode)	>1000 cycles (6C)	RT	233
14 M LiTFSI in DMC/water	$Li_4Ti_5O_{12}$//graphite	4.1 V	n/a	50 cycles (0.2 A g^{-1})	RT	235
9.25 m LiTFSI + 3.1 LiOTf in DMC/water	Nb_2O_5//graphite	4.0 V	n/a	300 cycles (0.2 A g^{-1})	RT	236
$Li_4(TEGDME)(H_2O)_7$	$Li_4Ti_5O_{12}$//$LiMn_2O_4$	4.2 V	120 W h kg^{-1} (total electrode)	500 cycles (3C)	RT	244
50 wt% Li(LiOH)PAA	TiO_2/$LiTi_2(PO_4)_3$// $LiMn_2O_4$/$LiNi_{0.5}Mn_{1.5}O_4$	2.7 V	142.2 W h kg^{-1} (total electrode)	100 cycles (0.5C)	RT	245
Mixture of 7 m NaOTf in water and 8 m NaOTf in PC	$NaTi_2(PO_4)_3$//$Na_3V_2(PO_4)_3$	2.8 V	45 W h kg^{-1} (total electrode)	100 cycles (10C)	RT	237
LiTFSI + Zn(TFSI)$_2$ (Li^+:Zn^{2+} = 20 in molar) in DES/water	Zn//$LiMn_2O_4$	>2.5 V	224.6 W h kg^{-1} (cathode)	600 cycles (0.1, 0.5, 1C)	RT	238
LiTFSI/H_2O/(EMIM-TFSI)$_{2.0}$	Nb_2O_5//AC	4.7 V	51.9 W h kg^{-1} (total electrode)	3000 cycles (1 A g^{-1})	RT	239
15.3 m LiTFSI in AN/water	$Li_4Ti_5O_{12}$//$LiMn_2O_4$	4.5 V	173 W h kg^{-1} (total electrode)	1000 cycles (5C)	RT, 0 °C	240
2 M $ZnSO_4$ in EG/water	Zn//PANI/V_2O_5	2.8 V	1700 W h kg^{-1} (cathode)	>250 cycles (0.2 A g^{-1})	−40 °C to RT	241
2 M $ZnSO_4$ in Anti-M-50%	Zn//PANI	∼2.5 V	n/a	2000 cycles (5 A g^{-1})	RT, −10 °C	242
1.5 M LiI in DMF/water	Zn//LiI	2.8 V	n/a	2000 cycles (0.2 mA cm^{-2})	RT, −20 °C	243

exhibit high capacity at both RT and 0 °C.[240] In addition, ethylene glycol (EG) has been widely used as antifreeze in engine coolant owing to its high boiling point and relatively low freezing point (−12 °C). When mixed with water, its freezing point can be further reduced (even to −40 °C), while the solvation interaction of Zn^{2+} with H_2O is partly reduced by the introduction of EG, contributing to fewer side reactions such as the HER on the Zn anode side. In a reported work by Li's group, the portion of EG in the mixture was optimized to 40% in volume, considering both ionic conductivity and ESW, which drove the Zn//PANI–V_2O_5 battery to more than 250 cycles under a current density of 0.2 A g^{-1} at −20 °C.[241] Qiao's group proposed a route using low-cost antisolvents, in which, for example, methanol was added to $ZnSO_4$ aqueous electrolyte to weaken the Zn^{2+} solvation sheath and minimize water activity by strengthening the interaction between the free and coordinated water molecules with antisolvents. The Zn reversibility was significantly boosted in the antisolvent electrolyte of 50% methanol in volume (anti-M-50%) at low or elevated temperatures. Based on the anti-M-50% electrolyte, the merits of the Zn//PANI coin cell/pouch cell were impressive, even repeatedly charged/discharged to 2000 cycles at −10 °C.[242] Hybridizing solvents were also applied to ARFBs by Yu et al., who systematically studied a wide range of salts (LiCl, Li_2SO_4 and LiTFSI) and solvents (dimethoxyethane, DME; tetraethylene glycol dimethyl ether, TEGDME; acetonitrile, AN; and dimethylformamide, DMF). Finally, 1.5 M LiI in DMF/water was chosen because of its 2.8 V ESW and retained ionic conductivity at low temperatures, which enabled the successful operation of Zn//LiI ARFBs at −20 °C for 150 cycles with nearly no capacity loss.[243] The merits of the works involving hybrid-solvent electrolytes are summarized (Table 2) based on representative papers in the literature.[233,235–245] Also, depending on the merits, it can be concluded that the strategy of hybridizing solvents is promising if a balance among wide

ESW, high ionic conductivity, low freezing point and cost can be found.

3.6. Electrode/current collector–electrolyte interface tuning

Interface tuning is a common strategy for all types of electrolytes, while the goals of tuning can be generally classified into thermodynamics (chemical and thermal stability) and kinetics (charge and mass transportation). Aqueous electrolytes possess superior interfacial kinetics and wettability, and thus it is more importance to cover the shortage in thermodynamics. The SEI can kinetically stabilize electrolytes at potentials far beyond their thermodynamic stability limits, allowing cell reactions to proceed reversibly. However, it failed to occur in aqueous electrolytes until the discovery of WiSE. The formation mechanism of an SEI in WiSE are possibly contributed by two pathways, as follows: (1) reduction of anion complexes or clusters and (2) reduction of O_2 and CO_2 dissolved in the electrolyte (Fig. 14a),[246] implied by combining various spectroscopic, electrochemical and computational techniques.

3.6.1. Solid electrolyte interface. The in situ constructed-SEI in WiSEs not only enabled a series of high voltage/energy density ARLiBs with unprecedented stability, but also brought high flexibility and even "open configurations", which have been hitherto unavailable for any LiB chemistries.[75,77,202] In contrast, in Zn^{2+}-based aqueous systems, severe the HER during Zn plating/stripping makes the in situ formation of SEI impossible. As mentioned for the electrolyte additive strategy, some additives were added to facilitate the formation of an SEI in ARZiBs. Wang at el. used 0.5 m $Me_3EtNOTF$ additive to build a fluorinated and hydrophobic interphase that conducts Zn^{2+}, while suppressing the HER through the decomposition of alkylammonium ions.[177] Meanwhile, the same group developed inorganic a ZnF_2–$Zn_5(CO_3)_2(OH)_6$–organic bilayer SEI based on a low-concentration aqueous $Zn(OTF)_2$–$Zn(NO_3)_2$ electrolyte, mutually considering Zn^{2+} diffusion (inorganic
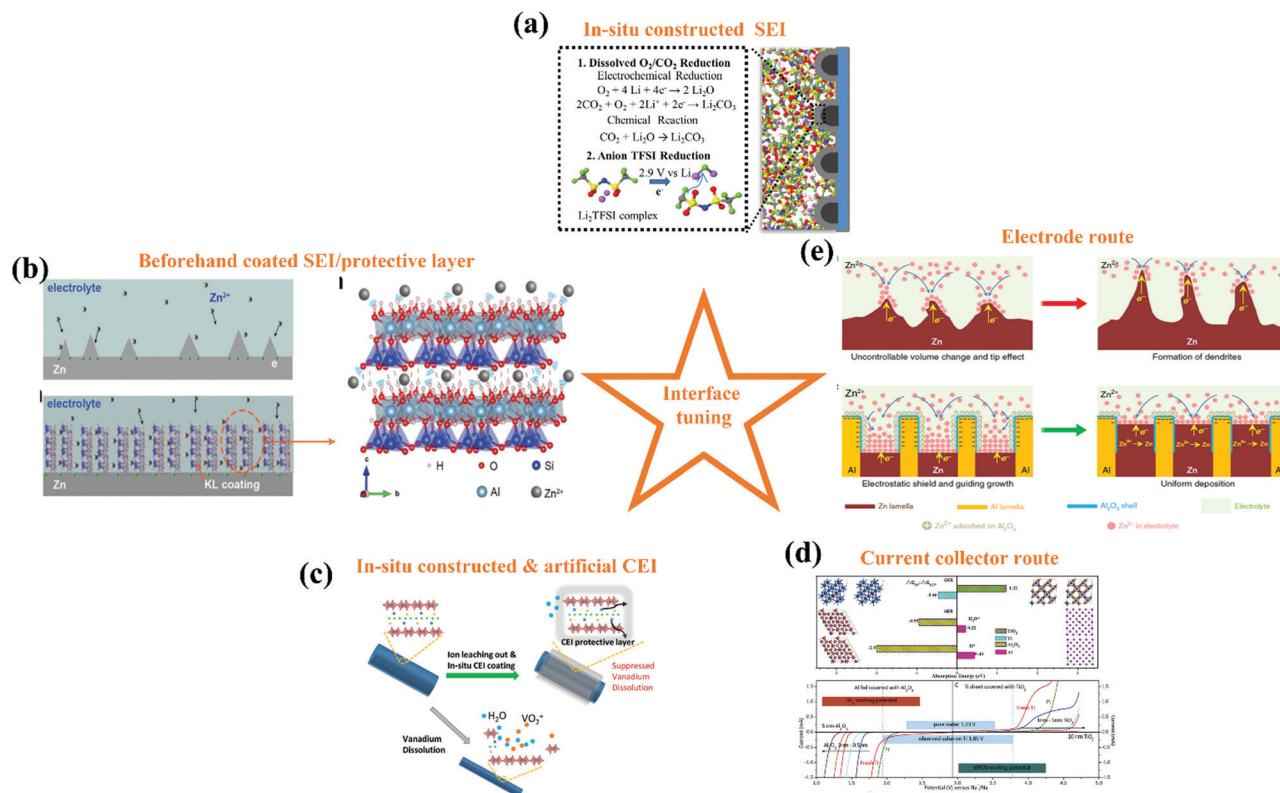
Fig. 14 (a) SEI formation mechanisms in WiSE.[246] (b) Schematic diagrams of Zn deposition process on bare Zn and KL−Zn with a detailed schematic diagram of confined Zn^{2+} transmission in kaolin.[250] (c) Illustration of the *in situ* CEI layer strategy design.[252] (d) Stability of Al and Ti current collectors in 15 m $NaClO_4$ aqueous electrolyte.[254] (e) Schematic illustration of eutectic strategy for dendrite and crack suppression.[257]

inner layer) and water inactivation (organic outer layer). A $Zn_5(OH)_8(NO_3)_2 \cdot 2H_2O$ layer was initially formed on the Zn anode surface *via* the self-terminated chemical reaction of NO_3^- with Zn^{2+} and OH^-, and then it converted into Zn^{2+} conducting $Zn_5(CO_3)_2(OH)_6$, promoting the formation of ZnF_2 as the inner layer. Meanwhile, the organic-dominated outer layer was generated by the reduction of OTf^-.[247]

Another type of interfacial engineering is pre-coating an SEI/protective layer, which is more mechanically robust than and *in situ*-grown SEI. In the WiSE system, a pre-coated anode-protected layer was prepared by adding 0.5 M LiTFSI and 10 wt% PEO to a mixture of 1,1,2,2-tetrafluoroethyl-2′,2′,2′-trifluoroethyl ether (HFE) and DMC (95 : 5 in volume), vigorously heating and stirring at 75 °C, which stabilized the graphite anode in a WiBSE and guaranteed a full cell with a working voltage of 4.0 V.[248] The HFE–PEO protective gel was applied to another graphite anode in the same WiBSE, paired with the cathode of halogen conversion–intercalation chemistry, which not only provided a working voltage of more than 4.0 V but also considerably high capacity of 243 mA h g^{-1} (for total electrode mass).[76] Besides ARLiBs, pre-coated protective layers were massively used on the surface of Zn metal anodes for the purpose of dendrite-control.[249] A layer of sieve-element function (selective channel of Zn^{2+}) and uniform-pore distribution (≈ 3.0 nm) of a kaolin was prepared and coated on a Zn metal anode for alleviating dendrite and corrosion issues.

Owing to the selective channel of Zn^{2+} and narrow distribution pore diameter of kaolin (Fig. 14b), homogeneous Zn^{2+} migration confined by this channel was achieved with dendrite-free deposition. Moreover, the coated kaolin (KL)–Zn anode exhibited long-time stability (800 h under current density of 1.1 mA h cm^{-2}), and accordingly suppressed side reactions at the anode surface/interface. This property was further verified by the KL-Zn//MnO_2 cell with high initial specific capacity and good capacity retention and a reasonably well-preserved morphology, as characterized by SEM.[250] A porous nano-$CaCO_3$ coating was discovered to possess the ability to guide uniform and position-selected Zn stripping/plating at the nano-$CaCO_3$-layer/Zn metal anode interfaces. This Zn-deposition-guiding ability was mainly ascribed to the porous nature of the nano-$CaCO_3$-layer, considering the discovery of a similar functionality (even though relatively inferior) in Zn metal anodes coated with porous acetylene black or nano-SiO_2 layers. The coated Zn anode was matched with a CNT–MnO_2 cathode in $ZnSO_4$ + $MnSO_4$ electrolyte, showing a 42.7% higher discharge capacity than bare Zn metal anode (177 *vs.* 124 mA h g^{-1} at 1 A g^{-1}) after 1000 cycles.[251]

3.6.2. Cathode electrolyte interface. Compared with the SEI, the CEI has been rarely reported, but it is still worthy to be investigated and applied for improving the stability of the cathode–electrolyte interface against side reactions and cathode dissolution. One general strategy to construct a CEI

for suppressing the dissolution of vanadium-based cathodes in aqueous electrolytes and beyond was proposed, which introduced Sr ions into vanadium oxide layers as a sacrifice guest, leaching from the vanadium-based cathode as an *in situ* CEI coating layer on the surface (Fig. 14c).[252] In ARLIBs, it is generally accepted that CEIs can only be formed in super-concentrated electrolytes containing fluorine-based organic anions (TFSI⁻, OTf⁻, *etc.*), while in a traditional nitrite-based aqueous electrolyte (pH-adjusted saturated $LiNO_3$), a CEI was initiatively discovered on the surface of the $LiNiO_2$ cathode with the composition of Li_2CO_3 and LiOH, as demonstrated by transmission electron microscopy (TEM) and X-ray photoelectron (XPS). Under the protection of the CEI, the capacity retention of $LiNO_2$ was significantly enhanced in comparison of that in 1 M $LiNO_3$ + LiOH (pH = 10) aqueous electrolyte after 50 cycles.[253]

3.6.3. Current collector. In the study regarding the HME of $Li(TFSI)_{0.7}(BETI)_{0.3} \cdot 2H_2O$, the effect from current collector to the ESW was confirmed, which could further expand the observed ESW when changing the cathode current collector to Ti and that of the anode into Al.[208] Zhu *et al.* reported that oxidizing an Al current collector to Al_2O_3 (3 nm thickness surface) for the anode and Ti current collector to TiO_2 (5 nm thickness surface) for the cathode could expand the ESW of 15 M $NaClO_4$ aqueous electrolyte to 3.5 V (Fig. 14d). This wide ESW enabled the TiS_2 anode of SiBs to exhibit a low working potential (1.5 V *vs.* Na/Na⁺) for the first time. Thus, a full cell coupling a TiS_2 anode with PBA cathode in 15 M $NaClO_4$ aqueous electrolyte demonstrated a working voltage of 2.6 V and cyclic life up to 1000 times (30C rate) with a high energy density of 100 W h kg⁻¹.[254] In Zn metal anode-based ARBs, the substrates (current collectors) can also affect Zn stripping/plating. Archer's group found that graphene with a low lattice mismatch for Zn was shown to be effective in driving the deposition of Zn with a locked crystallographic orientation relation. The resultant epitaxial Zn anodes achieved exceptional reversibility in 2 M $ZnSO_4$ aqueous electrolyte (10 000 cycles) and 1000 cycles of full-cell charging/discharging together with an α-MnO_2 cathode.[255]

3.6.4. Electrode. In aqueous supercapacitor systems, tuning the electrode itself was also reported as a method to widen the ESW. In that work, the W atoms in the WO_3 crystal were partially replaced by Mo atoms, thus introducing oxygen vacancies. The negative limitation of the ESW was tunable between −0.4 and −1.2 V *vs.* SHE in 1 M Li_2SO_4 aqueous electrolyte owing to the consolidation process-customized band gap and HER overpotentials of the Mo-substituted WO_3 electrode.[256] Zn alloying is another electrode route-pertaining interface, especially alloying with Al. Eutectic-composition alloying of Zn and Al as an effective strategy substantially tackled the irreversibility issues of Zn metal anodes by making use of their lamellar structure composed of alternating Zn and Al nano lamellas. The lamellar nanostructure not only promoted Zn stripping from the precursor eutectic $Zn_{88}Al_{12}$ (at%) alloys, but produced core/shell Al/Al_2O_3 interlamellar nano-patterns *in situ* to guide the subsequent growth of zinc (Fig. 14e),

enabling dendrite-free Zn stripping/plating for more than 2000 h in oxygen-free aqueous electrolyte of 2 M $ZnSO_4$.[257] Zn–Al alloying was also employed in an ARAiB, which consisted of an Al_xMnO_2 cathode, a Zn substrate-supported Zn–Al alloy anode, and an $Al(OTf)_3$ aqueous electrolyte. The featured alloy interface layer could effectively alleviate the passivation and suppress the dendrite growth, ensuring ultralong-term stable Al stripping/plating. The relevant architected cell exhibited a record-high discharge voltage plateau near 1.6 V and specific capacity of 460 mA h g⁻¹ for over 80 cycles.[258] Generally, interface tuning can be another universal method for ameliorating aqueous electrolyte and any other electrolytes, which is worthy to be investigated more deeply. The performance of representative works is summarized in Table S4 (ESI†).

3.7. Beyond concentrated electrolyte

The benefits of salt-concentrated electrolytes towards ARBs have been intensively claimed here, while type kind of electrolyte has to use salts with high solubility, restricting its applications in scale and scope. Therefore, the routes concerning breaking the ceiling of salt solubility, thereby introducing more cost-effective salts with relatively low solubility, and further broadening ESW emerge, which can be classified into de-solvation/salting-out and solubility enhancement.

3.7.1. De-solvation. Zhou's group developed a new liquid electrolyte for Li metal batteries with de-solvated Li⁺ ("Li⁺ de-solvated electrolyte"), which was merely composed of inactive "frozen-like" solvent and crystal-like salt solute.[259] The addition of salts to the concentrated electrolytes could effectively eliminate the abundance of free solvents in the electrolytes and make the concentrated electrolytes more aggregative than their original counterparts. Specifically, the electrolyte configuration evolved from solvent-separated ion pair (SSIP)-dominated structures to contact ion pair (CIP)-dominated structures (Fig. 15a).[260] This type of beyond concentrated electrolyte was even more aggressive than the saturated state and was composed of only crowded solvent-depleted CIPs without any free solvents.[260] Tao's group introduced this concept in aqueous electrolytes with inexpensive inorganic salts.[55,226,261] An "oversaturated gel electrolyte" (OSGE) was simply prepared with PVA and saturated $LiNO_3$ at 95 °C. Subsequently, the excess salt was crystallized at room temperature, which was dispersed equally by the continuous room-temperature saturated gel (RTSG), forming a heterogeneous morphology (Fig. 15b). The continuous ion pathway ensured the considerable ionic conductivity of OSGE, regardless of the existence of ion-insulated crystallized salt, while the ESW was further expanded compared with that of the RTSGE due to the further compacted CIPs (Fig. 15c). Moreover, the stability window of the OSGE was still wide enough at elevated temperatures even at 80 °C, ensuring the desirable elevated temperature performance of ARLiBs.[55] Meanwhile, a perchlorate OSGE (1 m $Zn(ClO_4)_2$ + 10 m $LiClO_4$–PVA) was also employed in Zn–Li HiBs by the same group, which showed an almost dendrite-free morphology with better cyclic stability.[226] Yan *et al.* applied this strategy for the fabrication of electrolytes for low-temperature
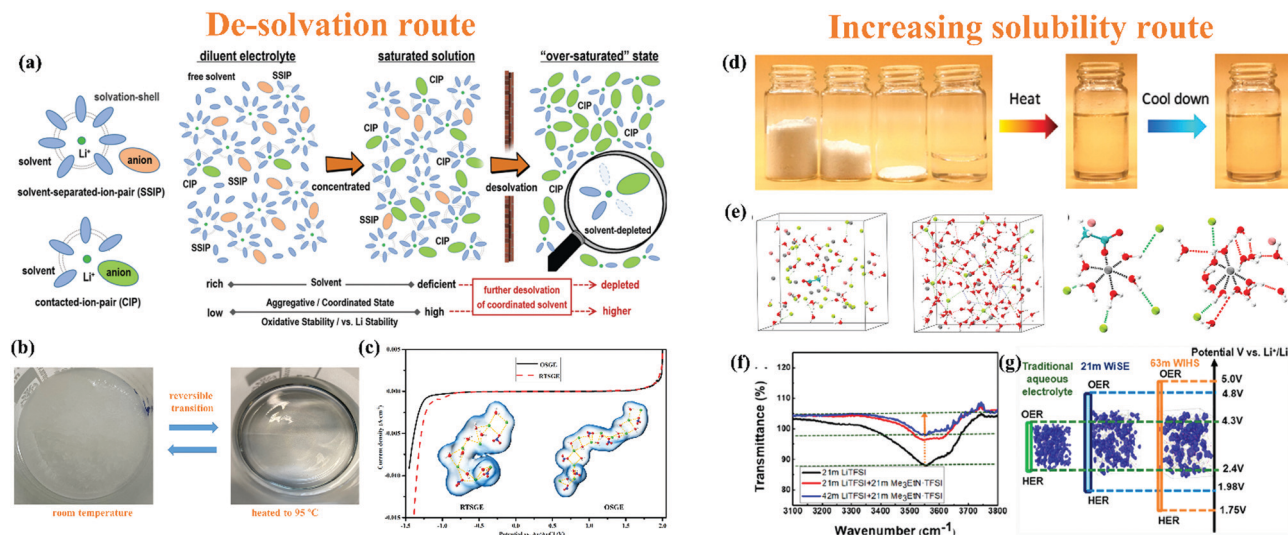
This journal is © The Royal Society of Chemistry 2022

Energy Environ. Sci., 2022, **15**, 1805–1839 | 1831

Fig. 15 (a) Design idea of further depletion of solvent molecules in the Li$^+$ solvation sheath.[260] (b) Optical images of top view of OSGE at RT and 95 °C.[55] (c) Comparison of ESW and Li$^+$ solvation sheath between OSGE and RTSGE.[55] (d) WSOE$_{45}$-1 prepared by stoichiometric amounts of ZnCl$_2$, ZnBr$_2$, Zn(OAc)$_2$, and water.[263] (e) Snapshots and extracted typical molecules conformations of MD simulation on WSOE$_{45}$-1 and 5 m ZnBr$_{0.5}$Cl$_{1.5}$ aqueous solution.[263] (f) FTIR spectra of WiSE, 42 m WiHS, and 63 m WiHS electrolytes.[220] (g) MD simulation results and ESWs of traditional aqueous electrolyte, WiSE and WiHS electrolyte.[220]

Zn-ion capacitors, which possessed superior ionic conductivity (even 1.3×10^{-3} S cm^{-1} at -60 °C) based on Zn(ClO$_4$)$_2$ salty ice, which is attributed to the unique 3D ionic transport channels inside this ice.[262]

3.7.2. Increasing solubility. Beside de-solvation/salting-out, the solubility increasing route was also attempted. A ZnCl$_2$ + ZnBr$_2$ + Zn(OAc)$_2$ aqueous electrolyte with a record super-solubility of up to 75 m was reported, which broke through the physical solubility limit, owing to the formation of acetate-capped water–salt oligomers (WSOs) bridged by Br$^-$/Cl$^-$–H and Br$^-$/Cl$^-$/O–Zn^{2+} interactions (Fig. 15d and e). This supersoluble electrolyte drove a high-performance DiB to display a reversible capacity of 605.7 mA h g^{-1} (corresponding energy density of 908.5 W h kg^{-1}).[263] A 63 m "water-in-hybrid-salt" (WiHS) electrolyte (42 m LiTFSI + 21 m Me$_3$EtN·TFSI) was prepared, which doubled the solubility of LiTFSI due to the inert salt based on the asymmetric ammonium cation of Me$_3$EtN$^+$. The FTIR spectrum in Fig. 15f reveals that the hydrogen bonding network of the WiHS electrolyte was severely disrupted, leading to a further broadened ESW (Fig. 15g).[220] The performance of representative works is summarized in Table S5 (ESI†). Basically, the mechanism behind beyond concentrated electrolytes still needs more studies, especially more fundamental studies, although some excellent works about this electrolyte tuning strategy have been reported.

4. Future perspective and conclusions

To mitigate the challenges of narrow ESWs, electrode dissolution/side reactions and temperature-variation instability of aqueous electrolytes, various strategies including electrolyte additive, pH management, salt concentration, electrolyte gelling, hybrid solvent, interface tuning, and breaking through salt solubility limitation were reported intensively during the past five years. The relevant achievements are remarkable, promoting ARBs in energy storage systems rapidly, particularly the achievements in salt-concentrated electrolytes. The beyond concentrated electrolytes can be included in salt-concentrated electrolytes, together with "solvate ionic liquid", "super-concentrated", "solvent-in-salt", and "localized concentrated" electrolytes, which are inherited from "polymer-in-salt" electrolytes.[264] At present, the salt-concentrated strategy is the most effective and efficient for high-energy and high-stability ARBs, whereas the cost of the salt is a challenge for large-scale applications. In the future, the hybrid solvent strategy can be more competitive if better non-aqueous solvents are discovered, which not only can reduce the cost, but also generate more stable electrode/electrolyte interfaces, thereby stabilizing ARBs. The artificial SEI/CEI can be another promising method; however, it is technically more difficult to create than hybrid solvents, and thus may take longer to be developed.

Despite the significant progress, there are still some potential challenges for the further commercialization of ARBs. Firstly, simulation and characterization towards aqueous electrolytes need to be improved. The parameters of MD simulation for the solvation sheath and DFT calculation for the electrode–electrolyte interface should be pre-set conscientiously rather than intentionally for supporting the as-obtained experimental results. In the case of the experimental characterization of the ion solvation structure, Raman, FTIR and NMR spectroscopy are used mostly as indirect methods, while seldom works have been reported using direct methods. X-ray nanoimaging was utilized for understanding the benefits of WiSEs, which provided direct evidence for the stability of WiSEs compared with conventional aqueous electrolytes.[265] However, that was

1832 | *Energy Environ. Sci.*, 2022, **15**, 1805–1839

This journal is © The Royal Society of Chemistry 2022

micron/sub-micron characterization, failing to approach the ion solvation sheath with a sub-nanosize. *In situ* liquid cell TEM was reported to reveal the nanoscale mineralization pathways of hydroxyapatite, which exhibits potential to characterize liquid aqueous electrolytes.[266] Secondly, the necessity of high concentration should be reconsidered.[267,268] For instance, in the $ZnCl_2$ system, the concentration of 7.5 m rather than 30 m in the saturated state was selected as the optimum concentration for modulating the electrolyte structure, and thus suppressing the freezing of water,[215] implying that, in some cases, too concentrated may be as bad as too diluted. Moreover, seawater can function as a desirable electrolyte for ARZiBs with a stable interfacial process through a Zn–Mn alloy anode,[269] further demonstrating that suitable concentration and rational interfacial design are more critical than pursuing even more concentrated electrolytes. Further, Tarascon *et al.* indicated that there was still a long way to apply WiSEs, the most popular salt-concentrated species, because of their fragile *in situ*-grown SEI and poor elevated-temperature performances.[270] The most evident benefit induced by salt-concentrated electrolytes is their expanded ESWs, and thus higher energy density of ARBs by pairing with high-working voltage electrodes. However, the electrode kinetics and mass transportation in salt-concentrated systems are usually undesirable due to their high viscosity and sluggish interfacial process. Nanosized electrodes can be an effective way to overcome kinetic issues, which balance the wide ESWs of the electrolyte and high capacity of the electrode when utilized in salt-concentrated electrolytes.[92,212,261] Besides their relatively low working voltage, ZABs and ARFBs are regarded as effective aqueous chemistries to significantly improve the energy density through their dramatically enhanced capacity, which are promising alternatives for the salt-concentrated strategy. To some extent, ZABs and ARFBs are suitable substitutes for LiBs owing to both their high energy density and excellent safety,[159,160,271] which are equally important in the future. The last issue is the gap between industry and academics. In fact, reporting the performance based on a limited number of metrics does not give a realistic picture of the battery performance required for practical use. Although it is not necessary to force the standardization of the electrode and button cell design for fundamental research, it is of paramount importance to understand the influence of button cell design, fabrication, and testing protocol on the tested results, providing more reliable results as guidelines for future studies and applications.[272,273] For real applications, the issue of self-discharge in ARBs should not be neglected, which is not only induced by macroscopical and microcosmic short circuit and electrode dissolution, but also direct chemical reactions (corrosion) between the electrode and electrolyte, especially for Zn foil electrodes. The reported long cyclic life of Zn metal-based batteries is normally obtained by testing a button cell immediately, neglecting the aging effects. Using Zn foil as both the working electrode and current collector will cause many problems when the battery is scaled up. Therefore, it is necessary to build up a Zn powder/current collector configuration with a longer calendar life.[274]

As mentioned above, ZABs and ARFBs with high capacity (high energy density) are promising for large-scale energy storage. Among the ARFBs, $Zn//Br_2$ and $Zn//I_2$ batteries are kinetically better than the Fe//Cr battery, while Zn corrosion is obstructive together with the corrosion of ARFBs. In the case of ZABs, besides the issues with the Zn metal anode, the sluggish kinetics of the ORR/OER at the cathode side also results in large polarization and low energy efficiency. The introduction of light has been demonstrated to boost the reaction kinetics of the ORR/OER, leading to enhanced electrochemical performances.[275] Therefore, the synergic effect of electricity and light can cultivate thermodynamically and kinetically better ZABs, if the theoretical understanding of the photoelectrochemical process at oxygen cathodes is deeper, whilst relevant characterization technology becomes more advanced. Overall, aqueous energy storage systems have been extensively investigated through the development of novel electrolyte concepts, while there are still challenges to be tackled before their large-scale applications.

Conflicts of interest

There are no conflicts to declare.

Acknowledgements

Notes and references

1 M. C. Hänsel, M. A. Drupp, D. J. A. Johansson, F. Nesje, C. Azar, M. C. Freeman, B. Groom and T. Sterner, *Nat. Clim. Change*, 2020, **10**, 781–789.

2 J. H. R. Lambers, *Science*, 2015, **348**, 501–502.

3 S. M. S. U. Eskander and S. Fankhauser, *Nat. Clim. Change*, 2020, **10**, 750–756.

4 O. Babacan, S. De Causmaecker, A. Gambhir, M. Fajardy, A. W. Rutherford, A. Fantuzzi and J. Nelson, *Nat. Energy*, 2020, **5**, 720–728.

5 N. Bauer, S. K. Rose, S. Fujimori, D. P. van Vuuren, J. Weyant, M. Wise, Y. Cui, V. Daioglou, M. J. Gidden, E. Kato, A. Kitous, F. Leblanc, R. Sands, F. Sano, J. Strefler, J. Tsutsui, R. Bibas, O. Fricko, T. Hasegawa, D. Klein, A. Kurosawa, S. Mima and M. Muratori, *Clim. Change*, 2018, **163**, 1553–1568.

6 C. E. Thomas, *Int. J. Hydrogen Energy*, 2009, **34**, 6005–6020.

7 X. Zeng, M. Li, D. Abd El-Hady, W. Alshitari, A. S. Al-Bogami, J. Lu and K. Amine, *Adv. Energy Mater.*, 2019, **9**, 1900161.

8 M. Tran, D. Banister, J. D. K. Bishop and M. D. McCulloch, *Nat. Clim. Change*, 2012, **2**, 328–333.

9 Y. Lu, X. Rong, Y.-S. Hu, L. Chen and H. Li, *Energy Storage Mater.*, 2019, **23**, 144–153.

10 A. Yoshino, *Angew. Chem., Int. Ed.*, 2012, **51**, 5798–5800.

This journal is © The Royal Society of Chemistry 2022

Energy Environ. Sci., 2022, **15**, 1805–1839 | 1833

11 M. Armand and J. M. Tarascon, *Nature*, 2008, **451**, 652–657.
12 W. Lee, S. Muhammad, C. Sergey, H. Lee, J. Yoon, Y.-M. Kang and W.-S. Yoon, *Angew. Chem., Int. Ed.*, 2020, **59**, 2578–2605.
13 Q. Wang, L. Jiang, Y. Yu and J. Sun, *Nano Energy*, 2019, **55**, 93–114.
14 D. Wang, J. Coignard, T. Zeng, C. Zhang and S. Saxena, *J. Power Sources*, 2016, **332**, 193–203.
15 G.-L. Zhu, C.-Z. Zhao, J.-Q. Huang, C. He, J. Zhang, S. Chen, L. Xu, H. Yuan and Q. Zhang, *Small*, 2019, **15**, 1805389.
16 G. Girishkumar, B. McCloskey, A. C. Luntz, S. Swanson and W. Wilcke, *J. Phys. Chem. Lett.*, 2010, **1**, 2193–2203.
17 S. Evers and L. F. Nazar, *Acc. Chem. Res.*, 2013, **46**, 1135–1143.
18 A. Parasuraman, T. M. Lim, C. Menictas and M. Skyllas-Kazacos, *Electrochim. Acta*, 2013, **101**, 27–40.
19 F. Zheng, M. Kotobuki, S. Song, M. O. Lai and L. Lu, *J. Power Sources*, 2018, **389**, 198–213.
20 Q. Pang, A. Shyamsunder, B. Narayanan, C. Y. Kwok, L. A. Curtiss and L. F. Nazar, *Nat. Energy*, 2018, **3**, 783–791.
21 D. Bin, Y. Wen, Y. Wang and Y. Xia, *J. Energy Chem.*, 2018, **27**, 1521–1535.
22 T. Famprikis, P. Canepa, J. A. Dawson, M. S. Islam and C. Masquelier, *Nat. Mater.*, 2019, **18**, 1278–1291.
23 W. Zhao, J. Yi, P. He and H. Zhou, *Electrochem. Energy Rev.*, 2019, **2**, 574–605.
24 J. Janek and W. G. Zeier, *Nat. Energy*, 2016, **1**, 16141.
25 S. Xin, Y. You, S. Wang, H.-C. Gao, Y.-X. Yin and Y.-G. Guo, *ACS Energy Lett.*, 2017, **2**, 1385–1394.
26 M. Galiński, A. Lewandowski and I. Stępniak, *Electrochim. Acta*, 2006, **51**, 5567–5580.
27 J. Liu, C. Xu, Z. Chen, S. Ni and Z. X. Shen, *Green Energy Environ.*, 2018, **3**, 20–41.
28 H. Manjunatha, G. S. Suresh and T. V. Venkatesha, *J. Solid State Electrochem.*, 2011, **15**, 431–445.
29 W. Tang, Y. Zhu, Y. Hou, L. Liu, Y. Wu, K. P. Loh, H. Zhang and K. Zhu, *Energy Environ. Sci.*, 2013, **6**, 2093–2104.
30 A. Gurung, J. Pokharel, A. Baniya, R. Pathak, K. Chen, B. S. Lamsal, N. Ghimire, W.-H. Zhang, Y. Zhou and Q. Qiao, *Sustainable Energy Fuels*, 2019, **3**, 3279–3309.
31 L. Yue, J. Ma, J. Zhang, J. Zhao, S. Dong, Z. Liu, G. Cui and L. Chen, *Energy Storage Mater.*, 2016, **5**, 139–164.
32 A. Manuel Stephan, *Eur. Polym. J.*, 2006, **42**, 21–42.
33 Y. Wang and W.-H. Zhong, *ChemElectroChem*, 2015, **2**, 22–36.
34 X. Yuan, F. Ma, L. Zuo, J. Wang, N. Yu, Y. Chen, Y. Zhu, Q. Huang, R. Holze, Y. Wu and T. van Ree, *Electrochem. Energy Rev.*, 2021, **4**, 1–34.
35 Z. Chang, Y. Yang, M. Li, X. Wang and Y. Wu, *J. Mater. Chem. A*, 2014, **2**, 10739–10755.
36 Z. Liu, Y. Huang, Y. Huang, Q. Yang, X. Li, Z. Huang and C. Zhi, *Chem. Soc. Rev.*, 2020, **49**, 180–232.
37 N. Alias and A. A. Mohamad, *J. Power Sources*, 2015, **274**, 237–251.
38 M. Pasta, C. D. Wessells, R. A. Huggins and Y. Cui, *Nat. Commun.*, 2012, **3**, 1149.

39 X. Wu and X. Ji, *Nat. Chem.*, 2019, **11**, 680–681.
40 A. Eftekhari, *Adv. Energy Mater.*, 2018, **8**, 1801156.
41 J.-Y. Luo, W.-J. Cui, P. He and Y.-Y. Xia, *Nat. Chem.*, 2010, **2**, 760–765.
42 X. Wang, Y. Hou, Y. Zhu, Y. Wu and R. Holze, *Sci. Rep.*, 2013, **3**, 1401.
43 J. O. G. Posada, A. J. R. Rennie, S. P. Villar, V. L. Martins, J. Marinaccio, A. Barnes, C. F. Glover, D. A. Worsley and P. J. Hall, *Renewable Sustainable Energy Rev.*, 2017, **68**, 1174–1182.
44 H. Kim, J. Hong, K.-Y. Park, H. Kim, S.-W. Kim and K. Kang, *Chem. Rev.*, 2014, **114**, 11788–11827.
45 J. Yue, L. Lin, L. Jiang, Q. Zhang, Y. Tong, L. Suo, Y.-S. Hu, H. Li, X. Huang and L. Chen, *Adv. Energy Mater.*, 2020, **10**, 2000665.
46 Q. Nian, J. Wang, S. Liu, T. Sun, S. Zheng, Y. Zhang, Z. Tao and J. Chen, *Angew. Chem., Int. Ed.*, 2019, **58**, 16994–16999.
47 K. Xu, *Chem. Rev.*, 2014, **114**, 11503–11618.
48 M. Li, C. Wang, Z. Chen, K. Xu and J. Lu, *Chem. Rev.*, 2020, **120**, 6783–6819.
49 J. B. Goodenough, *Solid State Ionics*, 1994, **69**, 184–198.
50 N. Mahmood, T. Tang and Y. Hou, *Adv. Energy Mater.*, 2016, **6**, 1600374.
51 J. B. Goodenough and Y. Kim, *Chem. Mater.*, 2010, **22**, 587–603.
52 M. Ishikawa, M. Ihara, M. Morita and Y. Matsuda, *Electrochim. Acta*, 1995, **40**, 2217–2222.
53 K. Xu, *J. Electrochem. Soc.*, 1999, **146**, 4172.
54 S. G. Chen, R. Lan, J. Humphreys and S. W. Tao, *ACS Appl. Energy Mater.*, 2020, **3**, 2526–2536.
55 S. Chen, P. Sun, B. Sun, J. Humphreys, P. Zou, K. Xie and S. Tao, *Energy Storage Mater.*, 2021, **37**, 598–608.
56 K. Xu, *Chem. Rev.*, 2004, **104**, 4303–4418.
57 W. B. Kirby, *Linden's Handbook of Batteries*, McGraw-Hill Education, New York, 5th edn, 2019.
58 A.-K. Kontturi, K. Kontturi, L. Murtomäki and D. J. Schiffrin, *J. Chem. Soc., Faraday Trans.*, 1994, **90**, 2037–2041.
59 J. C. Bachman, S. Muy, A. Grimaud, H.-H. Chang, N. Pour, S. F. Lux, O. Paschos, F. Maglia, S. Lupart, P. Lamp, L. Giordano and Y. Shao-Horn, *Chem. Rev.*, 2016, **116**, 140–162.
60 M. A. Ratner, P. Johansson and D. F. Shriver, *MRS Bull.*, 2000, **25**, 31–37.
61 J. G. Smith and D. J. Siegel, *Nat. Commun.*, 2020, **11**, 1483.
62 Z. Zhang and L. F. Nazar, *Nat. Rev. Mater.*, 2022, DOI: **10.1038/s41578-021-00401-0**.
63 D. J. Siegel, L. Nazar, Y.-M. Chiang, C. Fang and N. P. Balsara, *Trends Chem.*, 2021, **3**, 807–818.
64 J. Huang, Z. Guo, Y. Ma, D. Bin, Y. Wang and Y. Xia, *Small Methods*, 2019, **3**, 1800272.
65 W. Li, J. R. Dahn and D. S. Wainwright, *Science*, 1994, **264**, 1115–1118.
66 Q. T. Qu, Y. Shi, S. Tian, Y. H. Chen, Y. P. Wu and R. Holze, *J. Power Sources*, 2009, **194**, 1222–1225.
67 J. F. Whitacre, A. Tevar and S. Sharma, *Electrochem. Commun.*, 2010, **12**, 463–466.

1834 | *Energy Environ. Sci.*, 2022, **15**, 1805–1839

This journal is © The Royal Society of Chemistry 2022

68 S. I. Park, I. Gocheva, S. Okada and J.-I. Yamaki, *J. Electrochem. Soc.*, 2011, **158**, A1067.

69 D. Bin, F. Wang, A. G. Tamirat, L. Suo, Y. Wang, C. Wang and Y. Xia, *Adv. Energy Mater.*, 2018, **8**, 1703008.

70 X. Pu, H. Wang, D. Zhao, H. Yang, X. Ai, S. Cao, Z. Chen and Y. Cao, *Small*, 2019, **15**, 1805427.

71 Q. Qu, L. Li, S. Tian, W. Guo, Y. Wu and R. Holze, *J. Power Sources*, 2010, **195**, 2789–2794.

72 C. D. Wessells, S. V. Peddada, R. A. Huggins and Y. Cui, *Nano Lett.*, 2011, **11**, 5421–5425.

73 S. Liu, G. L. Pan, N. F. Yan and X. P. Gao, *Energy Environ. Sci.*, 2010, **3**, 1732–1735.

74 T. Tomai, S. Mitani, D. Komatsu, Y. Kawaguchi and I. Honma, *Sci. Rep.*, 2014, **4**, 3591.

75 L. Suo, O. Borodin, T. Gao, M. Olguin, J. Ho, X. Fan, C. Luo, C. Wang and K. Xu, *Science*, 2015, **350**, 938–943.

76 C. Yang, J. Chen, X. Ji, T. P. Pollard, X. Lü, C.-J. Sun, S. Hou, Q. Liu, C. Liu, T. Qing, Y. Wang, O. Borodin, Y. Ren, K. Xu and C. Wang, *Nature*, 2019, **569**, 245–250.

77 L. Suo, O. Borodin, W. Sun, X. Fan, C. Yang, F. Wang, T. Gao, Z. Ma, M. Schroeder, A. von Cresce, S. M. Russell, M. Armand, A. Angell, K. Xu and C. Wang, *Angew. Chem., Int. Ed.*, 2016, **55**, 7136–7141.

78 H. Jiang, W. Shin, L. Ma, J. J. Hong, Z. Wei, Y. Liu, S. Zhang, X. Wu, Y. Xu, Q. Guo, M. A. Subramanian, W. F. Stickle, T. Wu, J. Lu and X. Ji, *Adv. Energy Mater.*, 2020, **10**, 2000968.

79 X. Wu, Y. Qi, J. J. Hong, Z. Li, A. S. Hernandez and X. Ji, *Angew. Chem., Int. Ed.*, 2017, **56**, 13026–13030.

80 C. Li, J. Wu, F. Ma, Y. Chen, L. Fu, Y. Zhu, Y. Zhang, P. Wang, Y. Wu and W. Huang, *ACS Appl. Energy Mater.*, 2019, **2**, 6984–6989.

81 C. Li, W. Yan, S. Liang, P. Wang, J. Wang, L. Fu, Y. Zhu, Y. Chen, Y. Wu and W. Huang, *Nanoscale Horiz.*, 2019, **4**, 991–998.

82 Z. Rong, R. Malik, P. Canepa, G. Sai Gautam, M. Liu, A. Jain, K. Persson and G. Ceder, *Chem. Mater.*, 2015, **27**, 6016–6021.

83 M. Li, J. Lu, X. Ji, Y. Li, Y. Shao, Z. Chen, C. Zhong and K. Amine, *Nat. Rev. Mater.*, 2020, **5**, 276–294.

84 X. Wu, A. Markir, Y. Xu, C. Zhang, D. P. Leonard, W. Shin and X. Ji, *Adv. Funct. Mater.*, 2019, **29**, 1900911.

85 L. Wei, L. Zeng, M. C. Wu, H. R. Jiang and T. S. Zhao, *J. Power Sources*, 2019, **423**, 203–210.

86 W. Manalastas Jr, S. Kumar, V. Verma, L. Zhang, D. Yuan and M. Srinivasan, *ChemSusChem*, 2019, **12**, 379–396.

87 X. Zeng, J. Hao, Z. Wang, J. Mao and Z. Guo, *Energy Storage Mater.*, 2019, **20**, 410–437.

88 D. Kundu, B. D. Adams, V. Duffort, S. H. Vajargah and L. F. Nazar, *Nat. Energy*, 2016, **1**, 16119.

89 W. J. Wruck, *J. Electrochem. Soc.*, 1991, **138**, 3560.

90 G. Fang, J. Zhou, A. Pan and S. Liang, *ACS Energy Lett.*, 2018, **3**, 2480–2501.

91 C. Xu, B. Li, H. Du and F. Kang, *Angew. Chem., Int. Ed.*, 2012, **51**, 933–935.

92 S. Chen, R. Lan, J. Humphreys and S. Tao, *Energy Storage Mater.*, 2020, **28**, 205–215.

93 Y. Zeng, X. Zhang, Y. Meng, M. Yu, J. Yi, Y. Wu, X. Lu and Y. Tong, *Adv. Mater.*, 2017, **29**, 1700274.

94 Y. Jin, L. Zou, L. Liu, M. H. Engelhard, R. L. Patel, Z. Nie, K. S. Han, Y. Shao, C. Wang, J. Zhu, H. Pan and J. Liu, *Adv. Mater.*, 2019, **31**, 1900567.

95 D. Chao, W. Zhou, C. Ye, Q. Zhang, Y. Chen, L. Gu, K. Davey and S.-Z. Qiao, *Angew. Chem., Int. Ed.*, 2019, **58**, 7823–7828.

96 C. Liu, X. Chi, Q. Han and Y. Liu, *Adv. Energy Mater.*, 2020, **10**, 1903589.

97 C. Zhong, B. Liu, J. Ding, X. Liu, Y. Zhong, Y. Li, C. Sun, X. Han, Y. Deng, N. Zhao and W. Hu, *Nat. Energy*, 2020, **5**, 440–449.

98 G. G. Yadav, D. Turney, J. Huang, X. Wei and S. Banerjee, *ACS Energy Lett.*, 2019, **4**, 2144–2146.

99 C. Xie, T. Li, C. Deng, Y. Song, H. Zhang and X. Li, *Energy Environ. Sci.*, 2020, **13**, 135–143.

100 M. Li, Q. He, Z. Li, Q. Li, Y. Zhang, J. Meng, X. Liu, S. Li, B. Wu, L. Chen, Z. Liu, W. Luo, C. Han and L. Mai, *Adv. Energy Mater.*, 2019, **9**, 1901469.

101 G. Li, W. Chen, H. Zhang, Y. Gong, F. Shi, J. Wang, R. Zhang, G. Chen, Y. Jin, T. Wu, Z. Tang and Y. Cui, *Adv. Energy Mater.*, 2020, **10**, 1902085.

102 F. Mo, Z. Chen, G. Liang, D. Wang, Y. Zhao, H. Li, B. Dong and C. Zhi, *Adv. Energy Mater.*, 2020, **10**, 2000035.

103 H. Li, C. Han, Y. Huang, Y. Huang, M. Zhu, Z. Pei, Q. Xue, Z. Wang, Z. Liu, Z. Tang, Y. Wang, F. Kang, B. Li and C. Zhi, *Energy Environ. Sci.*, 2018, **11**, 941–951.

104 D. Wang, H. Li, Z. Liu, Z. Tang, G. Liang, F. Mo, Q. Yang, L. Ma and C. Zhi, *Small*, 2018, **14**, 1803978.

105 X. Zeng, J. Liu, J. Mao, J. Hao, Z. Wang, S. Zhou, C. D. Ling and Z. Guo, *Adv. Energy Mater.*, 2020, **10**, 1904163.

106 D. Chao, C. Ye, F. Xie, W. Zhou, Q. Zhang, Q. Gu, K. Davey, L. Gu and S.-Z. Qiao, *Adv. Mater.*, 2020, **32**, 2001894.

107 W.-J. Song, S. Lee, G. Song and S. Park, *ACS Energy Lett.*, 2019, **4**, 177–186.

108 V. Verma, S. Kumar, W. Manalastas Jr, R. Satish and M. Srinivasan, *Adv. Sustainable Syst.*, 2019, **3**, 1800111.

109 S. Zečević, L. Gajić, A. R. Despić and D. M. Drazić, *Electrochim. Acta*, 1981, **26**, 1625–1631.

110 S. Liu, J. J. Hu, N. F. Yan, G. L. Pan, G. R. Li and X. P. Gao, *Energy Environ. Sci.*, 2012, **5**, 9743–9746.

111 F. Wang, X. Fan, T. Gao, W. Sun, Z. Ma, C. Yang, F. Han, K. Xu and C. Wang, *ACS Cent. Sci.*, 2017, **3**, 1121–1128.

112 Y. Zhang, K. Cheng, K. Ye, Y. Gao, W. Zhao, G. Wang and D. Cao, *Electrochim. Acta*, 2015, **182**, 971–978.

113 Y. Mizuno, M. Okubo, E. Hosono, T. Kudo, K. Oh-ishi, A. Okazawa, N. Kojima, R. Kurono, S.-I. Nishimura and A. Yamada, *J. Mater. Chem. A*, 2013, **1**, 13055–13059.

114 L. Chen, J. L. Bao, X. Dong, D. G. Truhlar, Y. Wang, C. Wang and Y. Xia, *ACS Energy Lett.*, 2017, **2**, 1115–1121.

115 C. Lee and S.-K. Jeong, *Chem. Lett.*, 2016, **45**, 1447–1449.

116 S. Gheytani, Y. Liang, F. Wu, Y. Jing, H. Dong, K. K. Rao, X. Chi, F. Fang and Y. Yao, *Adv. Sci.*, 2017, **4**, 1700465.

117 K. F. Blurton and A. F. Sammells, *J. Power Sources*, 1979, **4**, 263–279.

This journal is © The Royal Society of Chemistry 2022

Energy Environ. Sci., 2022, **15**, 1805–1839 | 1835

118 J.-S. Lee, S. Tai Kim, R. Cao, N.-S. Choi, M. Liu, K. T. Lee and J. Cho, *Adv. Energy Mater.*, 2011, **1**, 34–50.

119 T. Zhang, N. Imanishi, S. Hasegawa, A. Hirano, J. Xie, Y. Takeda, O. Yamamoto and N. Sammes, *J. Electrochem. Soc.*, 2008, **155**, A965.

120 T. Zhang, N. Imanishi, Y. Takeda and O. Yamamoto, *Chem. Lett.*, 2011, **40**, 668–673.

121 Z. Chang, X. Wang, Y. Yang, J. Gao, M. Li, L. Liu and Y. Wu, *J. Mater. Chem. A*, 2014, **2**, 19444–19450.

122 K. Hayashi, K. Shima and F. Sugiyama, *J. Electrochem. Soc.*, 2013, **160**, A1467–A1472.

123 Y. Li and H. Dai, *Chem. Soc. Rev.*, 2014, **43**, 5257–5275.

124 J. Fu, R. Liang, G. Liu, A. Yu, Z. Bai, L. Yang and Z. Chen, *Adv. Mater.*, 2019, **31**, 1805230.

125 S. Liu, W. Han, B. Cui, X. Liu, F. Zhao, J. Stuart and S. Licht, *J. Power Sources*, 2017, **342**, 435–441.

126 M. A. Deyab and Q. Mohsen, *Renewable Sustainable Energy Rev.*, 2021, **139**, 110729.

127 N. Chawla, *Mater. Today Chem.*, 2019, **12**, 324–331.

128 B. T. Hang, T. Watanabe, M. Egashira, I. Watanabe, S. Okada and J.-I. Yamaki, *J. Power Sources*, 2006, **155**, 461–469.

129 Y. Boyjoo, H. Shi, Q. Tian, S. Liu, J. Liang, Z.-S. Wu, M. Jaroniec and J. Liu, *Energy Environ. Sci.*, 2021, **14**, 540–575.

130 S. Rehman, M. Pope, S. Tao and E. McCalla, *Energy Environ. Sci.*, 2022, **15**, 1423–1460.

131 H.-J. Peng, J.-Q. Huang and Q. Zhang, *Chem. Soc. Rev.*, 2017, **46**, 5237–5288.

132 S. Yun, S. H. Park, J. S. Yeon, J. Park, M. Jana, J. Suk and H. S. Park, *Adv. Funct. Mater.*, 2018, **28**, 1707593.

133 S. Licht and D. Peramunage, *J. Electrochem. Soc.*, 1993, **140**, L4–L6.

134 X. Wu, A. Markir, Y. Xu, E. C. Hu, K. T. Dai, C. Zhang, W. Shin, D. P. Leonard, K.-I. Kim and X. Ji, *Adv. Energy Mater.*, 2019, **9**, 1902422.

135 N. Li, Y. Wang, D. Tang and H. Zhou, *Angew. Chem., Int. Ed.*, 2015, **54**, 9271–9274.

136 M. M. Gross and A. Manthiram, *Energy Storage Mater.*, 2019, **19**, 346–351.

137 Y. Zhao, D. Wang, X. Li, Q. Yang, Y. Guo, F. Mo, Q. Li, C. Peng, H. Li and C. Zhi, *Adv. Mater.*, 2020, **32**, 2003070.

138 Z. Chen, F. Mo, T. Wang, Q. Yang, Z. Huang, D. Wang, G. Liang, A. Chen, Q. Li, Y. Guo, X. Li, J. Fan and C. Zhi, *Energy Environ. Sci.*, 2021, **14**, 2441–2450.

139 Z. Chen, Q. Yang, F. Mo, N. Li, G. Liang, X. Li, Z. Huang, D. Wang, W. Huang, J. Fan and C. Zhi, *Adv. Mater.*, 2020, **32**, 2001469.

140 H. Ao, Y. Zhao, J. Zhou, W. Cai, X. Zhang, Y. Zhu and Y. Qian, *J. Mater. Chem. A*, 2019, **7**, 18708–18734.

141 H.-R. Yao, Y. You, Y.-X. Yin, L.-J. Wan and Y.-G. Guo, *Phys. Chem. Chem. Phys.*, 2016, **18**, 9326–9333.

142 L. Chen, Q. Gu, X. Zhou, S. Lee, Y. Xia and Z. Liu, *Sci. Rep.*, 2013, **3**, 1946.

143 X. Cao, L. Wang, J. Chen and J. Zheng, *J. Mater. Chem. A*, 2018, **6**, 15762–15770.

144 Y. Liu, Z. Wen, X. Wu, X. Wang, Y. Wu and R. Holze, *Chem. Commun.*, 2014, **50**, 13714–13717.

145 Z. Chang, Y. Yang, X. Wang, M. Li, Z. Fu, Y. Wu and R. Holze, *Sci. Rep.*, 2015, **5**, 11931.

146 J. Yan, J. Wang, H. Liu, Z. Bakenov, D. Gosselink and P. Chen, *J. Power Sources*, 2012, **216**, 222–226.

147 F. Wang, O. Borodin, T. Gao, X. Fan, W. Sun, F. Han, A. Faraone, J. A. Dura, K. Xu and C. Wang, *Nat. Mater.*, 2018, **17**, 543–549.

148 B. Zhang, Y. Liu, X. Wu, Y. Yang, Z. Chang, Z. Wen and Y. Wu, *Chem. Commun.*, 2014, **50**, 1209–1211.

149 X. Wang, F. Wang, L. Wang, M. Li, Y. Wang, B. Chen, Y. Zhu, L. Fu, L. Zha, L. Zhang, Y. Wu and W. Huang, *Adv. Mater.*, 2016, **28**, 4904–4911.

150 X. Wang, M. Li, Y. Wang, B. Chen, Y. Zhu and Y. Wu, *J. Mater. Chem. A*, 2015, **3**, 8280–8283.

151 T. Placke, A. Heckmann, R. Schmuch, P. Meister, K. Beltrop and M. Winter, *Joule*, 2018, **2**, 2528–2550.

152 L. Zhang, H. Wang, X. Zhang and Y. Tang, *Adv. Funct. Mater.*, 2021, 2010958.

153 X. Wu, Y. Xu, C. Zhang, D. P. Leonard, A. Markir, J. Lu and X. Ji, *J. Am. Chem. Soc.*, 2019, **141**, 6338–6344.

154 J. Ding, W. Hu, E. Paek and D. Mitlin, *Chem. Rev.*, 2018, **118**, 6457–6498.

155 Y.-g. Wang and Y.-y. Xia, *Electrochem. Commun.*, 2005, **7**, 1138–1142.

156 J. P. Zheng, *J. Electrochem. Soc.*, 2003, **150**, A484.

157 L. Athouël, F. Moser, R. Dugas, O. Crosnier, D. Bélanger and T. Brousse, *J. Phys. Chem. C*, 2008, **112**, 7270–7277.

158 L. Dong, X. Ma, Y. Li, L. Zhao, W. Liu, J. Cheng, C. Xu, B. Li, Q.-H. Yang and F. Kang, *Energy Storage Mater.*, 2018, **13**, 96–102.

159 Y. Yao, J. Lei, Y. Shi, F. Ai and Y.-C. Lu, *Nat. Energy*, 2021, **6**, 582–588.

160 Z. Li and Y.-C. Lu, *Adv. Mater.*, 2020, **32**, 2002132.

161 E. Sum and M. Skyllas-Kazacos, *J. Power Sources*, 1985, **15**, 179–190.

162 D. Ma, B. Hu, W. Wu, X. Liu, J. Zai, C. Shu, T. Tadesse Tsega, L. Chen, X. Qian and T. L. Liu, *Nat. Commun.*, 2019, **10**, 3367.

163 K. Schmidt-Rohr and Q. Chen, *Nat. Mater.*, 2008, **7**, 75–83.

164 P. Singh and B. Jonshagen, *J. Power Sources*, 1991, **35**, 405–410.

165 B. Li, Z. Nie, M. Vijayakumar, G. Li, J. Liu, V. Sprenkle and W. Wang, *Nat. Commun.*, 2015, **6**, 6303.

166 A. Price, S. Bartley, S. Male and G. Cooley, *Power Eng. J.*, 1999, **13**, 122–129.

167 Z. Li, G. Weng, Q. Zou, G. Cong and Y.-C. Lu, *Nano Energy*, 2016, **30**, 283–292.

168 Y. Xu, Y. Wen, J. Cheng, Y. Yanga, Z. Xie and G. Cao, *Novel Organic Redox Flow Batteries Using Soluble Quinonoid Compounds As Positive Materials*, World Non-Grid-Connected Wind Power and Energy Conference, Nanjing, 2009, pp. 475–478.

169 R. Feng, X. Zhang, V. Murugesan, A. Hollas, Y. Chen, Y. Shao, E. Walter, N. P. N. Wellala, L. Yan, K. M. Rosso and W. Wang, *Science*, 2021, **372**, 836.

1836 | *Energy Environ. Sci.*, 2022, **15**, 1805–1839

This journal is © The Royal Society of Chemistry 2022

170 D. Chao, W. Zhou, F. Xie, C. Ye, H. Li, M. Jaroniec and S.-Z. Qiao, *Sci. Adv.*, 2020, **6**, eaba4098.

171 S. S. Zhang, *J. Power Sources*, 2006, **162**, 1379–1394.

172 S. Guo, L. Qin, T. Zhang, M. Zhou, J. Zhou, G. Fang and S. Liang, *Energy Storage Mater.*, 2021, **34**, 545–562.

173 Z. Hou, X. Zhang, X. Li, Y. Zhu, J. Liang and Y. Qian, *J. Mater. Chem. A*, 2017, **5**, 730–738.

174 T. K. A. Hoang, M. Acton, H. T. H. Chen, Y. Huang, T. N. L. Doan and P. Chen, *Mater. Today Energy*, 2017, **4**, 34–40.

175 W. Xu, K. Zhao, W. Huo, Y. Wang, G. Yao, X. Gu, H. Cheng, L. Mai, C. Hu and X. Wang, *Nano Energy*, 2019, **62**, 275–281.

176 J. Hao, J. Long, B. Li, X. Li, S. Zhang, F. Yang, X. Zeng, Z. Yang, W. K. Pang and Z. Guo, *Adv. Funct. Mater.*, 2019, **29**, 1903605.

177 L. Cao, D. Li, T. Pollard, T. Deng, B. Zhang, C. Yang, L. Chen, J. Vatamanu, E. Hu, M. J. Hourwitz, L. Ma, M. Ding, Q. Li, S. Hou, K. Gaskell, J. T. Fourkas, X.-Q. Yang, K. Xu, O. Borodin and C. Wang, *Nat. Nanotechnol.*, 2021, **16**, 902–910.

178 Y. An, Y. Tian, K. Zhang, Y. Liu, C. Liu, S. Xiong, J. Feng and Y. Qian, *Adv. Funct. Mater.*, 2021, **31**, 2101886.

179 F. Wang, Y. Lin, L. Suo, X. Fan, T. Gao, C. Yang, F. Han, Y. Qi, K. Xu and C. Wang, *Energy Environ. Sci.*, 2016, **9**, 3666–3673.

180 Q. Nian, X. Zhang, Y. Feng, S. Liu, T. Sun, S. Zheng, X. Ren, Z. Tao, D. Zhang and J. Chen, *ACS Energy Lett.*, 2021, **6**, 2174–2180.

181 J. Cui, X. Liu, Y. Xie, K. Wu, Y. Wang, Y. Liu, J. Zhang, J. Yi and Y. Xia, *Mater. Today Energy*, 2020, **18**, 100563.

182 T. Sun, H. Du, S. Zheng, J. Shi and Z. Tao, *Adv. Funct. Mater.*, 2021, **31**, 2010127.

183 F. Yue, Z. Tie, S. Deng, S. Wang, M. Yang and Z. Niu, *Angew. Chem., Int. Ed.*, 2021, **133**, 14001–14005.

184 W. Li, W. R. McKinnon and J. R. Dahn, *J. Electrochem. Soc.*, 1994, **141**, 2310–2316.

185 W. Li and J. R. Dahn, *J. Electrochem. Soc.*, 1995, **142**, 1742–1746.

186 L. Bai, J. Zhu, X. Zhang and Y. Xie, *J. Mater. Chem.*, 2012, **22**, 16957–16963.

187 Z. Xie, Q. Su, A. Shi, B. Yang, B. Liu, J. Chen, X. Zhou, D. Cai and L. Yang, *J. Energy Chem.*, 2016, **25**, 495–499.

188 R. Demir-Cakan, M. Morcrette, J.-B. Leriche and J.-M. Tarascon, *J. Mater. Chem. A*, 2014, **2**, 9025–9029.

189 F. Wang, J. Tseng, Z. Liu, P. Zhang, G. Wang, G. Chen, W. Wu, M. Yu, Y. Wu and X. Feng, *Adv. Mater.*, 2020, **32**, 2000287.

190 H. Pan, Y. Shao, P. Yan, Y. Cheng, K. S. Han, Z. Nie, C. Wang, J. Yang, X. Li, P. Bhattacharya, K. T. Mueller and J. Liu, *Nat. Energy*, 2016, **1**, 16039.

191 F. Y. Cheng, J. Chen, X. L. Gou and P. W. Shen, *Adv. Mater.*, 2005, **17**, 2753–2756.

192 N. Zhang, F. Cheng, Y. Liu, Q. Zhao, K. Lei, C. Chen, X. Liu and J. Chen, *J. Am. Chem. Soc.*, 2016, **138**, 12894–12901.

193 W. Sun, F. Wang, S. Hou, C. Yang, X. Fan, Z. Ma, T. Gao, F. Han, R. Hu, M. Zhu and C. Wang, *J. Am. Chem. Soc.*, 2017, **139**, 9775–9778.

194 X. Guo, J. Zhou, C. Bai, X. Li, G. Fang and S. Liang, *Mater. Today Energy*, 2020, **16**, 100396.

195 L. Dai, Y. Wang, L. Sun, Y. Ding, Y. Yao, L. Yao, N. E. Drewett, W. Zhang, J. Tang and W. Zheng, *Adv. Sci.*, 2021, **8**, 2004995.

196 C. Li, W. Wu, S. Zhang, L. He, Y. Zhu, J. Wang, L. Fu, Y. Chen, Y. Wu and W. Huang, *J. Mater. Chem. A*, 2019, **7**, 4110–4118.

197 W. Fan, F. Liu, Y. Liu, Z. Wu, L. Wang, Y. Zhang, Q. Huang, L. Fu and Y. Wu, *Chem. Commun.*, 2020, **56**, 2039–2042.

198 X. Yuan, X. Wu, X.-X. Zeng, F. Wang, J. Wang, Y. Zhu, L. Fu, Y. Wu and X. Duan, *Adv. Energy Mater.*, 2020, **10**, 2001583.

199 Y. Yamada, J. Wang, S. Ko, E. Watanabe and A. Yamada, *Nat. Energy*, 2019, **4**, 269–280.

200 Q. Dong, X. Yao, Y. Zhao, M. Qi, X. Zhang, H. Sun, Y. He and D. Wang, *Chem*, 2018, **4**, 1345–1358.

201 C. Yang, L. Suo, O. Borodin, F. Wang, W. Sun, T. Gao, X. Fan, S. Hou, Z. Ma, K. Amine, K. Xu and C. Wang, *Proc. Natl. Acad. Sci. U. S. A.*, 2017, **114**, 6197–6202.

202 L. Chen, L. Cao, X. Ji, S. Hou, Q. Li, J. Chen, C. Yang, N. Eidson and C. Wang, *Nat. Commun.*, 2020, **11**, 2638.

203 L. Jiang, Y. Lu, C. Zhao, L. Liu, J. Zhang, Q. Zhang, X. Shen, J. Zhao, X. Yu, H. Li, X. Huang, L. Chen and Y.-S. Hu, *Nat. Energy*, 2019, **4**, 495–503.

204 D. Reber, R.-S. Kühnel and C. Battaglia, *ACS Mater. Lett.*, 2019, **1**, 44–51.

205 D. P. Leonard, Z. Wei, G. Chen, F. Du and X. Ji, *ACS Energy Lett.*, 2018, **3**, 373–374.

206 M. R. Lukatskaya, J. I. Feldblyum, D. G. Mackanic, F. Lissel, D. L. Michels, Y. Cui and Z. Bao, *Energy Environ. Sci.*, 2018, **11**, 2876–2883.

207 C. Zhang, J. Holoubek, X. Wu, A. Daniyar, L. Zhu, C. Chen, D. P. Leonard, I. A. Rodríguez-Pérez, J.-X. Jiang, C. Fang and X. Ji, *Chem. Commun.*, 2018, **54**, 14097–14099.

208 Y. Yamada, K. Usui, K. Sodeyama, S. Ko, Y. Tateyama and A. Yamada, *Nat. Energy*, 2016, **1**, 16129.

209 Q. Zheng, S. Miura, K. Miyazaki, S. Ko, E. Watanabe, M. Okoshi, C.-P. Chou, Y. Nishimura, H. Nakai, T. Kamiya, T. Honda, J. Akikusa, Y. Yamada and A. Yamada, *Angew. Chem., Int. Ed.*, 2019, **58**, 14202–14207.

210 S. Wu, Y. Qiao, S. Yang, J. Tang, P. He and H. Zhou, *ACS Catal.*, 2018, **8**, 1082–1089.

211 C.-Y. Chen, K. Matsumoto, K. Kubota, R. Hagiwara and Q. Xu, *Adv. Energy Mater.*, 2019, **9**, 1900196.

212 S. Chen, R. Lan, J. Humphreys and S. Tao, *Appl. Mater. Today*, 2020, **20**, 100728.

213 J. Zheng, G. Tan, P. Shan, T. Liu, J. Hu, Y. Feng, L. Yang, M. Zhang, Z. Chen, Y. Lin, J. Lu, J. C. Neuefeind, Y. Ren, K. Amine, L.-W. Wang, K. Xu and F. Pan, *Chem*, 2018, **4**, 2872–2882.

214 X. Tang, D. Zhou, B. Zhang, S. Wang, P. Li, H. Liu, X. Guo, P. Jaumaux, X. Gao, Y. Fu, C. Wang, C. Wang and G. Wang, *Nat. Commun.*, 2021, **12**, 2857.

215 Q. Zhang, Y. Ma, Y. Lu, L. Li, F. Wan, K. Zhang and J. Chen, *Nat. Commun.*, 2020, **11**, 4463.

216 H. Bi, X. Wang, H. Liu, Y. He, W. Wang, W. Deng, X. Ma, Y. Wang, W. Rao, Y. Chai, H. Ma, R. Li, J. Chen, Y. Wang and M. Xue, *Adv. Mater.*, 2020, **32**, 2000074.

This journal is © The Royal Society of Chemistry 2022

Energy Environ. Sci., 2022, **15**, 1805–1839 | 1837

217 H. Liu, C.-Y. Chen, H. Yang, Y. Wang, L. Zou, Y.-S. Wei, J. Jiang, J. Guo, W. Shi, Q. Xu and P. Cheng, *Adv. Mater.*, 2020, **32**, 2004553.

218 S. Wu, S. Hu, Q. Zhang, D. Sun, P. Wu, Y. Tang and H. Wang, *Energy Storage Mater.*, 2020, **31**, 310–317.

219 L. Suo, O. Borodin, Y. Wang, X. Rong, W. Sun, X. Fan, S. Xu, M. A. Schroeder, A. V. Cresce, F. Wang, C. Yang, Y.-S. Hu, K. Xu and C. Wang, *Adv. Energy Mater.*, 2017, **7**, 1701189.

220 L. Chen, J. Zhang, Q. Li, J. Vatamanu, X. Ji, T. P. Pollard, C. Cui, S. Hou, J. Chen, C. Yang, L. Ma, M. S. Ding, M. Garaga, S. Greenbaum, H.-S. Lee, O. Borodin, K. Xu and C. Wang, *ACS Energy Lett.*, 2020, **5**, 968–974.

221 M. H. Lee, S. J. Kim, D. Chang, J. Kim, S. Moon, K. Oh, K.-Y. Park, W. M. Seong, H. Park, G. Kwon, B. Lee and K. Kang, *Mater. Today*, 2019, **29**, 26–36.

222 W. Yang, X. Du, J. Zhao, Z. Chen, J. Li, J. Xie, Y. Zhang, Z. Cui, Q. Kong, Z. Zhao, C. Wang, Q. Zhang and G. Cui, *Joule*, 2020, **4**, 1557–1574.

223 Z. Wang, H. Li, Z. Tang, Z. Liu, Z. Ruan, L. Ma, Q. Yang, D. Wang and C. Zhi, *Adv. Funct. Mater.*, 2018, **28**, 1804560.

224 Z. Liu, H. Li, M. Zhu, Y. Huang, Z. Tang, Z. Pei, Z. Wang, Z. Shi, J. Liu, Y. Huang and C. Zhi, *Nano Energy*, 2018, **44**, 164–173.

225 G. Wang, X. Lu, Y. Ling, T. Zhai, H. Wang, Y. Tong and Y. Li, *ACS Nano*, 2012, **6**, 10296–10302.

226 S. Chen, R. Lan, J. Humphreys and S. Tao, *ACS Appl. Energy Mater.*, 2020, **3**, 2526–2536.

227 C. Yang, X. Ji, X. Fan, T. Gao, L. Suo, F. Wang, W. Sun, J. Chen, L. Chen, F. Han, L. Miao, K. Xu, K. Gerasopoulos and C. Wang, *Adv. Mater.*, 2017, **29**, 1701972.

228 J. Xie, Z. Liang and Y.-C. Lu, *Nat. Mater.*, 2020, **19**, 1006–1011.

229 W. Pan, Y. Wang, X. Zhao, Y. Zhao, X. Liu, J. Xuan, H. Wang and D. Y. C. Leung, *Adv. Funct. Mater.*, 2021, **31**, 2008783.

230 C. Dai, X. Jin, H. Ma, L. Hu, G. Sun, H. Chen, Q. Yang, M. Xu, Q. Liu, Y. Xiao, X. Zhang, H. Yang, Q. Guo, Z. Zhang and L. Qu, *Adv. Energy Mater.*, 2021, **11**, 2003982.

231 J. Yang, Z. Xu, J. Wang, L. Gai, X. Ji, H. Jiang and L. Liu, *Adv. Funct. Mater.*, 2021, **31**, 2009438.

232 M. Chen, W. Zhou, A. Wang, A. Huang, J. Chen, J. Xu and C.-P. Wong, *J. Mater. Chem. A*, 2020, **8**, 6828–6841.

233 F. Wang, O. Borodin, M. S. Ding, M. Gobet, J. Vatamanu, X. Fan, T. Gao, N. Eidson, Y. Liang, W. Sun, S. Greenbaum, K. Xu and C. Wang, *Joule*, 2018, **2**, 927–937.

234 S. Chen, P. Sun, J. Humphreys, P. Zou, M. Zhang, G. Jeerh, B. Sun and S. Tao, *ACS Appl. Mater. Interfaces*, 2021, **13**, 46634–46643.

235 J. M. Wrogemann, S. Künne, A. Heckmann, I. A. Rodríguez-Pérez, V. Siozios, B. Yan, J. Li, M. Winter, K. Beltrop and T. Placke, *Adv. Energy Mater.*, 2020, **10**, 1902709.

236 J. Zhu, Y. Xu, Y. Fu, D. Xiao, Y. Li, L. Liu, Y. Wang, Q. Zhang, J. Li and X. Yan, *Small*, 2020, **16**, 1905838.

237 H. Zhang, B. Qin, J. Han and S. Passerini, *ACS Energy Lett.*, 2018, **3**, 1769–1770.

238 J. Zhao, J. Zhang, W. Yang, B. Chen, Z. Zhao, H. Qiu, S. Dong, X. Zhou, G. Cui and L. Chen, *Nano Energy*, 2019, **57**, 625–634.

239 Q. Dou, Y. Wang, A. Wang, M. Ye, R. Hou, Y. Lu, L. Su, S. Shi, H. Zhang and X. Yan, *Sci. Bull.*, 2020, **65**, 1812–1822.

240 J. Chen, J. Vatamanu, L. Xing, O. Borodin, H. Chen, X. Guan, X. Liu, K. Xu and W. Li, *Adv. Energy Mater.*, 2020, **10**, 1902654.

241 N. Chang, T. Li, R. Li, S. Wang, Y. Yin, H. Zhang and X. Li, *Energy Environ. Sci.*, 2020, **13**, 3527–3535.

242 J. Hao, L. Yuan, C. Ye, D. Chao, K. Davey, Z. Guo and S.-Z. Qiao, *Angew. Chem., Int. Ed.*, 2021, **60**, 7366–7375.

243 L. Zhang and G. Yu, *Angew. Chem., Int. Ed.*, 2021, **60**, 15028–15035.

244 Y. Shang, N. Chen, Y. Li, S. Chen, J. Lai, Y. Huang, W. Qu, F. Wu and R. Chen, *Adv. Mater.*, 2020, **32**, 2004017.

245 X. He, B. Yan, X. Zhang, Z. Liu, D. Bresser, J. Wang, R. Wang, X. Cao, Y. Su, H. Jia, C. P. Grey, H. Frielinghaus, D. G. Truhlar, M. Winter, J. Li and E. Paillard, *Nat. Commun.*, 2018, **9**, 5320.

246 L. Suo, D. Oh, Y. Lin, Z. Zhuo, O. Borodin, T. Gao, F. Wang, A. Kushima, Z. Wang, H.-C. Kim, Y. Qi, W. Yang, F. Pan, J. Li, K. Xu and C. Wang, *J. Am. Chem. Soc.*, 2017, **139**, 18670–18680.

247 D. Li, L. Cao, T. Deng, S. Liu and C. Wang, *Angew. Chem., Int. Ed.*, 2021, **60**, 13035–13041.

248 C. Yang, J. Chen, T. Qing, X. Fan, W. Sun, A. von Cresce, M. S. Ding, O. Borodin, J. Vatamanu, M. A. Schroeder, N. Eidson, C. Wang and K. Xu, *Joule*, 2017, **1**, 122–132.

249 Q. Zhang, J. Luan, Y. Tang, X. Ji and H. Wang, *Angew. Chem., Int. Ed.*, 2020, **59**, 13180–13191.

250 C. Deng, X. Xie, J. Han, Y. Tang, J. Gao, C. Liu, X. Shi, J. Zhou and S. Liang, *Adv. Funct. Mater.*, 2020, **30**, 2000599.

251 L. Kang, M. Cui, F. Jiang, Y. Gao, H. Luo, J. Liu, W. Liang and C. Zhi, *Adv. Energy Mater.*, 2018, **8**, 1801090.

252 L. Zhang, B. Zhang, J. Hu, J. Liu, L. Miao and J. Jiang, *Small Methods*, 2021, **5**, 2100094.

253 C. Lee, Y. Yokoyama, Y. Kondo, Y. Miyahara, T. Abe and K. Miyazaki, *Adv. Energy Mater.*, 2021, **11**, 2100756.

254 Z. Hou, X. Zhang, H. Ao, M. Liu, Y. Zhu and Y. Qian, *Mater. Today Energy*, 2019, **14**, 100337.

255 J. Zheng, Q. Zhao, T. Tang, J. Yin, C. D. Quilty, G. D. Renderos, X. Liu, Y. Deng, L. Wang, D. C. Bock, C. Jaye, D. Zhang, E. S. Takeuchi, K. J. Takeuchi, A. C. Marschilok and L. A. Archer, *Science*, 2019, **366**, 645–648.

256 J. Li, L. An, H. Li, J. Sun, C. Shuck, X. Wang, Y. Shao, Y. Li, Q. Zhang and H. Wang, *Nano Energy*, 2019, **63**, 103848.

257 S.-B. Wang, Q. Ran, R.-Q. Yao, H. Shi, Z. Wen, M. Zhao, X.-Y. Lang and Q. Jiang, *Nat. Commun.*, 2020, **11**, 1634.

258 C. Yan, C. Lv, L. Wang, W. Cui, L. Zhang, K. N. Dinh, H. Tan, C. Wu, T. Wu, Y. Ren, J. Chen, Z. Liu, M. Srinivasan, X. Rui, Q. Yan and G. Yu, *J. Am. Chem. Soc.*, 2020, **142**, 15295–15304.

259 Z. Chang, Y. Qiao, H. Deng, H. Yang, P. He and H. Zhou, *Joule*, 2020, **4**, 1776–1789.

1838 | *Energy Environ. Sci.*, 2022, **15**, 1805–1839

This journal is © The Royal Society of Chemistry 2022

260 Z. Chang, Y. Qiao, H. Yang, H. Deng, X. Zhu, P. He and H. Zhou, *Energy Environ. Sci.*, 2020, **13**, 4122–4131.

261 S. Chen, P. Sun, J. Humphreys, P. Zou, M. Zhang, G. Jeerh and S. Tao, *Energy Storage Mater.*, 2021, **42**, 240–251.

262 Y. Sun, H. Ma, X. Zhang, B. Liu, L. Liu, X. Zhang, J. Feng, Q. Zhang, Y. Ding, B. Yang, L. Qu and X. Yan, *Adv. Funct. Mater.*, 2021, **31**, 2101277.

263 S. Cai, X. Chu, C. Liu, H. Lai, H. Chen, Y. Jiang, F. Guo, Z. Xu, C. Wang and C. Gao, *Adv. Mater.*, 2021, **33**, 2007470.

264 K. Xu, W. Xu and S. S. Zhang, *J. Non-Cryst. Solids: X*, 2022, **14**, 100088.

265 C.-H. Lin, K. Sun, M. Ge, L. M. Housel, A. H. McCarthy, M. N. Vila, C. Zhao, X. Xiao, W.-K. Lee, K. J. Takeuchi, E. S. Takeuchi, A. C. Marschilok and Y.-C. K. Chen-Wiegart, *Sci. Adv.*, 2020, **6**, eaay7129.

266 K. He, M. Sawczyk, C. Liu, Y. Yuan, B. Song, R. Deivanayagam, A. Nie, X. Hu, V. P. Dravid, J. Lu, C. Sukotjo, Y.-P. Lu, P. Král, T. Shokuhfar and R. Shahbazian-Yassar, *Sci. Adv.*, 2020, **6**, eaaz7524.

267 D. Chao and S.-Z. Qiao, *Joule*, 2020, **4**, 1846–1851.

268 Y.-S. Hu and Y. Lu, *ACS Energy Lett.*, 2020, **5**, 3633–3636.

269 H. Tian, Z. Li, G. Feng, Z. Yang, D. Fox, M. Wang, H. Zhou, L. Zhai, A. Kushima, Y. Du, Z. Feng, X. Shan and Y. Yang, *Nat. Commun.*, 2021, **12**, 237.

270 L. Droguet, A. Grimaud, O. Fontaine and J.-M. Tarascon, *Adv. Energy Mater.*, 2020, **10**, 2002440.

271 R. F. Service, *Science*, 2021, **372**, 890–891.

272 H. Li, *Joule*, 2019, **3**, 911–914.

273 Z. Lin, T. Liu, X. Ai and C. Liang, *Nat. Commun.*, 2018, **9**, 5262.

274 Q. Li, Y. Wang, F. Mo, D. Wang, G. Liang, Y. Zhao, Q. Yang, Z. Huang and C. Zhi, *Adv. Energy Mater.*, 2021, **11**, 2003931.

275 D. Du, Z. Zhu, K.-Y. Chan, F. Li and J. Chen, *Chem. Soc. Rev.*, 2022, **51**, 1846–1860.

This journal is © The Royal Society of Chemistry 2022

Energy Environ. Sci., 2022, **15**, 1805–1839 | **1839**